

VALIDATION OF A CAPACITANCE SNOW DENSITY PROBE IN AN AVALANCHE
FORECASTING SETTING

by

STEVEN MICHEAL CONGER

B.Sc., University of Utah, 2001

A THESIS SUBMITTED IN PARTIAL FULFILLMENT OF
THE REQUIREMENTS FOR THE DEGREE OF

MASTER OF SCIENCE

In

THE FACULTY OF GRADUATE STUDIES

(Geography)

THE UNIVERSITY OF BRITISH COLUMBIA

April 2007

© Steven Michael Conger, 2007

ABSTRACT

Snow profiles provide information of medium importance and uncertainty (Class II) about the characteristics of snow stratigraphy relative to patterns associated with avalanche formation and activity. Snow profiles are time consuming and limited to a specific location. It would be a valuable improvement to be able to sample more sites and gain more information in the same time required for one manual profile. I conducted a careful and systematic investigation of the Capacitec capacitance probe (Louge et al., 2002) developed as a potential snow density profile tool. The probe utilizes measurements of dielectric properties of snow that have been related to the snow sample's density (Cumming, 1952; Kuroiwa, 1962; Yosida et al., 1958). I tested the intended use of both the original prototype and an improved second-generation prototype in a field setting representative of avalanche forecasting conditions.

I investigated three hypotheses. The first tested whether bulk snow density measured by the probe is equal to or better than currently accepted practice. A supporting study determined the range of values for "accepted practice." The second hypothesis investigated whether a density profile as estimated by the probe is equal to or better than currently accepted practice. The third hypothesis examined whether characteristics associated with structure and stratigraphy in the snowpack could be identified in the information provided by the probe.

Detailed manual snow profiles with associated probe measurements were collected over a nine-day period from 23 February to 3 March 2006 in the Northern Selkirk Mountains of British Columbia, Canada. These data were used as a training-set for the construction of recursive partitioned models to estimate densities from probe output. Portions of the training-set were used as validation-sets along with two test cases representing spatial and temporal differences, gathered on 5 and 10 March 2006. The precision and accuracy of predictions against validation-sets and test cases were analyzed and cross-validation was performed for models representing different sizes, grain types, and lag times.

In the supporting study, I determined that "accepted practice" includes under sampling errors of 1 to 2%, variation within individual cutters of 0.8 to 6.2%, and significant variation between cutters of 3 to 12%. Given the mean of all samples is the accepted true value of the measured density, variation solely in cutter types provides "accepted practice" measurements that are within 12% of the true density.

In addressing the first hypothesis, I was able to create and validate models based on probe measurements that provide bulk density predictions accounting for 92% of the variability in the manual density measurements (97% in a unique case) and are within "accepted practice" values.

Mechanical problems with the tracking component of the probe prevented numerical comparison of predicted and manual profiles. Visual analysis ascertained that though predicted and measured density profile shapes were close, the probe profiles were generally not sufficiently close to the manual profile to replace it in representing the structure of the snow cover. One case utilizing a layer ageing proxy did fit close enough for practical use. The same mechanical issues prevented a full conclusion regarding the third hypothesis though my experience with the probe and manual observations suggests the nature of grain bonding plays a noticeable role in the properties measured.

TABLE OF CONTENTS

Abstract.....	ii
Table of Contents	iii
List of Tables	iv
List of Figures	v
Acknowledgements	vii
Dedication.....	viii
Chapter 1 Introduction	1
1.1 Motivation.....	1
1.2 Considerations of Scale.....	2
1.3 Research Hypotheses.....	3
Chapter 2 Supporting Theory and Previous Work.....	5
2.1 Snow Densification	5
2.2 Snow Profile Observations	6
2.3 Avalanche Forecasting Context.....	7
2.4 Snow Profile Application to Avalanche Forecasting	8
2.5 Snow Profile Probes	10
2.6 Dielectric properties and snow.....	13
2.7 Relevance	16
Chapter 3 Methods	18
3.1 Research Setting	18
3.2 Data Collection.....	20
3.3 Sources of Error.....	23
3.4 Experimental Design.....	25
3.5 Data Manipulation, Management, and Quality Assurance	26
Chapter 4 Supporting Investigation and Benchmark.....	30
4.1 New Manual Observation Method	30
4.2 Current Practice Benchmark.....	32
Chapter 5 Results: Density Model Development, Validation, and Analysis	40
5.1 Data.....	40
5.2 Model Development.....	41
5.3 Model Bulk Density Analysis.....	45
5.4 Predicted Density Profile Analysis.....	62
Chapter 6 Conclusions	71
6.1 Summary.....	71
6.2 Study Limitations.....	73
6.3 Future Work	73
Bibliography	76
Appendices	81
Appendix A Training-set Day Weather Observations.....	81
Appendix B Grain Notation	82
Appendix C Brush Comparison Summary and Test Results.....	83
Appendix D Training-set Manual Snow Profiles	86
Appendix E Observation and Variable Distributions.....	96
Appendix G Bivariate Fits for 50% Training-set Day Models and Validations	101
Appendix H Bivariate Fits for 1 Training-set day Model Examples.....	104
Appendix I Residual Plots for 1 Training-set day Model Examples	106
Appendix J JMP scripts for Select Models.....	108

LIST OF TABLES

Table 1. Blöschl's scale triplet applied to measurements taken during this study.	3
Table 2. Scale triplet summary of the vertical snow profile measurements.	3
Table 3. Density changes in relation to various metamorphic processes (after Bader, 1962).....	5
Table 4. Matrix describing the ratings used in combining relief characteristics of relative layer hardness with visual quality. (**Decreasing ability to differentiate layers).....	31
Table 5. Specifications and characteristics of density cutters tested in the randomized block experiment.	34
Table 6. Measurement error and cutter under sampling error estimates.	35
Table 7. Summary of density measurement error bar values for tested cutters when used with the experiment specific scale.....	35
Table 8. Result summary of randomized block analysis of density cutters.....	37
Table 9. Summary of Layers 1, 2 and 4 where null hypothesis of cutters measuring equal was rejected.	37
Table 10. Variances of cutter measurements with in layers.....	38
Table 11. Kolmogorov-Smirnov-Lilliefors test results of normal distribution for model variables.....	42
Table 12. Residual analysis of the single training-set day models in Figure 15 summarizing the standard deviation and Shapiro-Wilk statistic W testing normal distribution of residuals.....	51
Table 13. R ² and RMSE values for model and test case fits of 1, 2, and 3 consecutive day models illustrated in Figure 24.....	60
Table 14. Correlation matrix for parallel plunge variable movAvgXpt5cm values.....	74
Table 15. Description of grain notation used in field recording and study graphics.....	82
Table 16. Summary of brush characteristics and specifications.	83
Table 17. Brush test results.....	85

LIST OF FIGURES

Figure 1. Example of a time profile following Häfeli's description. 9

Figure 2. Cole - Cole plot (Argand diagram) of the relationship between real and imaginary components of the complex dielectric constant through frequencies from the static dielectric constant to the optical dielectric constant. 14

Figure 3. Location of research sites on British Columbia map (Parks highlighted in grey)..... 18

Figure 4. Illustration of second-generation probe following a full depth plunge, encoder, and backpack containing electronics. Upper right insert shows the PDA and A-D device, upper left insert shows the probe tip and collapsed avalanche probe shaft. 22

Figure 5. Typical field layout for data collection day. (a) The probe as left in place following the last plunge along line (b). (c) The area of previous day's data collection. (d) Area for next data collection day. 26

Figure 6. Typical data collection excavation showing the probe as left in place for vertical measurement reference following final plunge of day's sequence. Manual densities were measured directly adjacent to probe. 28

Figure 7. Various types of density cutters tested for variance, left to right: box (100 cc), wedge (200 cc), and tube (100 cc). 34

Figure 8. Graphic summary of sampling variance and weighing errors for density cutters evaluated for "accepted practice" benchmark. (Organized by sample layer and showing cutter mean densities.) 39

Figure 9. Scatter plot of model variables with .95 confidence interval ellipse 43

Figure 10. Example of two-split recursive partition tree from JMP IN output. 45

Figure 11. This graph shows the respective R² values calculated or precision for the bivariate fits between model predicted densities and the response variable used in creation of the various models. 46

Figure 12. Comparison of precisions for selected models applied to excluded training-set data of the percentage of change between model fit to training-set data and model fit of predicted densities for training-set data excluded from model construction. 48

Figure 13. Coefficients of determination for density prediction results relative to training-set size. 49

Figure 14. Summary of results for consecutively increasing sized training-sets shown as a percentage of change from the model fit to a single day validation-set..... 50

Figure 15. Comparison of selected one-day training-set model fits 51

Figure 16. Residual plot examples suggesting grain type influence on model errors..... 52

Figure 17. One-day model precisions by distance (days out) from prediction. 53

Figure 18. One-day model precisions organized by the prediction day. 54

Figure 19. Comparison of fit accuracy for selected models as suggested by RMSE analysis. 55

Figure 20. Accuracy comparison of increasing sized training-set models. 56

Figure 21. Accuracy of one-day training-set models applied to increasingly distant validation days. 57

Figure 22. Overall fits for one, 2, and 3 consecutive training-set day, interactively constructed model applied to validation-set. 58

Figure 23. Fits for non-interactive one, two, and three consecutive day training-set model, model cross validation, and validation set..... 59

Figure 24. Overall fits for one, two, and three consecutive training-set day, interactively constructed model applied to the test cases. 60

Figure 25. Exceptional overall fits for one, two, and three consecutive day training-set model, model cross validation, and validation set with inclusion of ageing proxy as an effect factor..... 61

Figure 26. Predicted density profiles shown in relation to the measured density profile for test case 1 based on one, two, and three-day training-set models. The heavier and darker line represents the predicted profile while the lighter line is the manually measured density profile. 63

Figure 27. Modeled density profiles for test case 1 shown in conjunction with the manual snow profile. The heavier and darker line represents the predicted profile while the lighter line is the manually measured density profile. Left to right: 3 March training-set, 2-3 March training-set, and 1-3 March training set. 64

Figure 28. Predicted density profiles for Test Case 2 based on one, two, and three-day training-set models. The heavier and darker line represents the predicted profile while the lighter line is the manually measured density profile. 65

Figure 29. Modeled density profiles for test case 2 shown in conjunction with the manual snow profile. The heavier and darker line represents the predicted profile while the lighter line is the manually measured density profile. Left to right: 3 March training-set, 2-3 March training-set, and 1-3 March training set. 66

Figure 30. Predicted density profiles for 3 March validation-set based on one, two, and three-day training-set models. The heavier and darker line represents the predicted profile while the lighter line is the manually measured density profile.	67
Figure 31. Modeled density profiles for 3 March validation-set shown in conjunction with the manual snow profile. Left to right, 2 March training-set, 1-2 March training-set, and 29 Feb – 2 March training-set.	68
Figure 32. Predicted density profiles for 3 March validation-set based on one, two, and three-day training-set models including ageing proxy. The heavier and darker line represents the predicted profile while the lighter line is the manually measured density profile.	69
Figure 33. Modeled density profiles utilizing the ageing proxy shown in conjunction with the manual snow profile for March 3 validation-set. Left to right, 2 March training-set, 1-2 March training-set, and 29 Feb – 2 March training-set.	70
Figure 34. Traces of movAvgXpt5cm variable for parallel plunges 30 cm apart. The order of the plunges left to right are 1, 2, 3, 4, 5, 11, 10, 9, 8, 7, 6 that correspond to the plunge numbers in Table 5. Relative hand hardness layering is shown for reference in grey.	74
Figure 35. Illustration of varying vertically segregated volume percentages sampled by a wedge-type density cutter when inserted horizontally.	75
Figure 36. New snow and height at Fidelity 23 February through 3 March 2006.	81
Figure 37. Air temperatures at Fidelity 23 February through March 3 2006.	81
Figure 38. Snow profile for 23 February 2006.	86
Figure 39. Snow profile for 25 February 2006.	87
Figure 40. Snow profile for 26 February 2006.	88
Figure 41. Snow profile for 27 February 2006.	89
Figure 42. Snow profile for 28 February 2006.	90
Figure 43. Snow profile for 1 March 2006.	91
Figure 44. Snow profile for 2 March 2006.	92
Figure 45. Snow profile for 3 March 2006.	93
Figure 46. Snow profile for 5 March 2006.	94
Figure 47. Snow profile for 10 March 2006.	95
Figure 48. Recursive partitioning tree for density prediction model based on 50% of training-set days at 5 splits.	99
Figure 49. Recursive partitioning tree for density prediction model based on 50% of training-set days at 10 splits.	99
Figure 50. Recursive partitioning tree for density prediction model based on 50% of training-set days at 15 splits.	100

ACKNOWLEDGEMENTS

I am grateful for the research funding support of Canadian Mountain Holidays and the National Sciences and Engineering Research Council of Canada. This study also received in-kind support from Parks Canada Glacier Park Avalanche Control Section and Capacitec Inc. I was supported in part by a University of British Columbia International Partial Tuition Scholarship and the Jared Stanley Memorial Scholarship.

Many exceptional people provided assistance and insight along the way. I thank my supervisor Dr. Dave McClung and committee member Dr. Brett Eaton for their support and guidance. Appreciation is due to Bruce McMahon, Jeff Goodrich, Johann Schleiss, Eric Dafoe, Jim Phillips, Dean Flick, and Mark Harrison of the Avalanche Control Section; Chris Borstad and Rob Burrows of the UBC Avalanche Research Group; and Kellie Erwin for field assistance.

A special thanks goes to the mentors and friends whom always had time for questions, discussions, and encouragement: Duan Bowles, Knox Williams, R.A. Schmidt, Doug Fesler, Sue Ferguson, Ed LaChapelle, Bill Harrison, Chris Landry, Dave McClung, Kirk Bachman, Chris Borstad, Jeffrey Conger, Liam Fitzgerald, Daniel Howlett, Clair Israelson, Peter Schorey, John Tweedy, Niko Weis and numerous members of the Canadian and American Avalanche Associations. I was fortunate to have the camaraderie of the ASARC cohort during time spent at Rogers Pass: Catherine Brown, Dave Gauthier, James Floyer, and Laura Bakermans.

I thank my parents Jerry and Shirley Conger for ensuring I grew up skiing and enjoying the mountains.

Finally, I wish to thank Tannis Dakin for her unfaltering support of this endeavour and enthusiasm for the next adventure.

To Simon and Coby

Chapter 1 INTRODUCTION

My study focuses on observations of the snowcover during avalanche formation. It specifically investigates an electronic probe (snow sonde) proposed to gather snow profile observations relevant to prediction of avalanche activity.

Snow profiles provide information of medium importance and uncertainty (Class II) about the characteristics of snow stratigraphy relative to patterns associated with avalanche formation and activity. Snow profiles are time consuming and limited to a specific location. Improvement to this activity would be in the form of faster information collection and more sampling sites over the time required for just one manual profile. The holy grail of snow profile observation has been described as the development of non-destructive testing techniques for describing the three-dimensional extent of layers while providing information about density and grain size (Colbeck, 1991).

A portable capacitance snow-sounding instrument was developed by Capacitec Inc. as a potential snow density profile tool utilizing a measurement concept d originated in research by others (Cumming, 1952; Kuroiwa, 1962; Yosida et al., 1958). A density profile can serve as a proxy for snow pack characteristics such as strength and are important in evaluation of potential avalanche formation.

I conducted a careful and systematic investigation testing the intended use of both the original prototype and an improved second-generation prototype in a field setting representative of avalanche forecasting conditions. In supporting studies, two preliminary analyses were conducted. First, a standardized and reproducible field method for layer identification at an appropriate scale was developed. This addressed a complication of high-resolution snow sondes in providing information on fine scales relative to the snow cover thickness that are difficult to compare to classically scaled, manual profile measurements. The second was an analysis to establish a benchmark for “currently accepted practice” representing variance present in field density measurements.

1.1 Motivation

I have taken on the challenge of gaining the technique and skill of researcher and aspirant scientist after fifteen plus years as a practitioner in the field of avalanche education, forecasting, and mitigation. In this effort, I find myself revisiting classic techniques to determine the assumptions they are based on and whether such suppositions still serve their ultimate goals of predicting avalanche activity.

I am standing in a rectangular hole dug in the snow at tree line near 51 degrees north latitude. It is nine-thirty in the morning in late February. The snow pit is approximately two and a half meters deep with a north-facing, plumb wall that is slightly more than two meters across; the ends of the pit are half that distance wide. The five cubic meters and 1,500 kg of snow have been excavated by hand in over 250 shovel loads. When the day is done, I will move all this snow a second time back into the hole. This exercise has gone on each day directly adjacent to the prior day's area for several days and will continue several more without break. I have not kept tally of how many snow pits I have dug during my career. Digging snow pits is the standard method of observing the profile of the snowpack and gaining information about its structure. It is a tangible activity in a field of inquiry plagued with uncertainty and is not without limitations.

A snow profile is a point observation in a spatially and temporally dynamic medium. I am in full agreement with LaChapelle's (1985) admonishment that individuals often "are found in an ostrich-like position scrutinizing snow crystals with a hand lens while concrete evidence of snow behaviour goes ignored." Yet, I continue to dig as I also continue to observe and learn, seeking observations or scales of observation not yet utilized that will reduce our uncertainty in forecasting avalanche activity. I am motivated to know if it is possible to dig smarter, maybe less, and know more about what I am unable to see and how I might pass on such a skill or technique to other practitioners or students.

During the winter of 2004/2005, I began a project to determine through field investigation and experimentation how instability present at a slope feature is related spatially to the slope around it. I proposed to use the Capacitec snow sonde (Louge et al., 2002) designed to measure electrical properties of the snow. However, fieldwork immediately illustrated that the probe required substantiation for use in any experimental exploration. Thus, the project became one of instrument validation, which is necessary for adoption of the probe by avalanche forecasters.

In this study, I investigate a manner of observing, recording, and presenting stratigraphic information about a point observation of snowpack structure. For as Colbeck (1991) cautions, "While theory has been enormously helpful in understanding snow's behaviour, further theoretical developments without direct observations to support the assumptions and test the conclusions can be dangerous."

1.2 Considerations of Scale

Scale is essential in understanding and analyzing geographically based measurements and their change over space and time. Scale issues develop when measurement scales for observations supporting understanding and prediction differ from the scales on which avalanche phenomenon processes occur over multiple spatial and temporal extents. Walker and Walker (1991) used Delcourt and Delcourt's 1988 spatial definitions of macro (10^{10} to 10^{12} m²), meso (10^6 to 10^{10} m²), and micro (10^0 to 10^6 m²) scales to characterize areal extent in their conceptual "time-space" of landscape disturbance in the Arctic. Landry (2001) extended Walker and Walker's period of disturbance versus spatial scale to the avalanche phenomenon and increased microscale to include 10^{-3} to 10^6 m² in his "avalanche time – space". Caution must be exercised and convincing rules regarding regions of validity must be used when extrapolating observations or model relationships between spatial scales (i.e. scaling).

Blöschl (1996) provides a framework to describe scale through the measurement triplet of extent, spacing, and support. Extent refers to the coverage of the observation in space or time. Spacing is the distance (temporal or spatial) between observations. Support describes the volume of the sample. Hägeli and McClung (2000) adopted this triplet for avalanche measurements and models.

Scaling issues present in avalanche formation and activity prediction often involve the estimation of general conditions over larger areas or periods from point observations or estimation of point conditions from general conditions. This compounds the avalanche forecasting process and must be addressed through observation techniques and sampling strategies. The same issues are present when comparing observations from one day to the next or from one area to another as in this study.

Snow processes present in the extent, spacing, and support of this study occur on the microscale. The microstructure of the snowpack is arrangement of several grains and their respective

bond condition. Individual grain bonds are on the order of less than 0.1 cm, strain softening of those bonds during fracture are on the order of 100 grains (McClung and Schaerer, 2006). Slab failure in an avalanche generally occurs between 0.5 to 1 m deep. The probe samples a volume of less than 100 grains.

Table 1 conveys the relationships between three perspectives of the triplet applied to categorical differences in the data collection process. The first column is the actual measurement taken by the probe as it penetrates vertically through the snow. A profile is the product of a vertically referenced set of measured voltages. Profiles can be physically very near to each other or represent differences due to topography (e.g. elevation, aspect, slope). Different sample days represent change in meteorological conditions as well as metamorphic change in the snow cover.

	X & Y measured voltages	Profiles	Sampling Days
Extent	~2 meters vertical and ~2 minutes	2 meters horizontal and 15 minutes for 11 plunges	160 m ² and weeks
Spacing	Randomly with an average of 5 samples per cm	~30 cm	Change in height of snow surface, snow and air temperatures over hours.
Support	.57 cm ³	Product of capacitance value extent, spacing, and support triplet	Product of profile support times day spacing

Table 1. Blöschl's scale triplet applied to measurements taken during this study.

Vertical Scale	Probe Measurements	Manual Densities	Manual Temperatures
Extent	~2 meters vertical and ~2 minutes	~2 meters vertical and ~120 minutes	~2 meters vertical and ~10 minutes
Spacing	Randomly with an average of 5 samples per cm	<2 cm (stacked and relatively continuous)	5 cm
Support	Averaged to 0.5 cm vertical region	3 cm	.5 cm

Table 2. Scale triplet summary of the vertical snow profile measurements.

1.3 Research Hypotheses

Accurate snowpack observations are a cornerstone of both understanding avalanche formation and avalanche forecasting. In this study, I attempt to advance abilities in retrieving an accurate profile of snowcover stratigraphy, without time consuming excavation, at accuracy comparable to accepted state of practice.

A portable capacitance snow-sounding instrument was introduced in 1998 as a potential snow density profile tool specifically for snow hydrologists and avalanche forecasters. Limited measurements made with a prototype during concept demonstration showed correspondence between probe values and

measured values of snow density with individual errors smaller than 20% (Louge et al., 1998a). The probe is intended for operational use. Far less error is assumed to be present in density measurements by avalanche practitioners, therefore acceptance requires further validation. This study addresses the following hypotheses in support of its validation:

H_{o1}: The bulk snow density measured by the probe is equal to or better than currently accepted practice.

H_{o2}: A density profile, as estimated by the probe, is equal to or better than currently accepted practice.

H_{o3}: Characteristics associated with the structure in the snowpack can be identified in the information provided by the probe.

The analysis and conclusions must be both relevant and significant if they are to be trusted by a working forecaster and accepted within the scientific community. This is reflected in the development of the research plan and selection of methods. To this end, field data collection was done in locations representative of specific ones used by avalanche forecasters in support of the types of decisions they make.

A common metric used by other researchers to evaluate snow profile probe performance has been the average of measurement values over the length of the profile (e.g. (Birkeland et al., 1995; Brown and Birkeland, 1990; de Quervain and Meister, 1986; Kronholm, 2004; Perla, 1970)). This is valid for consideration of bulk characteristics but not for the interfaces and step-like stratigraphy relationships important to avalanche forecasting. Identification of layering from electronic probe information in analogous applications such as well logging has been done through visual analysis. This has also been the case for snow (Kronholm, 2004).

There were concepts that required development during this research to build a case supporting the null hypotheses. A benchmark for “currently accepted practice” was needed. The variance present in density measurement tools currently used in snow profile work was analyzed in a supporting investigation to establish a value range for “accepted practice”.

The advent of high-resolution snow profile probes introduces an additional challenge since they generally measure at a scale far finer than classical manual techniques. A component of this investigation was the development of a manual, reproducible layer identification technique to expose or highlight stratigraphy variation suggested by the probe output.

Chapter 2 SUPPORTING THEORY AND PREVIOUS WORK

This chapter provides background and a base of knowledge through a literature review that discusses the physical processes present in the snow cover affecting density, snow stratigraphy observations and records, the context in which snow profiles are used to support avalanche forecasting, the development of probes to gather snow profiles, and electrical properties utilized by the capacitance probe for measurements.

2.1 Snow Densification

Density is a measurement of the mass per unit volume. In dry snow, the volume is filled with a mixture of ice and air. Since air has negligible mass, it is therefore a measurement of the amount of ice mass present in the given volume. The size, shape and arrangement of grains in a specimen of snow determine its texture, while the stratigraphy or layering seen in profiles is its structure (Colbeck et al., 1990). Both texture and structure influence the density of a sample of snow. Metamorphism of the snow results in a change of texture and structure (Bader, 1954).

Density of snow on the ground is known to change over time and increasing depth in a general trend towards greater density. If this process goes uninterrupted, the stratigraphy is ultimately altered from metamorphosed snow to firn to glacial ice assuming the snow is not subjected to extreme temperatures. Bader attributed metamorphism as a cause of increasing density and natural settling of the snow, suggesting densification is a result of the metamorphism process that predominates in each layer (Table 3). His original metamorphism discussion used the terms destructive and constructive that correspond to present terminology of low growth rate resulting in rounding of grains or high growth rate resulting in faceting of grains respectively.

Metamorphism Process	Description Relative to Density Change	Observed Density Changes
Destructive (Rounding)	Loss of original shape resulting in fine grain snow (0.5 to 1 mm)	150 to 250 kg/m ³ (Further metamorphism relies on plastic densification by load if dry; pressure metamorphism)
Constructive (Faceting)	Development of faces, edges, vertices (2 to 8 mm)	200 to slightly more than 300 kg/m ³
Melt	Coarse grained, rounded to 3 mm and clusters to 15 mm	Any density up to that of ice
Pressure	Mechanical deformation of dry snow	450 to 830 kg/m ³

Table 3. Density changes in relation to various metamorphic processes (after Bader, 1962).

Bader (1962) also observed that when he heaped disaggregated snow originally denser than 150 kg/m³ and having undergone destructive metamorphism (rounding) in the cold, the resulting density was approximately 500 kg/m³. He took this to indicate that an irregular arrangement existed in the original sample composed of randomly oriented intersecting chains of grains and that as density increased, the average number of grains in contact increased. He described this micro-structure as a porous, permeable

aggregate in which the grains might move into the large pore spaces as the structure is deformed thus increasing the density, i.e. grain rearrangement.

Arons and Colbeck (1995) analyzed the data of Yosida and others (1955) regarding observed characteristics of snow texture in relation to density. Arons and Colbeck made a generalization that the number of bonds (joints) per square millimetre decreased as the density increased over 30 days while the percent distribution of joint order (number of bonds per grain) remained nearly unchanged. However, for the increase of density from approximately 120 kg/m^3 to approximately 240 kg/m^3 the number of bonds is seen to increase by slightly more than 22% in their presentation of these data.

An increase in density can also be considered as a reduction of volume occupied by a given mass. Brown (1980) described a volumetric constitutive law based on neck growth between ice grains to account for pore space collapse in densities greater than 300 kg/m^3 . He illustrated a good fit with experimental data over the range of 100 to 600 kg/m^3 through stating that volumetric deformation in low-density snow is determined by inter-granular glide and inelastic deformation of grains and necks. This model has been used with success in the physical SNOWPACK model (Bartelt and Lehning, 2002).

Early descriptions called density the most significant index property of snow (Bader, 1962). Mellor (1964) called it a useful single property indicator with some correlation to grain packing, bond concentration, and structural characteristics. Mechanical and thermal properties significant to avalanche formation have been related partly or largely to snow density such as intrinsic permeability, thermal conductivity, diffusivity, (LaChapelle, 1961) and strength (Colbeck, 1991).

Generally, the hardness of snow increases as its density increases, though layers may exist adjacent to each other at nearly the same density but different hardness. Hardness is more closely related to strength than density. Strength is closely related to bond formation (McClung and Schaerer, 2006). Shapiro and others (1997) suggest this apparent relationship between density and mechanical properties seems to exist because both the mechanical properties and the density depend on the nature of the bonding/grain contacts. However there is no unit of hardness independent of the measurement device (Gubler, 1975). Thus, density measurements are basic to all calculations of force and stress, and therefore fundamental to most snowpack mechanical investigations.

In summary, though various theories exist on the true nature of densification, it is generally observed that grain shape and mass along with size and number of bonds per grain relate directly to the density of a sample. Multiple processes are occurring that result in increasing density depending on the location within the snowpack. Changes in any or each of these will influence the density of the sample, thus variations of each may be masked if one solely considers the density measurement of a snow sample.

2.2 Snow Profile Observations

Snow profiles are the record of observations made of the stratigraphy and characteristics of layers within the snowpack. They are made in various topographical locations depending on the type of decision their information is to support. Just as the structure of the snowcover is a snapshot of its chronological deposition and changes at a unique point in time, an individual snow profile is a record of observations made at of this structure at a unique location.

Paulke and Welzenbach both included detailed cross-sections of snow cover and cornice stratigraphy in their publications (Pielmeier and Schneebeli, 2003a). Seligman (1936) provided simple drawings of snow sections to convey the information in his discussions of strata and examples of dangerous vertical layer sequences. The importance placed on this visual communication of snowpack structure is evident in the historical progression of profile illustrations from 1939 (Bader et al., 1954), through their de facto adoption (USDA Forest Service, 1961), varying techniques for grain representation (Pielmeier and Schneebeli, 2003a), and establishment of drafting and symbology standards (Associate Committee on Geotechnical Research, 1982; Schaefer et al., 1954).

Observation and recording guidelines and standards for snow profiles have been established and adopted in North America (Canadian Avalanche Association, 2002; Greene et al., 2004). International standards for describing seasonal snow on the ground have been recognized (Colbeck et al., 1990) and are presently being revised by the International Union of Geodesy and Geophysics Commission for the Cryospheric Sciences (2005). These provide a uniform lexicon for communication both text and visually through drafting, notation, and symbology specification. Figures 38 to 46 in Appendix D provide examples. Additional work has been accomplished in Canada to establish electronic communication standards (Hägeli, 2005). Snow profile specific field books for recording and graphing the stratigraphy have been in existence since 1980 (Conger, 1980). Computer software has been developed to graph and store snow profile information (Kahrl, 2003; Kelly, 2005; Sims, 2005).

2.3 Avalanche Forecasting Context

Empirical understanding of avalanche formation in the 1800s by winter inhabitants of the western North American mountains is illustrated through narratives with reference to “snow slide weather” (Green, 1987) and the use of dynamite to initiate failure in “combs of snow” to shorten travel times into mines (Wells, 1964). Avalanche research and forecasting gained hold in the alpine countries of Europe during the later half of the 1800’s including published discussion of these topics. Seligman (1936) was the first to describe scientific investigation of the avalanche phenomenon in English. He drew from personal experience in the Alps and translation of earlier German publications. His was the primary source of knowledge in the North American snow community for decades (Atwater, 1968; Fraser, 1966).

Early alpinists alluded to the layered nature of the snow in accounts of glacier travel and exploration (Tyndal, 1861). In their broad review of the history of snow stratigraphy developments, Pielmeier and Schneebeli (2003a) attribute Swiss forester Coaz with first describing a relationship between snow cover stratigraphy and avalanche formation in 1881. Seligman (1936) quoting Zumstein and deSaussure ascribes Agassiz as having known about stratification even earlier in 1840. During the first four decades of the 1900s, Paulke pioneered detailed investigations and descriptions published in German of snow stratigraphy (Seligman, 1936).

Modern avalanche forecasting began during the 1930s simultaneously in the European Alps and the North American Wasatch Mountains with each location focusing on somewhat divergent paths. Engineers, mineralogists, and foresters began organized research with the survey of snow profiles and experimental investigations at Davos, Switzerland in a belief that the key to avalanche formation was knowing what layers develop into sliding surfaces (Niggli, 1954). U.S. Forest Service Snow rangers at

Alta, Utah began development of forecasting techniques with the belief that it was the “nature with which the snow fell” and focused on storm related observations (Atwater, 1968). The paths were not combined until some time later through describing the process of avalanche forecasting by Shoda (LaChapelle, 1980) and codifying forecasting with the description of the avalanche triangle: terrain, snowpack, weather (Fredston and Fesler, 1984).

LaChapelle (1980) concluded that the psychological process of forecasting originates in right-brain thinking. To the observer, the surface of the mantle of white snow covering a slope is all that is seen. This effectively hides the structure of the snowcover of which knowledge is key to understanding formation and activity of avalanches. It is unseen. From this, the assumption can be made that unseen information is visualized (imagined) in the brain to better understand it and unseen information is therefore better communicated in a visual medium; thus visual information about snow structure (snow profiles) plays a fundamental role in forecasting. McClung and Schaerer (2006) contribute that even though most of the process relies on inductive reasoning it also includes deductive reasoning that results from targeted education, physical laws, deterministic and probabilistic models.

2.4 Snow Profile Application to Avalanche Forecasting

LaChapelle (1980) described avalanche forecasting’s focus as interpreting uncertainties. He organized the information used for forecasting in three data classes according to their level of entropy relative to the amount of uncertainty associated with the information: Class I – low entropy, Class II – medium entropy, and Class III – high entropy. He placed stratigraphy (snow profiles) in the middle at medium entropy (Class II). The use of data classes in forecasting was advanced by McClung (1993). Recently, the use of snowpack factors is included as Class I information for positive test results revealing structure necessary for avalanching such as test shear quality (McClung and Schaerer, 2006).

Expert knowledge was codified through structured interviews that elicited an avalanche forecaster’s assignment of importance to snow profile information (McClung, 1995). This was a successful effort to verify and validate expert profile interpretation as a skill. The results were used in the development of an automated snow profile assistant that calculated a “certainty factor” for individual layers depending on the accumulated potential for the layer to play a role in future avalanching based in characteristics of layers throughout the observed snow profile.

Few attempts have been made to analyze the effectiveness of snow profile use in avalanche forecasting. During the San Juan Avalanche Project, four avalanche forecasters’ combined accuracy of whether natural avalanches were likely or artificially triggered avalanches were possible during a 24-hour period varied between 58% and 90%. In a summary of observations deemed significant by the four, only one (wind speed and direction) was unanimously chosen. However, study plot snow stratigraphy was chosen by three of the four as were old snow stability, new snow load and loading rate (LaChapelle, 1974).

In her Ph.D. dissertation, Ferguson (1984) concluded that an unstable slab structure could be identified from traditional snow profile observations and sufficiently quantified for numerical analysis. However, no single parameter in a snow profile could be identified with instability, but a linear combination of five parameters could explain 72% of the variance relating to instability.

In another test, 58 practising avalanche forecasters were presented with 35 graphical fracture-line snow profiles from Canada, U.S. A., and Switzerland. The actual bed surfaces were masked and subjects were requested to select where they believed a sliding surface could exist. Results suggested that snow profile interpretation is correlated to multiple years and location specific experience. Profiles with strong discontinuities at the bed surface were more often identified correctly than those with subtle instabilities (LaChapelle and Ferguson, 1980). This highlights the importance “profile shape” plays in the forecaster’s mind.

Profile shape was the focus in a study of fifty years of ramsonde profiles taken on April 1 on the Weissfluhjoch above Davos Switzerland combined with seasonal regional avalanche records. This resulted in the characterization between stable and “bad” profiles with six general profile patterns (de Quervain and Meister, 1986). Two of the six corresponded to “stable” years with the balance characterized on one end by spring full-depth avalanches and on the other to high and very severe avalanche seasons.

A specific example of snow profile use in avalanche forecasting was the construction of time profiles. The time profile was introduced in 1939 to visually summarize and compare individual observations over a season (Häfeli et al., 1954). The time profile is the history of the snowcover represented by a continuous line referencing the height above the ground of the snow surface and date specific snow pack information. Inserted at the appropriate date are vertical profiles of the snow temperature, density, and stratification as indicated by the ram penetrometer and visually identified layers (Figure 1). A time profile provides what LaChapelle (1961) described as the ability to inspect individual properties separately (e.g. density, crystallography, temperature) in their relation to snow layer evolution.

I am not aware of the inclusion of time profiles in the forecasting process by any operation, due I believe to the amount of time required to manually create and update them. As a substitution, such profile comparison is done solely through snow profiles in chronological order back to front on clipboards organized by location of information, e.g. drainage or avalanche path.

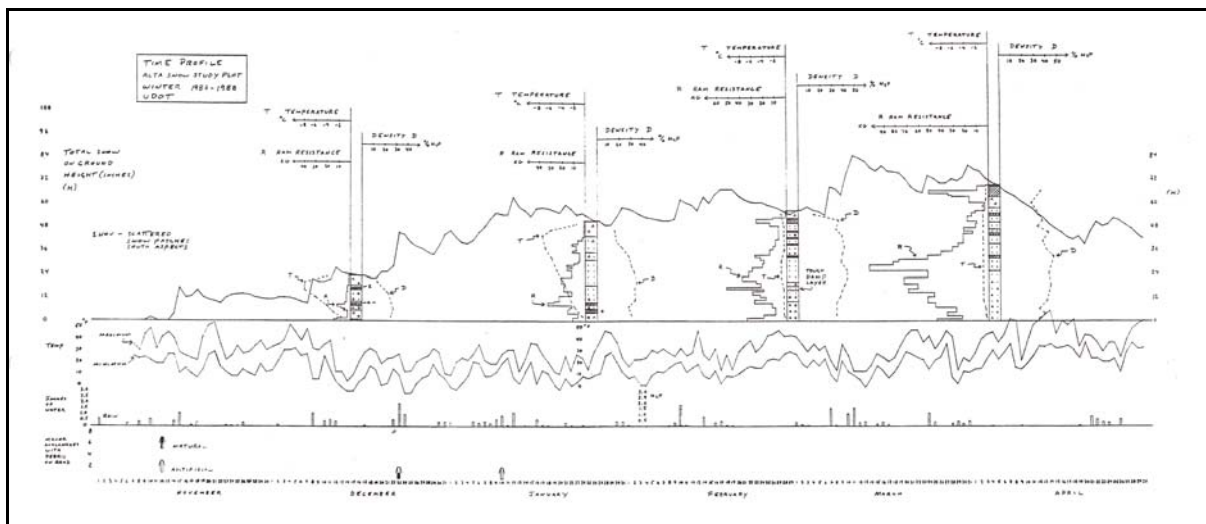


Figure 1. Example of a time profile following Häfeli’s description.

A graphic display of snow cover evolution model output provides a predicted time profile that is utilized in the current French CROCUS and Swiss SNOWPACK avalanche forecasting programs (Bartelt and Lehning, 2002; Brun et al., 1992; Durand et al., 1999; Lehning et al., 1998). This represents one of the fundamental benefits of the model and could represent a return to wider use of time profiles.

Modifications to the original time profile concept included the addition of meteorological and avalanche occurrence observations and development of a storm plot (Atwater and Koziol, 1952). The graphical combination of contributing factors and occurrences assisted in developing rules of thumb for avalanche path specific forecasts. The automatic computer graphing of weather and snowfall measurements from automated weather stations has replaced the storm plot for many avalanche-forecasting operations in monitoring “the nature in which the snow falls” (Hägeli and Atkins, 2002; Tremper, 1992).

2.5 Snow Profile Probes

The holy grail of snow profile observation has been described as the development of non-destructive testing techniques for describing the three-dimensional extent of layers while providing some information about their density and grain size (Colbeck, 1991). The concept of probing the snow to gather information about its hidden stratigraphy is not new. In 1936, Seligman described a sounding practice he said was “strongly urged” in Zdarsky’s 1929 writing: *Beiträge zur Lawinekunde*. Seligman stated, “If the sounding stick pushes straight down into the snow with great ease, the internal cohesion of the snow particles is very low either through newness, extreme cold, or wetness.” He described his sonde as a double pointed ski pole, which when the grip is removed exposed a second sharp point.

The rammsonde¹, a cone penetrometer, was also introduced in 1936 as a simple test to assess the relative strength of layers without digging a profile (Häfeli, 1954). A sectional shaft of metal tube with a 60-degree conical tip that is slightly larger than the shaft diameter is successively driven through the snowpack by the weight of the instrument and the impact of a known weight dropped from a measured height. Knowing the drop height, the weights, and the vertical change in cone tip depth, a ram resistance number is calculated representing penetration resistance in kilograms, which when graphed as a profile provides a representation of the snowpack stratigraphy. The ram profile is not completely quantitative as a measurement or in physical interpretation though it is reproducible and provides an instructive picture of the mechanical state (de Quervain and Meister, 1986). The ram continues to be used. A handful of avalanche forecasting operations gather monthly or more regular ram profiles from snow study plots and other snow profile observation sites. Procedures are described in observation standard publications (Canadian Avalanche Association, 2002; Greene et al., 2004)

The Cooperative Avalanche Research Laboratory at Montana State University developed the portable snow resistograph to give a generalized strength or cohesiveness profile that possessed a relationship to load. It was designed to be swift and simple thus allowing widespread sampling of the snowpack (Bradley, 1965). It operated in the opposite vertical direction as the ram. The resistograph was pushed to the bottom of the snowpack and rotated 90 degrees allowing horizontal blades on the end to position in undisturbed snow before being withdrawn. An ingenious paper roll recording device integrated

¹ Often referred to using the interchangeable terms; rammsonde, ram, and ram penetrometer.

to the instrument scribed a profile as it was withdrawn. It operates on the assumption that the resistance is approximately equal to the breaking strength of the snow measured in grams per centimetre squared. It performed at a quicker pace (approximately 10 cm/sec) than an equal depth ram test. Bradley was not able to make any firm conclusions at the time of the original publication. Disadvantages included operator sensitivity, a considerable learning curve, weight (3 kg) and cost; the latter two prevented its acceptance as a field instrument (Brown and Birkeland, 1990).

Though not a probe in the sense described thus far, a nuclear isotope snow-profiling gauge was developed during the mid 1960s that warrants inclusion here. Four gauges were deployed throughout the western United States. The gauge consisted of two parallel vertical tubes; one containing a radioactive source the other a sensor. The source and the sensor were automatically lifted in unison by cables up the tubes sampling the snowcover in 1.27 cm increments at a rate of 9.5 cm / minute when activated. When the gauge was not in use, the source and sensor were stored below ground in a lead shielded portion of the tube. The system was controlled by and data were transmitted via phone line to a base station computer. Cost of the system was placed at US\$8,000 to \$10,000 with the computer base station at US\$6,000 to \$9,000 (1972 dollars, unadjusted) (Randolph et al., 1972).

One gauge was deployed at Red Mountain, Colorado and evaluated as part of the San Juan Avalanche Project. The standard deviation was calculated between manual and profiling gauge density values at 5 cm intervals on seven days during the winter 1971-72. The deviations ranged from 9 to 17 kg/m³ and were used to calibrate the profiler during the remainder of the project. Comparisons were made between the gauge profile and ram profiles, and the gauge's ability to illustrate the development of structurally weak depth hoar was described (Armstrong, 1976). The nuclear profiling gauge has not been used since the San Juan Avalanche Project.

A similar, portable device utilized a standard Mount Rose snow water equivalent sampler in which a radioactive source and sensor were lowered once the core had been taken, removed from the tube, and the tube replaced in the vacated sampling shaft. It used a backscatter measurement from a 5 cm thick, 60 cm "doughnut" of snow outside the tube to estimate densities (Young, 1976). No record of this device's further use or deployment was located.

A novel device was developed that allowed the extraction of a 15.6 cm thick, 35.8 cm wide, and 123.5 cm tall snow section as a more efficient option than the bonfire or dye method of highlighting stratigraphy for profile analysis (Harrison, 1982). Other than its original use in studies of snow failure under compaction, the device has not seen further use.

Though not a "profiling" probe, the Finnish Snow-fork was introduced in 1986 (Sihvola and Tiuri, 1986) and subsequently improved (Kendra et al., 1994). This dielectric probe was designed to measure density and wetness of the snow once the stratigraphy is exposed through excavation. It is currently commercially available (Tokka Oy, 2005).

A prototype digital resistograph was developed by Tim Dowd and Bob Brown at Montana State University to allow rapid, repeated sampling and provide strength profiles comparable to the ram penetrometer that could be digitally stored and graphically presented in the field at the time of sampling (Dowd, 1984). Simultaneously, the use of frequency modulated continuous wave radar to return snow

profiles was being explored in Europe (Gubler and Hiller, 1984). Other than this reference and another (Ellerbruch and Boyne, 1980) to the beginnings of work relating to snow water equivalence, profiling using radar is not discussed here.

The digital resistograph was improved in 1988. The previous problems associated with the digital resistograph included a low data storage volume of 25 profiles. In the improved version, the instantaneous plotting function was dropped and the profile storage was improved using EPROM modules capturing 150 profiles at a time, which could be changed in the field. The original digital resistograph had shown that the readings were not significantly affected by the insertion rate. Study of the improved resistograph indicated that index values of three profiles when averaged over the length of the profile presented a standard deviation that was 6% of the mean value. This was compared to a larger, similarly calculated deviation for adjacent ram profiles that was 10.3% of the average ram value. However, their overall conclusion was that the digital resistograph was equal in performance to the ram with similar correlation between averaged profiles. The improved version was used by Birkeland (1995) in his spatial study of average resistance normalized for depth over a uniform avalanche slope. Both the digital resistograph and ram require an experienced operator (Brown and Birkeland, 1990).

A prototype fibre optic probe to determine snow layering was introduced in 1991 and advanced during the following years to include multiple sensors measuring optical, mechanical, and electrical properties. The digital snow sonde weighed 20 kg and was designed to provide identification of coarse or fine snow by reflectivity, soft or hard penetration force by load cell, and wet or dry snow through AC conductivity over a vertical depth up to 1.2 meters. One test each in the cold room of a dry snow block and a wet snow block illustrated signal responses relative to two layers in each block (Abe et al., 1998).

Two other probes were introduced in 1998, the SnowMicroPen (Schneebeli and Johnson, 1998; Schneebeli et al., 1998) and the Capacitec probe (Louge et al., 1998a; Louge et al., 1998b). The SnowMicroPen (SMP) is a penetrometer with a relatively small (5 mm) diameter conical tip that is motor driven through the snowpack at 6 to 20 mm / sec. The cone is the rammsonde standard 60-degrees and the force signal is measured every 0.004 mm. A textural index consisting of a ratio of the mean grain size divided by the density of the snow was found to have a significant correlation to the force signal (Pielmeier et al., 2001). Investigations of the signal response as thin layer boundaries are crossed by the tip have enabled identification of individual layers (Kronholm, 2004). Technical problems that have rendered 50% of profiles unusable for analysis affect the SMP's reliability in recent studies (Kronholm, 2004).

The Capacitec probe is a hand pushed sonde that measures electrical properties (capacitance) of the snow to create a density profile. It was designed, it's concept feasibility established, and an industry needs assessment accomplished under a U.S. Army research grant (Louge et al., 2002). This probe is described further in the instrumentation section of the methods chapter.

The Himachal Safety Systems SABRE penetrometer was introduced in 2002. It is an electronic, lightweight, and portable penetrometer based on a tip located force sensor and accelerometer (Mackenzie and Payten, 2002). The accelerometer signal was shown to visually compare well between

two plunges. One example was shown of its similarity to a standard hand hardness test. This probe is currently undergoing modification and evaluation (Floyer and Jamieson, 2006).

The comparison of the resistograph to the rammsonde described earlier was one of three studies contrasting performance of probes to other methods for snow profiles. Pielmeier and Schneebeli (2003b) compared hardness profiles measured by hand hardness, rammsonde, and SnowMicroPen against surface section images. They found that the SMP profile captured the stratigraphic features identified in the surface sections nearly completely. Hand hardness profiles captured 80 % and ram hardness profiles only 60 % of the features. They cautioned in their conclusion that “classical stratigraphic methods should be applied with great care to quantitative comparisons”.

Harper and Bradford (2003) investigated the spatial variability of stratification processes, especially densification, in the accumulation zone of an Alaskan glacier using multiple methods. During a three-day period, a 20 meter by 20 meter area was explored using the Finnish Snow-fork, classic snow profiles, ground-penetrating radar, and back-illuminated columns. They found “good” agreement between density profiles with a range of 100 to 350 kg/m³ taken by the three methods but varying levels of detail. Classic profiling revealed 5 to 8 layers in the upper 2 meters of the snowpack. Dielectric measurements taken at discrete 5 cm vertical intervals revealed at least twice as many layers as did the radar. Analysis of the backlit column identified two orders of magnitude more.

2.6 Dielectric properties and snow

The previous section contained the research and development of various probes and technologies that have been introduced to gather snow profiles. The Capacitec probe is the topic of this study. This section includes an overview of the electrical properties utilized by the probe and a history of their snow research use.

A material’s permittivity (ϵ) is a physical property (Equation 1). It is it’s a measurement of the materials ability to store electrical potential energy (D coulombs / m²) when exposed to an electrical field (E volts / m) (Coelho, 1979). The permittivity of vacuum is approximately 8.854×10^{-12} farads per meter (F/m) and known as the electric constant.

$$\epsilon = \frac{D}{E} \quad (1)$$

A material through which the energy required to establish an electrical field can be recovered in whole or part is described as being dielectric. Its permittivity is given relative to that of vacuum and known as the materials dielectric constant. Capacitance is a property of a system of conductors and dielectric material that permits storage of an electrostatic charge.

Cole and Cole called the behaviour of permittivity “absorption conductivity” and described as the complex dielectric constant (ϵ^*) fitting the dimensionless equation:

$$\epsilon^* = \epsilon' - i\epsilon'' \quad (2)$$

Where ϵ' is the dielectric constant, the real component
 ϵ'' is the loss factor, the imaginary component

$$i = \sqrt{-1}$$

The real component describes the electrical field that is recovered once “the poles are reversed. The loss factor describes the portion that is not recovered (disbursed) and lost to the generation of heat.

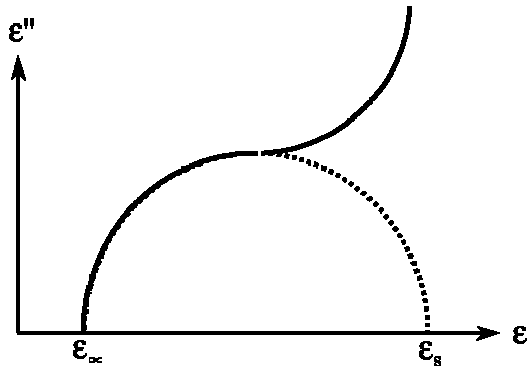


Figure 2. Cole - Cole plot (Argand diagram) of the relationship between real and imaginary components of the complex dielectric constant through frequencies from the static dielectric constant to the optical dielectric constant.

Ice was investigated as a dielectric material with the first experimentation on the frequency dependence of the dielectric properties of ice attributed to J. Errera in 1924 (Auty and Cole, 1952; Kuroiwa, 1962). A graphic representation known as the Cole-Cole plot of the Debye relation (Equation 3) allows estimation of values over a full range of frequencies. The Cole-Cole plot is semi-circular for ideal conditions (dashed curve in Figure 2). However, actual measurements of snow (solid line in Figure 2) do not follow the curve in the lower frequencies near the static dielectric constant due to imperfections and impurities (Yosida et al., 1958). This shape is also described as representative of a double layer capacitor (Coelho, 1979).

Variations in dielectric constant measurements were attributed to voids and impurities in ice samples by Auty and Cole (1952) who through careful experimentation were able to describe dielectric dispersion using the Debye relation:

$$\epsilon^*(\omega) = \epsilon_{\infty} + \frac{\epsilon_s - \epsilon_{\infty}}{1 + i\omega\tau} \quad (3)$$

- Where
- ω is the angular frequency
 - τ is the relaxation time
 - ϵ_{∞} is the optical dielectric constant
 - ϵ_s is the static dielectric constant

Cumming (1952) investigated radar echoes from snow-covered terrain and microwave energy attenuation by snowstorms. He studied the permittivity and loss tangent (ϵ'/ϵ'') of snow and ice at a frequency of 9.375 GHz. He attempted to make his samples of cut snow blocks as homogeneous as possible and found no relation between crystal structure and the dielectric loss tangent. Though his frequency was outside the focus of this study, it is important to note that he attached no significance to one or two cases where the loss tangent appeared to have a permanent increase following warming the

sample to 0°C and chilling it to an unmentioned lower temperature. This suggests a possible change from the ice grains responding dielectrically individually to a condition with little or no distinction between grains or bonds and effectively responding as a large ice mass rather than a lattice.

Ambach's 1958 German publication is one of the first descriptions of the relationship between the capacitance of snow and its water equivalent content (Evans, 1965).

A number of experiments were done by the Institute of Low Temperature Science exploring the dielectric properties of snow and ice at frequencies from 0.5 KHz to 1,000 KHz (Yosida et al., 1958). Their discussion begins with the statement that snow always contains impurities making matters regarding snow's dielectrics a hopeless issue; however, I assume for the purpose of this in-situ study that impurities are homogenous within the layer of their deposition and may accentuate layer definition. They demonstrated that impurities resulted in effects on the dielectric constant (real) and loss factor (imaginary) and that by extrapolating a "pure snow" the Debye relation remained valid.

Tests were conducted on non-compacted snow samples placed in an ebonite container with electrodes inserted vertically into the snow. A fundamentally important conclusion relative to this study was that snow's influence on ϵ' is more evident at low alternating current (A.C.) frequencies. This supports the notion that the amplifier frequency of the Capacitac probe at 3.9 KHz may be better suited to suggest grain or structure differences than those at higher frequencies.

Yosida and others (1958) also concluded that the snow density and the dielectric values were not the same unless the ice structure of the snow was the same. They proposed use of Wiener's *formzahl* (u) formula (Equation 4) for a two component dielectric mixture to characterize the structural relationship of grains in the snowpack. Additionally, they estimated appropriate limits to the range of ϵ' values for the same snow densities. The formzahl is a strong conceptual link between theory and actual geometry. However, it must be correlated to known structure before its value has a physical meaning (Arons and Colbeck, 1995).

$$\frac{\epsilon_s - 1}{\epsilon_s + u} = q \left(\frac{\epsilon_i - 1}{\epsilon_i + u} \right) + (1 + q) \left(\frac{\epsilon_a - 1}{\epsilon_a + u} \right) \quad (4)$$

where: ϵ_s is the dielectric constant of snow

ϵ_i is the dielectric constant of ice (3.15 (Cumming, 1952))

ϵ_a is the dielectric constant of air (1 (Yosida et al., 1958))

$q = \frac{\rho_s}{\rho_i}$ is the sample density of snow / density of ice

The multiple frequency investigation of snow was continued by Kuroiwa (1962) exploring the change in dielectric properties resulting from freezing wet snow and ageing granular or compact snow. He sampled natural snow, cut in blocks, and placed between electrodes to form the condenser. His experimental data had a better fit to formzahl limits $10 < u < 25$ than Yosida and others (1958). Notable is his exploration of changes in the dielectric constant and loss factor due to ice grain bonding. Compact

snow was disaggregated and packed in a condenser (capacitor). Measurements were taken over the range of 0.5 kHz to 1,000 kHz for a series of days at 0, 16, 40, 70, 113, and 143 hours. The real component increased from near 12 to near 26 over this period. He concluded a calculated increase in the formzahl from 20.9 to 263 as evidence of progressive growth of ice bonds between grains, the sample and the electrodes. The higher value is the first mention of a formzahl in such a range.

Denoth (1982) described control of the dielectric constant and loss tangent at frequencies less than 100 MHz by idealized grain or cluster shape. He used porosity based on known density and liquid water content as his response variable. He argued that use of shape was more suitable for wet snow as opposed to dry snow and suggested it as a method of classification in lieu of sieving or visual observation. He could attribute no significance to grain size. This marked a time when concentration on snow dielectrics shifted to wet snow, liquid water content and density related to melt and wet snow. A second focus on higher frequencies related to remote sensing.

Little work has been done regarding the dielectric properties of dry snow since Kuroiwa (1962), Yosida and others (1958). Only recently, have Takei and Maeno (2003) studied the dielectric properties of snow near the melting point. They concluded that above -0.6 °C the mechanical properties of the snow samples related to the properties of the boundary rather than the ice substrate.

2.7 Relevance

Shapiro and others (1997) recommended investigating dielectric measurement as an index property for tests designed to be sensitive to the snowpack microstructure in their review of snow mechanics and effort to encourage the expanded use of snow mechanics in applied problems. The Capacitec probe non-destructively measures the dielectric properties of a small volume of snow that represents several grains, their respective microstructure and bonding.

The volume of measurement is 3 mm vertically and extends 13 mm into the snow pack from the face of the sensors. The extent, spacing, and support of this measurement should be adequate to sample thin layers for in their dielectric properties. A relationship has been described between the dielectric measurements of snow versus those of air resulting in values associated with the volume of ice in the sample (Kuroiwa, 1962; Louge et al., 2002; Yosida et al., 1958). Based on this, it should be possible to model an in-situ relationship between the probe dielectric measurements and manually measured density at a fine scale near the resolution provided by the spacing and support of the probe measurements.

Snow profile shape relative to hardness determined from continuous vertical probe measurements of snow structure have been shown to contribute Class II avalanche forecasting information (de Quervain and Meister, 1986; Schweizer et al., 1998). The demonstrated dielectric measurement and density relationship combined with the apparent relationship between density and mechanical properties should be sufficient to utilize a snow density profile from information gathered by a validated Capacitec probe.

An additional benefit may result through detailed investigation of the Capacitec probe; it is has been suggested that heat conduction, electrical, and mechanical properties of the ice lattice of the snow cover strongly depend on the bonds and must be related to the same geometrical properties (Arons and Colbeck, 1995). The frequency at which the probe excites the ice lattice to make a measurement has

been shown to be influenced by the structure within which the field is being generated (Cumming, 1952; Takei and Maeno, 2003; Yosida et al., 1958). If an index of geometry such as formzahl can be successfully correlated to observed structure using the probe measurements, snow profiles observed through use of the probe might provide highly useful information in avalanche forecasting.

Chapter 3 METHODS

This chapter contains the setting, data collection, sources of error, and data processing used for this inquiry and analysis. The research methods described in this section, though unique to the specifics of snow cover investigation of avalanche formation, reflect fundamental field methods utilized in physical geography (Jones, 1968).

3.1 Research Setting

3.1.1 Location and Climate

Field work was conducted during the months of January, February, March, and early April of 2005 and 2006; in the Selkirk Mountains near Rogers Pass between the towns of Golden and Revelstoke in southern British Columbia, Canada (Figure 3).

During both field seasons, the bulk of field data collection for this study was done in a large, flat area directly adjacent to the study plot at the Mount Fidelity Observatory. The Avalanche Control Section of Parks Canada Glacier National Park maintains the Observatory site at 1905 meters above sea level as part of their avalanche forecasting and control program for the Park and this segment of the Trans-Canada Highway (Schleiss, 1990). Snow and weather measurements have been recorded at this upper-elevation observation and research site since 1966 and the site has been the location of numerous avalanche related studies.

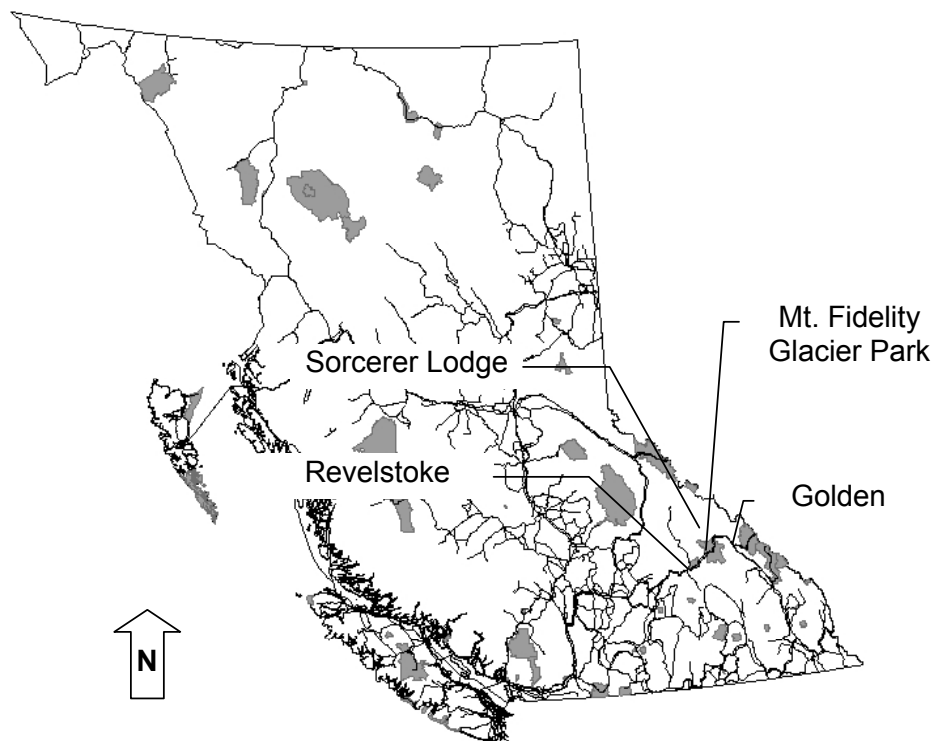


Figure 3. Location of research sites on British Columbia map (Parks highlighted in grey).

The Selkirk Mountains are one of four individual ranges that make up the Columbia Mountains located in the southeast interior of British Columbia; bordered on the west by the interior plateau and on

the east by the Rocky Mountain Trench (Robinson, 1987). The portion of the Trans Canada Highway between Revelstoke and Golden traverses the lowest route between the Sir Donald and Hermit Ranges of the Selkirk Mountains at Rogers Pass located in Glacier National Park. The Selkirk Mountains lie in the “Interior Wet Belt” (British Columbia Natural Resources Conference, 1956) second only to the Vancouver Island and Coastal Mountains in annual precipitation. Interestingly, Hægeli and McClung (2003) classify Mount Fidelity in the maritime snow climate based on Mock and Birkeland’s snow climate scheme (2000) while the remainder of the Columbia’s are placed in the Transitional snow climate. Mock and Birkeland’s scheme uses the criteria of >80 mm average rain to classify maritime, and Mount Fidelity is very near to the threshold (82 mm average). Hægeli and McClung rightfully question the validity of this scheme since it misses the critical beginning month of November. Regardless, the Mount Fidelity location does exhibit traits characteristic of being on the up slope side of the pass. Reflecting this, the snow climate of the area is subdivided by local experts into the milder temperatures - heavy snowfall western zone, colder – lighter snowfall eastern zone, and the summit of Rogers Pass where both sub-zones mix creating unstable weather (Schleiss, 1990). The observed weather conditions for the period of the study are presented in Appendix A.

3.1.2 First Field Season

The first field season (2004 – 2005) was plagued by confounding weather and equipment difficulties. At the onset of the first field season, initial field procedure and equipment operation techniques were practiced during the second week of January 2005. Towards the end of January, a severe storm with heavy rain to unusually high elevations moved through the entire province. This created a hard and thick crust that delayed fieldwork until mid-February. A relatively dry and clear period occurred during much of February with shallow accumulation (~1m) over the impenetrable January storm layer. A period of unseasonably warm air temperatures during later February and early March created moist and wet snow surface conditions. This effectively limited the probes ability by introducing a layer of moisture to the sensor surface and rendering measurements out of range. This provided an opportunity to explore various methods for layout spatial sampling both in flat terrain and across slopes. Use of a high accuracy (sub centimetre) Global Positioning System to survey sampling positions was investigated. The high latitude, steep incline, and generally north facing aspect characteristic of the selected avalanche slopes made it difficult to obtain adequate satellite constellations required to achieve the desired (i.e. low) location measurement uncertainties. These problems rendered this method of surveying inadequate for spatial studies of selected slopes similar to avalanche start zones. Manual methods using rod and chain with an inclinometer proved satisfactory.

A second-generation prototype probe and encoder base was delivered by Capacitec in mid-March, 2005. Near average weather had returned but the snowcover was quickly losing the stratigraphy and variation characteristic of dry snow. Two data collection platforms accompanied the newer probe and base. The first was a tablet pc running a Labview® based program that quickly proved inadequate due to programming bugs. The second was a newer version of a palm held device and analog to digital (A-D) converter. The palm held system allowed a maximum sample-recording rate of 40 Hz rather than the earlier 5 Hz. Data were recorded to allow comparison of the two probes and a handful of data collection

days were undertaken with the second generation probe and palm held device before field work ended the first week of April. The new probe and palm device generally operated as desired, providing the necessary information to plan data collection with it the following season.

3.1.3 Second Field Season

Careful analyses of the second-generation probe vertical travel, encoder roller movement, and signal output was undertaken at the onset of the second field season in order to isolate measurement errors uncovered during the first field season. Another important change was the switch to an accurate electronic scale for sample weighing rather than the density cutter provided scale. Two supporting investigations, that are described later, were undertaken in the field before data collection with the probe.

Mid way through the second field season and following a multi-day series at Fidelity Observatory, two sets of field day data were gathered approximately 25 kilometres due north in the Selkirk for comparison of findings from the primary research site. These two sets were collected at a remote backcountry location near Sorcerer Lodge. One set just below tree line near the lodge's weather observation plot. The second set from a flat open area in the alpine, chosen for its exposure to winds and likely stratigraphy.

Additional data sets were gathered during March and early April 2006 for further investigation of grain type, instability tests, and their relationship to the probe measurements. These data were collected at the Mount Fidelity study plot area.

3.2 Data Collection

Data collection is the process of capturing raw or primary data from a single source or from multiple sources. Measurements and observations were made and recorded manually as well as electronically during this study. This section contains a discussion of instrumentation, methods, sources of measurement error, and experimental design.

3.2.1 Instrumentation

This study focused on the use and validation of a specific snow measurement instrument, a capacitance probe manufactured by Capacitec Incorporated located in Ayer, Massachusetts. Several components make up the probe. The primary elements are the capacitance sensors located in a chisel-shaped tip that is fit to the end of a lance-like probe. Electrical wiring connects the sensors to an electronic "rack" enclosure containing circuit boards to process the various signals from the components and pass them on to the data collection platform. The rack weight is 3.5 kg and is carried in a backpack. Connected to the rack by wiring is a depth encoder base (2.3 kg) that tracks the vertical movement of the probe shaft. Signal recording was accomplished with an analog to digital (A-D) converter attached to a personal data assistant (PDA) and connected by wires to the rack. Power is supplied by DC batteries in the rack, A-D converter, and PDA.

Louge and others (2002) provide an explanation of the physics and conceptual description of the electronics associated to the measurements made by the probe. Three electrodes make up the measurement surfaces: sensor, ground, and guard. The electronics measure the impedance Z (ohms) between the sensor and ground while a buffer amplifier maintains the guard at the same sinusoidal

voltage as the sensor (current I / impedance Z). The output is the rectified guard voltage (V_g) that is kept proportional to the sensor voltage and is related to the capacitance (C) between the ground and sensor surfaces through an empirical relationship. The amplitude of the sensor current is kept constant by controlling the voltage (V_r) across a reference impedance. The electronics exploit the phase lag between V_r and V_g to approximate a relationship between the real (Y') and imaginary (Y'') components of the sample's complex dielectric constant.

Laboratory calibration of the probe provides empirical equations that allow the extraction of the real and imaginary parts of the complex dielectric constant of the sample (Y^*). The electronics then output voltages over a specific range. The output channel 1 voltage (X) is proportional to the real component and the output channel 2 voltage (Y) is proportional to the imaginary component.

Use of the early prototype of the probe (season 1) was plagued with difficulties. It was a two-piece, 2.5-meter lance designed to be driven into the snow in a hammer-drop fashion like the ram penetrometer. Early on, it was discovered that the probe did not require hammering and could easily penetrate the dry snow by smooth, hand over hand, pushing. Snowpack conditions included a very solid, rain soaked and frozen old snow surface formed in January 2005 on all aspects and elevations near the research site. This substrate, still close to the surface in early February, effectively stopped deeper penetration. The buried rain crust and the soft, compressible new surface snow resulted in an immediate change of technique from that originally described for the probe. The encoder base was rigged to a pair of skis allowing it to be moved across the snow surface avoiding disturbance and compression in the area under the encoder that altered the snow and vertical reference point. The hammer, heaviness of the lance itself and its length made smooth vertical movement through the relatively shallow (less than 1 meter) snowpack difficult and visibly caused lateral movement to the probe's axis at the lance tip. The hammer was removed and only the lower section of the probe was used. It was observed that the constant cylindrical shape of the probe body laterally stabilized the penetration axis once that point along the probe's length was 10 to 15 centimetres into the snowpack.

During the preliminary evaluation of the first probe, a visually identified, thin (1 cm) and clearly separate layer was not reflected in the probe measurement values. This led to consultation with the probe manufacturer in order to achieve greater sensitivity for the probe. Different amplifier gain settings were tested until one was found that maintained continuity within the measurement range for all types of available snow as well as showing discernable differences between similar, soft layers. However, continued difficulty was experienced during the first field season in resolving an adequate number of samples vertically ensuring measurement relatively close and above, within, and relatively close and below thin layers (≤ 1 cm). This was due to the data collection device's recording rate upper limit of 5 Hz. The lack of an adequate combination of measurement support and spacing along with a lack of variable continuity, amplifier calibration changes, and near daily system troubleshooting rendered the data set inappropriate for any conclusive analysis.

A second-generation probe was received late in the first field season. Its design made it easier to transport and use. The sensors were located in a chisel-shaped, stainless steel tip fit to the end of a modified collapsible avalanche probe (upper left, Figure 4). The depth encoder incorporated four legs

allowing it to sit above the snow surface without influencing the area to be sampled along with easy view of the probe tip as it approached and penetrated the surface. This also made it easy for repositioning without sinking into the snow (Figure 4). Signal recording continued to be performed with an A-D converter attached to a PDA. The new configuration consisted of a Palm® Tungsten T3 handheld computer with a Datastick® Systems DAS-1245 data collection module with four single-ended analog inputs. Datastick Connection™ 3.5 software was run on the T3 to monitor and record measurements in real time and store them in Palm OS™ databases on the Palm handheld. The DAS-1245 was powered by an external rechargeable battery (Datastick p/n:MH-DPB180M). The T3 relied on its internal rechargeable battery. Neither power source presented problems during fieldwork and battery use of 1 to 3 hours; however, screen visibility was often an issue due to cold air temperatures, sunlight, or water droplets from melting snow. Various weatherproof enclosures were tried without success. They became too stiff in the cold to allow the necessary screen tapping that controls Palm® operations.



Figure 4. Illustration of second-generation probe following a full depth plunge, encoder, and backpack containing electronics. Upper right insert shows the PDA and A-D device, upper left insert shows the probe tip and collapsed avalanche probe shaft.

Unlike the earlier setup, the new data acquisition device was unable to read negative voltages. The second-generation probe system was modified by Capacitec between field seasons with the addition of an adjustable offset for the Y channel of the probe responsible for the voltage signal associated to the

imaginary dielectric component. Additionally, the probe and amplifier were calibrated to capacitance and impedance in air at the optimal gain settings determined during the previous season.

3.2.2 Classic Manual Observations

Observation and recording standards outlined by the Canadian Avalanche Association (2002) were adhered to in making manual observations except where finer resolution or additional clarity of records was required. The exceptions included sampling spacing of snow pack temperatures, densities, and inclusion of a standardized method of using a brush to identify layering. Snow grain notations included non-standard terms that are described in Appendix B. The shaft of the probe was marked with an adhesive centimetre rule tape and left in place following plunges to be used for manual measurement of layer boundary positions. Snow temperatures were taken at 5 cm vertical spacing using one thermometer to avoid disparate measurements due to slight calibration differences. Temperatures were measured with a widely available digital thermometer that is commonly used for snow profile observations (Thermor Ltd. model PS100) The packaging that accompanies this rugged, waterproof thermometer describes an accuracy of $\pm 2.2^{\circ}\text{C}$. This is no doubt a printing error since a review of scientific instrument firms selling this model provided the specification of $\pm 0.56^{\circ}\text{C}$ for the range -17.8 to $+110^{\circ}\text{C}$. One thermometer was used and was calibrated to zero in ice-water slurry once a week. Snow densities were taken in nearly continuous vertical sampling with the top of one sample as close to the location of the bottom of the previous as possible.

3.3 Sources of Error

3.3.1 Instrumentation

Potential sources of measurement error or bias were identified. They included effects of the probe on the snow, instrument system performance, observation skill and technique.

Effects of the probe to the snow it was penetrating were investigated using the bonfire method (Nakaya et al., 1936) of highlighting grain textures. This technique involves igniting a shallow, flat pan of kerosene at the base of the pit wall. Soot from the flames is fanned towards the wall. The soot adheres to the exposed pit wall in a manner that visually highlights grain size and bonding. The design of the probe tip is chisel-like with the sensor on the flat front to create little disturbance of the snow density while the back is cut at an angle of ten degrees. Several shallow plunges were made along a line that allowed for a section view of half the cavity created once the probe was removed and a pit excavated. There were changes visible in the grain texture with a 10-power hand lens along the wall of the cavity where the snow had been displaced by the shaft but not in the region where only the chisel tip had been.

Investigation of the relative “zone of influence” was accomplished by observing the measurement values from a vertically stabilized probe with the sensor tip 15 cm below the surface. Foot penetration and compression of the snow to a depth of 20 to 25 cm along a line directly approaching the sensor face up to a location 5 cm away from the probe revealed no change in the signal. This was taken as an empirically acceptable minimum lateral limit between plunges.

The encoder base used a USDigital Corporation #H1-360-HS ball-bearing, optical, and incremental shaft encoder (a sensor of mechanical motion) to track the rotation of the probe guide wheel

and measure the vertical distance traveled by the probe. It is unknown whether the systematic errors described here were unique to this application or attributable to the products involved. The error was reproducible and highly predictable, allowing its influence to be isolated.

The encoder generated a voltage relative to one-degree rotation increments. The voltage was progressive until it rolled over at a maximum value near 5.0 VDC at about the first third of the 11th rotation. The voltage was converted to a “wheel” count by the data acquisition module and software. Each count ostensibly represented 0.057 cm travel of the probe. However, a rounding error occurred in a saw tooth pattern and altered the measurement scale. Additionally, the encoder generated a random negative voltage value at its reset to zero and associated value of 38 for the wheel count. This occurred again when the count rolled over at a value of 3360. A non-elegant but satisfactory solution was arrived at through diligent experimentation to match recorded wheel count with an accurate distance values. My confidence is high that the probe measurements are accurate ± 0.1 cm relative to the wheel count locations except in the cases where profile measurement is shallower than 2.2 cm or deeper than 191.2 cm from the surface. The error induced at the wheel count rollover was not resolved to a level of comfort for making analysis and conclusions for deeper layers.

A random measurement error was observed in the raw data. It is unknown which component of the system was responsible for this reproducible artifact. It was evident when the sensors were maintained in a stable environment, (i.e. stationary in either air or snow). With no associated movement of the encoder wheel, the recorded wheel count fluctuated plus or minus one or two counts (± 0.057 cm to 0.114 cm). Statistical review of this observed change in counts for the stationary wheel suggested a normal distribution. The assumption was made it represented random noise. Only the values associated with negative wheel count changes were cleaned during the data manipulation described in a later section. This suggests an error associated with the vertical location of a probe measurement to manual measurements of approximately ± 0.1 cm with a slight bias toward +0.1 cm.

Another error associated with the vertical location of a probe measurement to manual measurements resulted from operator technique. When the wheel counter was reset upon the probe tip touching the surface, it was difficult to visually determine the precise location of the tip from the position of the operator. The tip was always at or slightly under the surface. The sensors are located 0.9 cm from the tip. Visual inspection of the probe voltages when preparing the data for analysis suggested an identifiable difference between the last air and first snow measurements. Half this distance was assumed to be the surface, adjustment of the wheel counter reset position to this assumed snow surface position equalled the 0.9 cm offset of the sensors from the probe tip in the majority of instances. The largest variance was 0.5 cm.

I assume a vertical accuracy of probe measurements are ± 0.7 cm for this study based on the combination of these three error sources associated with the location of a probe measurement to manual measurements.

3.3.2 Observation Skill and Technique

Ferguson (1984) estimated the accuracy of observations to describe measurement errors associated with classic snow profile including thickness, hardness, grain type, size, layer density, and

temperature. These estimations were necessary since she coded each value numerically for analysis. Her examples of error causes remain valid in considering measurements taken by unknown observers. These examples include:

- Measuring layer depths along a line other than vertical,
- Varying hand hardness penetration force or instrument (gloved versus un-gloved),
- Unfamiliarity with grain types or unable to see shapes,
- Not disaggregating or not distinguishing between grain size range or mean size,
- Compressing or disturbing density sample upon extraction,
- Not allowing thermometers to equilibrate with environment.

These issues were avoided in my study since all manual measurements were taken by a single skilled observer. Sources of error in manual density measurement are discussed in the manual density measurement current practice section.

3.4 Experimental Design

Experimental design draws upon all the topics of the methods chapter. This section contains a description of the physical and temporal regiment that framed the data sets, isolated the differences to be measured, and minimized external effects on the information. Data were collected in a three-tiered sequence (represented by the column headings in Table 1). The first tier is the individual plunges. This technique is described in the following section under field data procedures.

The second tier is related to each day's sampling as laid out in the rectangular study plot area (Figure 5). A reference line was established perpendicular to the left or right boundary in the undisturbed area of the study plot adjacent to the previously sampled area. Eleven plunges were performed in a specific spatial alignment along this line. Beginning on the observer's left looking into the undisturbed area, the first plunge was done following the first tier procedures. Sampling was then moved right 25 cm and repeated. This was done until five good samples were taken. Sampling was then moved to a point near the right end of the reference at a spacing equal to the number of plunges on the left plus one. The procedures were repeated moving right to left with 25 cm between samplings until the final plunge occurred at the center of the sampling line.

The encoder base was then removed from the probe, leaving the probe in place for measurement reference using the rulings on the shaft with the sensor's position representing zero (Figure 6). The excavation for the manual snow profile, instability tests, and density measurements were then done in the area between the older, disturbed area and the line of plunges.

The third tier consisted of carefully marking the disturbed areas and systematically moving into undisturbed areas on following days with adequate spacing to ensure previous excavation did not influence the new sampling area. Two days were done moving left to right before moving forward into undisturbed area. The ground under the study plot area was near uniformly flat without large vegetation. A slight difference in relative snow depth was observed left to right looking towards the undisturbed area with the region on the left sometimes 5 to 10 cm deeper. Each excavation was refilled at the end of sampling to ensure limited horizontal influence of temperature to the snowpack between sampling days.

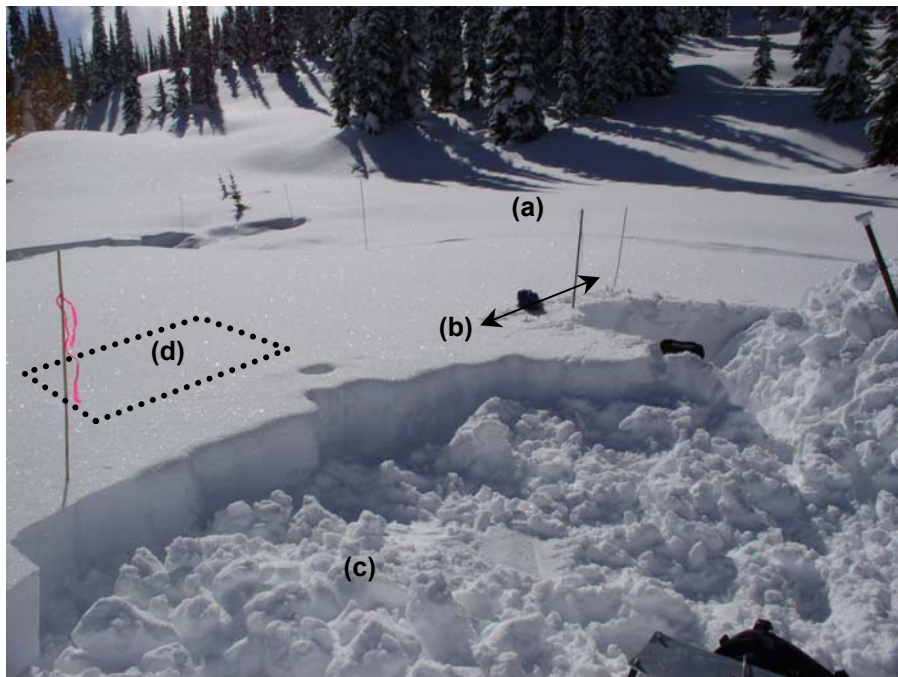


Figure 5. Typical field layout for data collection day. (a) The probe as left in place following the last plunge along line (b). (c) The area of previous day's data collection. (d) Area for next data collection day.

3.5 Data Manipulation, Management, and Quality Assurance

This section contains a description of the approach, standards, and methods of data recording, its subsequent archiving, and preparation for analysis used over the course of the study.

3.5.1 Field Records and Procedures

Both electronic and manual records were made in the field. Electronic files were saved on the Palm component of the data collection system described in the earlier instrumentation discussion. These were ASCII tab delimited text files. Daily notes were kept in a waterproof field book and snow profiles were recorded using an avalanche field book formatted for use of standardized observations and measurements (Canadian Avalanche Association, 2002).

The same procedure was followed each field session. Upon arriving at the location to be sampled, the probe was assembled and the electronics powered on for at least thirty minutes prior to measuring to ensure the circuitry was stabilized at the ambient temperature. Each electronic file consisted of one plunge or other designated observation such as the air calibration file done at the beginning of each data collection session. Once the system (probe and electronics) had stabilized over the thirty-minute period, a file was recorded of probe measurements with the sensor off the snow surface approximately one meter and shaded. This allowed for the probe measurement of base dielectric properties of the air on the day of sampling as well as thermistor measurements of air temperature in conjunction with a manual measurement. Dielectric measurements of air were necessary in converting recorded voltages from the probe measurement to real and imaginary components of the complex dielectric constant.

A new file was created for each plunge of the probe. File naming was automatically accomplished by the Dastack software running on the PDA using the date and time stamp, e.g.

21Feb2006(1039)DBData.txt for the data file began at 10:39 on 21 February 2006. A second file (e.g. 21Feb2006(1039)DBLog.txt) was also automatically created when a new file was begun. In the case of less than a minute elapsing before the need to begin a new file, the new file was manually named for the future minute and a note was recorded in the field book.

A systematic procedure was rigorously followed to ensure continuity beginning with positioning the encoder base at the sampling plunge location and followed in order by:

- 1) Testing rollers and encoder output.
- 2) Creating a new file set (*DBData.txt and *DBLog.txt),
- 3) Starting data recording, cleaning the sensor face,
- 4) Threading the probe through the encoder rollers and pausing with the probe tip at the snow surface maintaining the probe plumb,
- 5) Resetting the wheel count,
- 6) Checking the data on the PDA screen after beginning the plunge,
- 7) Plunging steady and smoothly to the ground,
- 8) Stopping data recording, removing the probe from the plunge and setting it aside, and
- 9) Creating a new file for the next plunge before making any notes in the field book.

The probe was left in place to the ground following the last plunge of the sequence and a new file was created. This final empty file set ensured that all data collection files were closed and saved since corruption of the final file of the day had been experienced the previous winter when downloading files from the PDA.

The simple check of the values and their changes upon the plunge entering the snowpack (step 6 above) and the values prior to removing the probe from the hole provided a quick quality assurance step. If the wheel count behaved appropriately and the values were within range, the plunge was counted as good.



Figure 6. Typical data collection excavation showing the probe as left in place for vertical measurement reference following final plunge of day's sequence. Manual densities were measured directly adjacent to probe.

3.5.2 File Transfer and Storage

At the end of each day upon returning from the field, data stored on the PDA was retrieved with a laptop via the manufacturer's supplied connection cradle. A copy was made of the entire set of files created that day and saved in a separate electronic folder named by the date providing simple navigation between files during analysis. File size was reviewed for any indications of problems such as failed plunge recording. File names were confirmed against related notations in the field book. Original file sets remained on the Palm until file backups were made both on a compact disk and remotely to the departmental server.

3.5.3 Data Manipulation and Preparation

In each case of a file being prepared for analysis, a copy was made from the original before manipulation. In a first tier of preparation, the .txt file was opened in Microsoft® Excel 2000². The wheel count value was used to identify various periods of the plunge record for cleaning from the file and those to be eventually used in analysis. Rows associated with all wheel count values prior to the reset value of 38 were deleted, as were rows associated with the probe at rest on the ground prior to ending the data recording. Due to the problems associated with the encoder described in the methods section, rows beyond the encoder-wheel rollover-point of 3360 counts were deleted as well. An automated procedure was then used to go through the remaining rows and delete all that represented a negative direction or zero step of the wheel count based on the assumption described earlier in sources of error. The file was then resaved as a .txt file to be imported into Excel in the next step.

² Subsequently referred to as Excel.

Descriptive statistics were calculated for the plunge data sets. Generally, the raw data for a plunge represented 800 to 1000 point measurements collected around five samples per cm at approximately 8 cm/sec. Once the data were prepared for analysis they represented 300 to 500 measurements at 2 to 3 samples per cm per plunge.

A complex master Excel file (workbook with multiple worksheets) was prepared to transform raw probe measurements into appropriate variables and combine the multiple electronic and manual observations into a single useful format. An individual file (Excel workbook) was created for individual plunges and named using the same convention (e.g. 21Feb2006(1039).xls). The .txt file containing the raw probe measurements (X and Y component voltages, distance wheel counts) was imported to the primary worksheet in the workbook. Another worksheet provided conversion information from reference wheel count to distance from surface. Using the “index” and “match” Excel functions, each measurement was assigned a location (distance from the surface) based on the recorded wheel count. A feature was included that allowed an offset adjustment of the probe tip from its reset point to a location appropriately matching the sensors relation to the snow surface.

Other observations including the densities, layer identification, stability test, and temperatures recorded in the snow profile field book were transcribed to individual worksheets in the workbook. Study plot readings (HS, HN, HST, and ram pen) for the season occupied another. A set of worksheets provided by Capacitec were included and linked to transform the raw voltages recorded from the probe to the real, imaginary, loss tangent, and complex dielectric constant based on design equations (Louge et al., 2002). The “index” and “match” Excel functions were then used to associate the raw voltages and calculated dielectric values to the other observations based on the distance to the surface. The information from the various worksheets was combined in graphs similar to classic snow profiles for visual analysis and reference on another worksheet.

An additional worksheet reformatted the information from the primary worksheet to a uniform scale. The uniform scale was set at a vertical increment of 0.057 cm representing one wheel count distance between references. Measurements from the primary worksheet were assigned to the appropriate distance from the surface value. This allowed for the calculation of moving averages over vertical distances either side of a known measurement point. A “half-centimetre” (0.513 cm or 9 wheel counts) moving average (0.285 cm above and 0.228 cm below due the wheel count) was calculated for the X and Y component voltages. This represented an up scaling from probe measurement extent to manual density measurement extent and a smoothing of raw measurements (0.061 volts RMSE for the X component and 0.022 volts RMSE for Y component). This was done so probe measurements and manual density measurements were comparable at the same resolution.

Chapter 4 SUPPORTING INVESTIGATION AND BENCHMARK

This chapter contains the analysis and results of efforts in developing concepts required to build a case supporting the null hypotheses. A supporting investigation was undertaken to develop a manual and reproducible layer identification technique to expose or highlight stratigraphy variation suggested by the probe output. A benchmark for “currently accepted practice” was established through variance comparison of density measurements made with cutters presently used in the field.

4.1 New Manual Observation Method

A layer identification technique to expose or highlight stratigraphy variation suggested by the probe output was developed during this study. It was clear at an early stage that classic methods of layer identification performed at a scale of spacing and support that was not appropriate to the closely spaced probe measurements. Pielmeier and Schneebeli (2003b) described this difficulty as well. It was important that this field method be repeatable and reproducible.

The classic method of hand hardness has many limitations: its accuracy is observer dependent, it is unable to test thin fist or 4 finger hard layers, and the ranking of such lesser hardness when occurring between harder layers is purely subjective. Ferguson (1984) estimated the uncertainty of hand hardness when converted to force as $\pm 5 \times 10^3 \text{ N/m}^2$. Additionally, McClung and Schaerer (2006) point out that important soft layers will be missed if the ICSI recommended 5 N force is used and recommend 1.5 N.

Thin section profiles and photography techniques were determined not to be options due to the time and equipment required. Andersen (1960) introduced the use of a brush to highlight layers. It was the likely candidate and previous work offered the following limited but encouraging guidance:

- Careful horizontal strokes will model out layers (USDA Forest Service, 1961).
- Brushing “... will help bring out the natural layering...” (Greene et al., 2004).
- One of three options to reveal changes of hardness and layer borders (McClung and Schaerer, 1993).
- “... it’s a good way to dull your pencil and fill up your field book with layers” (Anonymous Practitioner, personal communication, 2005).

Two steps were undertaken in this supporting study, first the selection of a “best” brush, and second, the development of a general method. Ten brushes (Table 16 Appendix C) in a range of styles and brush materials were selected representing examples of economical cost and widespread availability.

The criteria for development of the general method were set such that the results were: 1) reproducible, 2) comparable between pits and observers (repeatable), and 3) consistently identified changes in more than one hand hardness level from fist (F) or four finger (4F); and required nothing more than the brush.

The assumption on which the method is based is that the brush applies a uniform force of disaggregation to the grain structure on the face of the snowpit wall based on the stiffness of the brush. Disaggregation force is related to the density and strength of the layer (Mellor, 1964). However, no stiffness standards exist for paint brushes (American Society for Testing and Materials (ASTM), 2002). Using a test stand (DuPont Filaments, 1999) each brush’s stiffness was measured by displacing 2 cm of

the brush tip from the brush while it was held perpendicular to the measurement surface. The area pressured by the flexed brush and splayed end was measured to determine a value per unit of pressure to compare brushes.

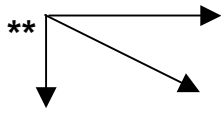
	Visible relief	Exaggerated relief	No relief present on profile wall
			
Easy to see layer boundaries and/or grains	1	2	3
Challenging to see layers and or grains	2	4	6
Difficult to see layers and or grains	3	6	9

Table 4. Matrix describing the ratings used in combining relief characteristics of relative layer hardness with visual quality. (**Decreasing ability to differentiate layers)

A matrix combining the ease of differentiating layers visually and the relative disaggregation of the grains was used to rate each test (Table 4). Field trials consisted of excavating a long trench exposing similar conditions at each point along the pit wall where testing was to occur. Multiple tests of each brush were completed, working into the pit wall and cleaning the back wall with a fresh shovel cut between each test.

The finalized method was utilized in flat terrain only, though tested for inclined terrain. The following description of the method includes instructions for its use on inclined terrain.

- 1) Prepare pit wall or column as customary with a shovel blade (a shaded column side wall if the method is to be used for an inclined snowpit).
- 2) Determine the upper layer representing fist or lowest hand hardness resistance.
- 3) Hold the brush perpendicular to the pit or column wall, brush lightly, smoothly, and parallel to the layering; with a full sweep across before beginning the return stroke. Across the pit wall for flat terrain and along the side of the column or pit wall for inclined terrain.
- 4) Exercise caution to maintain the brush handle perpendicular to the wall to ensure accurate results.
- 5) Count the number of strokes (each direction is counted individually) until the fist or lowest resistance snow is displaced by the brush to a depth equal to half the bristle length.
- 6) Move to an undisturbed area or re-prepare the pit wall or column side.
- 7) Brush the width of the wall or the length of the column side the number of strokes determined in the prior step.
- 8) Move the brush position down the wall or column one brush-width and repeat.
- 9) Continue to the bottom of the pit.
- 10) Record layering as: valley if relief is ≥ 1 cm or edges are square to adjacent faces, ridge or plateau depending on the shape of the top of the relief face. Annotate square edges.
- 11) Determine boundaries between classic hand hardness changes, e.g. F to 1F.

Table 17 in Appendix C contains the field trial results, ratings, and comments. The better-rated brushes fell in the mid range of pressure values. Thicker and stiffer brushes did not perform well, they damaged the surface making relief and layering difficult to see. Snow adhesion was a problem on synthetic brushes when snow and air temperature were warmer.

A drafting brush (brush I in Table 17) received the best overall rating and was the brush of choice. This brush distinguished thin F or 4F layers from adjacent layers that were harder or softer by one hand hardness level. Variations in the hardness relief of the lowest density layers (HN and HST) generally corresponded to subtle grain differences representing variations in near-surface conditions during deposition (wind and grain type) and variations in metamorphism occurring near the surface. Beyond this study, such results have potential to improve amateur observation quality for incorporation in snow profile analyses using threshold values.

4.2 Current Practice Benchmark

When an avalanche forecaster uses a snow density sampling kit for snow profile work, she or he rarely gives thought to the accuracy of the measurement provided by the device. When densities are utilized in published studies, accuracy is often not addressed other than in statements such as measurements were made according to observation standards (e.g. (Schweizer and Jamieson, 2001)).

Several density kits are commercially available and currently being used, as are a few that are no longer purchasable. These represent different styles of cutters for taking the volume sample as well as different weighing devices. Weighing devices such as spring scales, balances, or digital scales nominally have accuracy and environmental limits described in accompanying literature provided by the manufacture. For example, a Swiss 500g X 5g spring scale that accompanies a wedge-type cutter is described by the manufacture as having an accuracy of $\pm 0.3\%$ or about a gram and a half. This does not address the size of sample, i.e. such accuracy means something very different for a 100 cm^3 versus a 1000 cm^3 sample of the same density.

During the first season fieldwork the density kit “at hand” was used, which included a wedge-type cutter and a dial-spring scale. It was discovered that a non-linear relationship existed between actual and measured sample densities through comparison of measurements on a triple beam balance in the field with those of the spring scale being used. Such error resulting from “accepted practice” provided the impetus to evaluate variance in snow density measurements of various cutters for reference in evaluating the probes ability to discriminate snow density.

4.2.1 Standards Review

A review of described or specified techniques provided limited guidance. Very few details are included in current North American avalanche, weather and snow observation standards (Canadian Avalanche Association, 2002; Greene et al., 2004). These are limited to:

- Describing the use of wedge-type or smaller cutters for thin layers,
- Larger volume cutters for depth hoar,
- Insertion horizontal in the center of the layer, vertical if layer thickness exceeds cutter width, and in the pit sidewall for angled slopes.

The sole additional standard states that if more than one layer is sampled by the cutter it is described as bulk density (Greene et al., 2004). An observation of snow density competency or confidence (SDC) that describes sample quality as: 1) good sample 2) some loss of snow 3) full sample not possible due to too low of cohesion or too hard to sample was included in data standards for the Long Term Ecological Research McMurdo Dry Valleys Project (McMurdo Dry Valley LTER, 2000).

Other published works lent little to the topic of density cutter accuracy other than validation of an over sampling bias of up to 12% for snow survey devices used in total snowpack snow water equivalent measurement (e.g. (Peterson and Brown, 1975). A 10% combined sampling and weighing error in repeated density measurements with a 100 cc density cutter was described by Harper and Bradford (2003) during their small area spatial density investigation on an Alaskan glacier. The lone density cutter analysis was done as part of the San Juan Avalanche Project (Carroll, 1977).

Carroll (1977) determined there was no significant difference in measured snow densities when using 500 cc aluminium tube, 200 and 100 cc stainless steel box-type density cutters. Using a two-way analysis of variance to address random effects by operators, fifty samples per cutter per layer for three homogeneous layers were analyzed (N=150). Five operators took 10 samples each cutter per layer. He found insufficient evidence in all three layers to suggest significant difference in cutter type. He did find significant evidence that operator effect existed in the upper and lower layers at the 0.01 alpha-level, which he attributed to grain type and associated measurement difficulties that required greater experience. I assume that different weighing devices were used for the tube cutter versus the box cutters based on knowledge of the scale supplied with the box-type cutter kit and the weight characteristics of the tube cutter.

4.2.2 Density Cutter Types

A field experiment to determine the relative precision of snow density cutters was undertaken testing the 500 cc aluminium tube, 200 and 100 cc stainless steel box-type cutters evaluated by Carroll as well as a 200 cc stainless steel wedge-type cutter and a 100 cc stainless steel tube-type cutter. The “standard” 500 cc tube was originally described in English by Seligman (1936) and the sampling technique published in 1939 (Bader, 1954). Bader described the maximum measurement error as 0.25 to 1% for fine-grained and coarse-grained snow respectively. This cutter is commonly referred to as the Swiss or SIPRE (Snow, Ice, and Permafrost Research Establishment) cutter and sometimes the CRREL (Cold Regions Research and Engineering Laboratory) cutter. It is easily constructed from tube aluminium stock with one end sharpened chisel-like. The box-type cutter design originated at the Institute for Low Temperature Science and was manufactured in the U.S. by Hydro-Tech as the Taylor-LaChapelle density kit (Figure 7, left). The wedge-type cutter design is attributed to R.I. Perla and is manufactured by Snowmetrics in the U.S. However, the wedge-type cutter tested by me was made by Snow Research Associates and is no longer available (Figure 7, middle). The Wasatch Touring density kit with the small, 100 cc tube-type cutter (Figure 7, right) was designed by Steve Rosso and can be obtained through numerous sources worldwide. Specifications of the cutters are summarized in Table 5.



Figure 7. Various types of density cutters tested for variance, left to right: box (100 cc), wedge (200 cc), and tube (100 cc).

These density kits come with a variety of scales; hanging and dial mechanical spring scales, digital scales, and in the case of the Wasatch Touring model; a custom made balance device. Due to the measurement error experience described earlier and a desired design to compare cutters not scales, an appropriate digital scale was used for all experimental measurements. The scale was portable, waterproof, measured up to 1000g at a 0.5g resolution with accuracy of $\pm 1g$, an operating environment of $-10^{\circ}C$ to $40^{\circ}C$, and had a calibration accuracy of $\pm 0.1g$.

All the cutters were pushed horizontally into the layer being measured. This ensured they were sampling as close to the same stratigraphy as possible with vertical variation the same across each sample. The box-type cutters are supplied with a close fitting cap that slices the sample down both open ends of the cutter and snugly encloses the cutter. The wedge-type cutter has a sliding plate that slices the sample from the surrounding material as it is inserted along the open top edge of the cutter. Often this squeezed the cutter out of the sample area leaving a less than complete volume in the cutter. The tube-type cutters require using a flat metal piece such a crystal screen or spatula to cut away material from both open ends. There is regularly opportunity for low-density snow to fall out of these when removing them for weighing.

Cutter	Type	Measured Volume cc	Tare @ $-9^{\circ}C$ gm	Width cm	Diameter cm	Height cm	Length cm	Cutting Edge
Hydro-Tech 100	box	99	71	6		5.5	3	Y
Hydro-Tech 200	box	197.4	88.5	7		4.7	6	Y
SIPRE 500	tube	485.4	490		5.63		19.5	Y
Snow Research Associates 200	wedge	207.5	172	10		4.1	1.01	Y (on cutting plate)
Wasatch Touring 100	tube	99.2	47.5		3.71		9.18	N

Table 5. Specifications and characteristics of density cutters tested in the randomized block experiment.

4.2.3 Measurement and Sampling Error

A component of the density cutter analysis was estimation of measurement and sampling error. The measurement error was assumed to be the variation of density measurements resulting from the scale accuracy over the sampled range of densities. A Monte Carlo simulation was run 100 times for 100 randomly assigned errors within the stated scale accuracy resulting in the estimated measurement errors shown in Table 6. The sampling error was estimated using a similarly iterated Monte Carlo simulation. A potential under sampling error was assumed and calculated using a 0, 1, or 2 mm randomly assigned volume reduction at the open ends or top of the cutter. This was also done for the range of density measurements taken during the analysis and resulted in the estimated under sampling errors shown in Table 6.

Density Cutter	Measurement Accuracy	Percentage of Measurement	Cutter Under Sampling Error	Percentage of Measurement
HydroTech100	±4 kg/m ³	±1 to 4%	2 to 8 kg/m ³	-2%
HydroTech200	±2 kg/m ³	±1 to 2%	2 to 7 kg/m ³	-2%
SIPRE	±0.8 kg/m ³	±1%	1 to 5 kg/m ³	-1%
SRA	±2 kg/m ³	±1 to 2%	2 to 8 kg/m ³	-2%
Wasatch Touring	±4 kg/m ³	±1 to 4%	1 to 5 kg/m ³	-1%

Table 6. Measurement error and cutter under sampling error estimates.

Interpretation of these estimates is not straightforward; the estimated sampling errors do not include the likelihood of under sampling based on the relative ease of making an accurate measurement. Though the box cutters have the larger error (-2%), their design makes actual under sampling very unlikely, which was supported by experience. The wedge cutter often under sampled due to its design. The tube cutters, though smaller error percentages, also regularly under sampled due to the manner in which the snow is cut from the ends of a horizontally inserted tube. Combination of these observations, measurement and sampling error estimates therefore result in the error bar values associated with the scale used and are shown in Table 7.

Density Cutter	Density Measurement Error Bars
HydroTech100	±4%
HydroTech200	±2%
SIPRE	-2% to +1%
SRA	-4% to +2%
Wasatch Touring	-5% to +4%

Table 7. Summary of density measurement error bar values for tested cutters when used with the experiment specific scale.

4.2.4 Experimental Design and Sampling

A randomized block experimental design was chosen to focus measured effect on the density cutter as the treatment and to account for variability between sample areas (blocks). An experimental design evaluation day preceded data collection to ensure consistency and suitable techniques. Data for analysis were collected in the flats adjacent to the Mount Fidelity Station study plot on 3 field days: 15, 17 February 2006, and 29 March 2006. On each day, a rectangular pit was excavated in a previously undisturbed location such that the working area (approximately 70 cm thick and 130 cm across) was to the south of a deeper trench for standing. A small trench was cleared perpendicular to the standing area so a two-dimensional reference to the horizontal bedding of layers was visible. Each block included one sample per cutter, working from closest to the standing trench away and towards south. Sequencing of cutters within the block was randomized. In cutting and removing a sample, substandard ones (e.g., visible volume loss or non removable extraneous snow) were discarded and the sample was repeated until an adequate one was taken before moving on to the next cutter in sequence. Blocks progressed left to right along the same layer plane into a section undisturbed by the previous block. One experienced individual took all samples and measurements.

Layers for sampling were selected based on a visual observation of homogeneity, at least 10 cm thick and preferably 15 cm or more. On 15 February, the base of sample layer 1 was 33 cm down from the surface and consisted of small rounds; size 0.25 to 0.5 mm with limited evidence of past faceting on the larger sizes. The layer thickness was 12 cm. The wind speed was calm with the temperature ranging from -9.3°C at the start to -11.3°C near the end of data collection. Eight blocks were sampled.

On the 17th of February, two sets of twelve blocks were sampled in the same manner. The upper twelve blocks (layer 2) sampled were centered in a layer between 5 cm and 15 cm down from the surface. This layer consisted of decomposing fragments; size 1 to 2 mm with some faceting occurring. The second set of 12 blocks (layer 3) was taken from a thick layer and sample centers were relatively close to 57 cm below the surface.

Two sets of eight blocks were sampled on the 29th of March. The first set (layer 4) was taken directly above an old crust 7.5 cm down from the surface and represented the most heterogeneous layer sampled. This layer consisted of rapidly rounding grains, 0.5 mm in size. The second set of eight (layer 5) was taken 67 cm from the surface and consisted of moderately necked rounds, 0.5 mm in size.

4.2.5 Density Cutter Conclusions

A one-way analysis of variance (ANOVA) was used to test the null hypothesis that the means of each cutter were the same ($N=220$). Statistical analyses were performed using the JMP IN® Version 5.1 software package (Sall et al., 2003). The layers described above were analyzed and F-test results compared for an alpha-level of 0.05. In three of the five layers, results suggested rejecting the null hypothesis that the cutters were the same and therefore significantly different. Initial results also indicated blocking was not necessary in three of the five layers. Re-calculation of ANOVA results for those layers did not change the outcomes (Table 8).

Layer	No. of Blks	N	Prob > F		Null Hypothesis Result	Greatest density difference between cutters (kg/m ³)	Greatest cutter difference as % of layer mean density	Layer mean density (kg/m ³)	Greatest density difference between cutter mean & block mean (kg/m ³)	Greatest cutter & block difference as % of layer mean density
			Cutter	Block						
1*	8	40	0.0088 w/o blocking 0.0183	0.0747	Cutters significantly different	9.21	5%	195	5.8	3%
2*	12	60	0.0006	0.0002	Cutters significantly different	9.5	8%	119	5.4	5%
3	23	60	0.0701	0.1117	Unable to reject null	7.6	3%	255	4.8	2%
4*	6	30	<0.0001 w/o blocking <0.0001	0.1078	Cutters significantly different	18.7	12%	151	10.2	7%
5	6	30	0.1431 w/o blocking 0.1379	0.4196	Unable to reject null	24.9	7%	345	13.4	4%

Table 8. Result summary of randomized block analysis of density cutters.

All pairs were tested using the Tukey-Kramer Honestly Significant Difference to decrease committing a Type I error in the analyses. The results are shown in Table 9 summarizing the cutters that were suggested to be significantly different from others. In this table, cutters not connected by the same letter (A, B, C, etc) with in a layer were significantly different from the letter-connected sets. There was no threshold or pattern evident in the differences, e.g. 200 cc or tubular cutters always fell in the same groupings. However, in all cases where the cutters were significantly different, both the small box and small tube cutters were not different from the large tube.

	Layer 1		Layer 2			Layer 4	
HydroTech100	A	B		D			G
HydroTech200		B		E		F	
SIPRE	A	B	C	D	E		G
SRA	A	B	C			F	
Wasatch	A		C	D	E		G
Blocks		8		12			6
Layer mean density (kg/m ³)		195		119			151
Form		df & fc		rd			df
Size (mm)		1 - 2		0.5			1

Table 9. Summary of Layers 1, 2 and 4 where null hypothesis of cutters measuring equal was rejected.

ANOVA assumes the variances are equal within the treatments. Four statistical tests (O'Brian's, Brown-Forsythe, Levene's, and Bartlett's) were applied to each layer analysis to evaluate this assumption. In only layer 1, two of these tests suggest un-equal variances. Application of the Welch ANOVA (which weights observations by an amount inversely proportional to the variance) supported rejection of the null hypothesis for layer 1. A closer look at the individual variances is shown in Table 10.

Layer	HydroTech100		HydroTech200		SIPRE		SRA		Wasatch	
	Cutter StDev (kg/m ³)	as % of layer mean density	Cutter StDev (kg/ m ³)	as % of layer mean density	Cutter StDev (kg/ m ³)	as % of layer mean density	Cutter StDev (kg/ m ³)	as % of layer mean density	Cutter StDev (kg/ m ³)	as % of layer mean density
1*	4.9	2.5%	4.3	2.2%	1.5	0.8%	3.0	1.5%	6.7	3.4%
2*	4.2	3.5%	4.1	3.4%	3.4	2.9%	7.4	6.2%	6.0	5.0%
3	4.9	1.9%	6.5	2.5%	5.2	2.0%	7.4	2.9%	6.2	2.4%
4*	5.7	3.8%	3.7	2.5%	3.5	2.3%	6.0	4.0%	3.8	2.5%
5	14.3	4.1%	6.1	1.8%	17.4	5.0%	14	4.1%	15.3	4.4%

Table 10. Variances of cutter measurements with in layers.

In application, snow density measurements taken by various density cutters may be significantly different though there are expected ranges of precision. A conclusion can be made solely on the value ranges presented by the investigation without taking into account various reasons for the differences, e.g., stage of densification or mixture of metamorphism states. Without accounting for variation due to weighing devices, the “accepted” range of density measurements includes under sampling errors of 1 to 2%, variation within individual cutters of 0.8 to 6.2%, and variation between cutters of 3 to 12%. These ranges are illustrated in Figure 8 showing the mean layer densities of each cutter and relevant error bars for each tested layer. Interpretation of Figure 8 suggests that given the mean of all samples is the accepted to be the true value of the measured density, variation exclusively between cutter types provide “accepted practice” measurements that are within 12% of the true density.

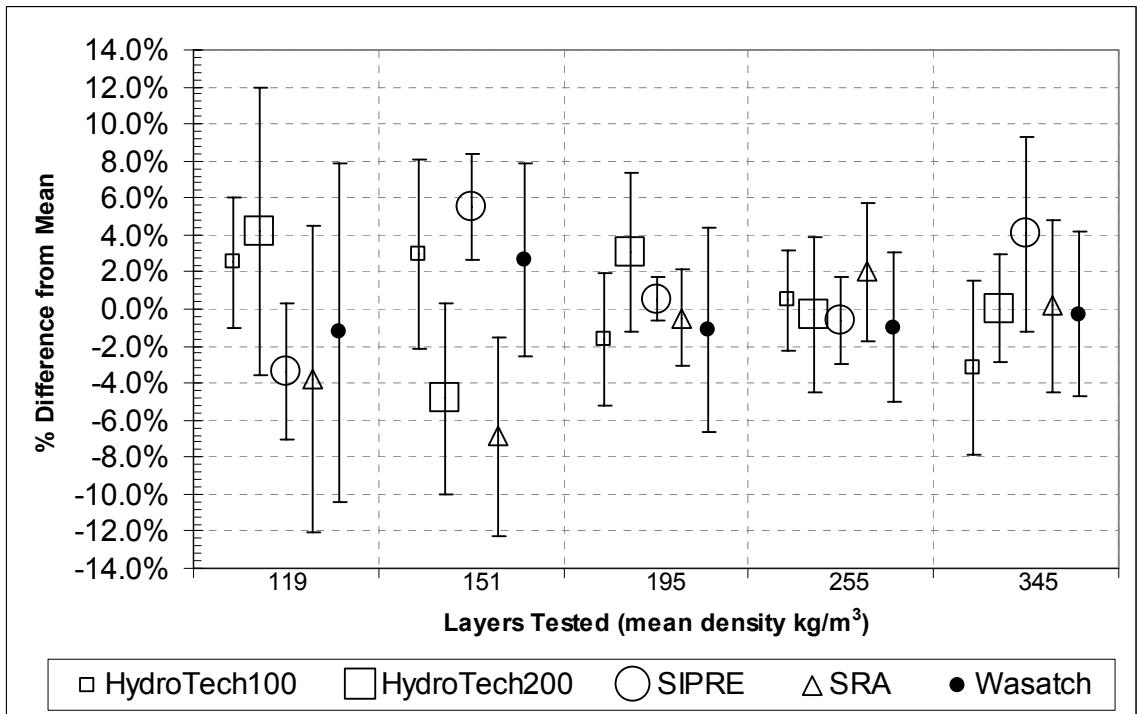


Figure 8. Graphic summary of sampling variance and weighing errors for density cutters evaluated for “accepted practice” benchmark. (Organized by sample layer and showing cutter mean densities.)

The HydroTech100 was chosen as the cutter used during the duration of the study. It and the Wasatch Touring tube cutter are the ones consistently near the mean density in Figure 8. The HydroTech model was chosen because it is easier to gather accurate samples with and removes a thinner section.

Chapter 5 RESULTS: DENSITY MODEL DEVELOPMENT, VALIDATION, AND ANALYSIS

This chapter contains a discussion on the development and analysis of several models based on correlation between manually observed density and probe-provided measurements. The models seek to answer the first two research hypotheses: 1) whether the bulk snow density measured by the probe is equal to or better than currently accepted practice, and 2) whether a density profile, as estimated by the probe, is equal to or better than currently accepted practice.

To assess strength of this correlation, several density prediction models were developed using probe measurements versus manual measurements as training-set data. Predictions of density were compared against validation-sets and test cases. The predictive models were also tested using cross-validation within the training-set data. Conclusions are based on interpretations of precision and accuracy of bulk density predictions and where the predictions fall in relation to “accepted practice”. Model predicted stratigraphy profiles are graphically compared to manual profiles. Statistical analyses were performed using the JMP IN® Version 5.1 software package (Sall et al., 2003).

5.1 Data

5.1.1 Field Measurements

Measurements collected over a nine-day period from 23 February to 3 March 2006 were selected as a calibration or training-set to determine models for estimating densities from probe output. Samples were taken on all days except 24 February, i.e. 8 of the 9 days. A description of daily weather conditions and manual snow profiles from each are presented in Appendix D. Following the multi-day series, data sets from two profiles were gathered approximately 25 kilometres due north of the same elevation on 5 and 10 March 2006. These were gathered to use as test cases against which models built on the training-set were compared. Test case 1 was from a snow profile two days after the last training-set day. The profile was just below tree line with very similar snow pack conditions to the training-set. The second test case was gathered five days later in a flat, open area in the alpine, chosen for its exposure to winds and likely contrasting stratigraphy.

Part of testing the probe in an avalanche-forecasting environment included using only the values returned by the probe. These included voltages representing the real and imaginary dielectric components and temperatures. The probe-mounted thermistor was unable to measure at a rate commensurate with the desired rate of plunge. This was due to the thermal characteristics of the metal tip. Thus, snow temperatures from manual measurements were used for analysis and model construction. Snow temperatures were inferred to the locations of the probe dielectric measurements based on the slope between physical temperature measurements.

5.1.2 Voltage Measurement versus Dielectric Values Assumptions

During the concept demonstration of the probe, a separate snowpress built by Capacitec was used to establish the density calibration. It was designed to accept a snow sample of known density and allow calibrated compression of the mass while measuring in the same manner as the probe. The

snowpress was not used during this study due to the belief it does not represent the physical grain and bonding differences in in-situ snow densification. This decision was supported by the following findings:

- Dielectric properties related to density change with bond growth (Yosida et al., 1958),
- Dielectric properties related to density change with age (Kuroiwa, 1962),
- Dielectric properties related to density change with temperature (Cumming, 1952; Takei and Maeno, 2003; Tiuri et al., 1984).

Difficulty was encountered using the vendor supplied spreadsheet for conversion of measurement voltages to dielectric values ϵ' and ϵ'' . The calculated dielectric values exhibited noticeably lower correlations to manual measured densities than the voltage measurements. The built-in spreadsheet computations use snowpress calibration values. Though the correlation discrepancy was attributed to not using the snowpress, the true source of the error induced in the spreadsheet calculations remained unidentifiable. The voltage measurements returned by the probe are representative of real physical conditions and dielectric properties present in the measurement volume (Louge, personal communication 2006). Therefore, the measurement voltages rather than the dielectric values were used for analysis and validation.

5.2 Model Development

5.2.1 Variables

Numerical models were constructed and analyzed with the following variables representing density, dielectric values, temperature, and layer age.

assignRho In all cases of the model development and analysis, the manual density measurement assigned to a probe measurement point was considered the response variable.

movAvgXpt5cm is an effect factor that is the half-centimetre moving average of X component voltages assigned to a probe measurement point.

movAvgYpt5cm is an effect factor that is the half-centimetre moving average of Y component voltages assigned to a probe measurement point.

Temperature was included as an effect since it varies in-situ rather than being held constant or controlled, as it had been in cited laboratory studies (Kuroiwa, 1962; Takei and Maeno, 2003; Yosida et al., 1958). Thermal conditions play a fundamental role in metamorphic state of snow grains. The temperature gradient is an index commonly used to determine what metamorphic regime a layer of snow is under (Armstrong, 1985). I believed this is an important effect variable for consideration in the analysis. Snow temperatures were inferred to the locations assigned to the probe measurements based on the slope between manual temperature measurements.

slopeTemp is the effect variable of snow pack temperature inferred to a probe measurement point.

TGslope is the effect variable that provides a proxy for the metamorphic process present at the probe measurement point. It is the calculated slope between the manual temperature measurements above and below the probe measurement point.

locat is the wheel count determined distance from the surface in centimetres after adjustment has been made to the 0 cm snow surface location relative to the position representing the probe sensor when reset of the wheel count occurred with the probe tip at the surface. Its use as an effect factor is as an assumed ordinal metric representing the temporal sequence of the layers.

Distribution of avalanche related data are often right-skewed (Bovis, 1976; Bovis, 1977). The distributions of my observations and variables are shown in Appendix E. A Lilliefors test (KSL) utilizing the Kolmogorov-Smirnov statistic to evaluate normality was applied to the distributions (Table 11). In all tests, the test statistic is larger than the critical value of 0.016 for an alpha of 0.05, therefore the null that the distribution is normal is rejected. Distribution graphs are included in Appendix E.

Variable	Test Statistic D (prob D>0.01 all cases)
movAvgXpt5cm	0.176
Log Transformed movAvgXpt5cm	0.041
movAvgYpt5cm	0.108
assignRho	0.116
slopeTemp	0.099
TGslope	0.186
locat	0.095

Table 11. Kolmogorov-Smirnov-Lilliefors test results of normal distribution for model variables.

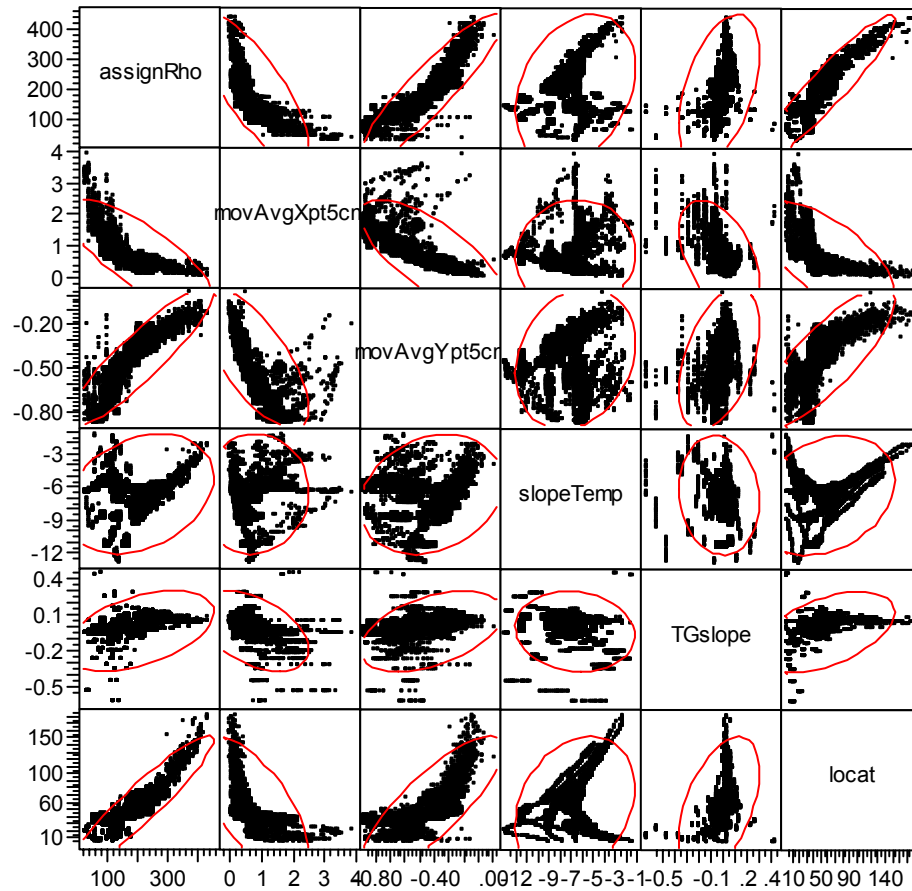


Figure 9. Scatter plot of model variables with .95 confidence interval ellipse

5.2.2 Density Model Development

The requirement of normal distribution for many multivariate statistical analyses (e.g. principle component analysis (PCA)) restricted choices of modeling techniques. Scatterplot analyses suggested a lack of linear relationships between variables (Figure 9). I chose recursive partitioning described by Friedman (1977) to explore variable relationships and create the density prediction model for the probe measurements. Unlike PCA, which assumes the vector that describes the least variance between factors is used to establish a numerical relationship; recursive partitioning maximizes the difference between factors as successive forks in a decision tree. Recursive partitioning is a robust method for data classification not requiring prior knowledge of distribution (Breiman et al., 1984). Recursive partition has been applied to avalanche data (Davis et al., 1999). They evaluated the importance of several avalanche contributory factors, including empirically derived ones, through the application of classification and regression trees. Davis and others argue that strength of recursive partitioning applied to avalanche data lies in its ability to over fit a model for exploratory purposes and provide a conservative prediction model.

A caution exists when using recursive partitioning to explore relationship. You cannot run an unrestrained number of new iterations until one provides the desired results. Ultimately, if the data is purely random, it will suggest significance at an alpha of 0.05 about 5% of the time.

The use of recursive partitioning in this study treats density correlation as a classification problem based on an assumption that density measurement is an index of change in volume resulting from metamorphic grain and bond change at a given environmental temperature. The metamorphic grain and bond change are manifested as variations in the real and imaginary dielectric values of the sample.

Recursive partitioning mimics the decision tree it creates as the construction process progresses through the data set examining both the factors and response variable at each new branch pair (split). This occurs at the primary split node and at subsequent nodes that represent the subset created by the previous split. At each split, an opportunity exists to use a cutting value for the factors that divides (partitions) the sample into groups above and below the value. The split in data is accomplished by selecting the factor and its associated cutting value that significantly separates the sample into two groups by separating the means of the response variable. This is done by examining the sums of squares due to the mean's differences (Sall et al., 2005).

Figure 10 provides an example of the JMP IN output tree of a three-split recursive partition model. In this example there are four factors being considered as effects on the response variable. At the first splitting node, all 3453 values of the response variable with mean 222.3 are considered. Factor 4 provides the opportunity to split the full set in half creating the largest sum of the squares of the residuals (candidate SS of 26,894,886). The cutting value for factor 4 in this split is < -0.329 or ≥ -0.329 . The second split is governed by which of the two new sets possesses the opportunity for the largest candidate sum of squares, in this example it is factor 2 in the subset factor 4 ≥ -0.329 . Factor 3 will create the largest candidate sum of squares (2,326,654) in the other factor 4 group however the candidate SS for factor 2 in that group is less than (3,268,744) thus the choice of splitting the factor 4 ≥ -0.329 subset. Logically this three-split tree would be written for application to another data set as:

```
If Factor 4  $\geq$  -0.329, Then
    If Factor 2  $<$ -6
        Then, assign prediction value 260.9
    Else, assign prediction value 352.4
Else, assign prediction value 139.1
```

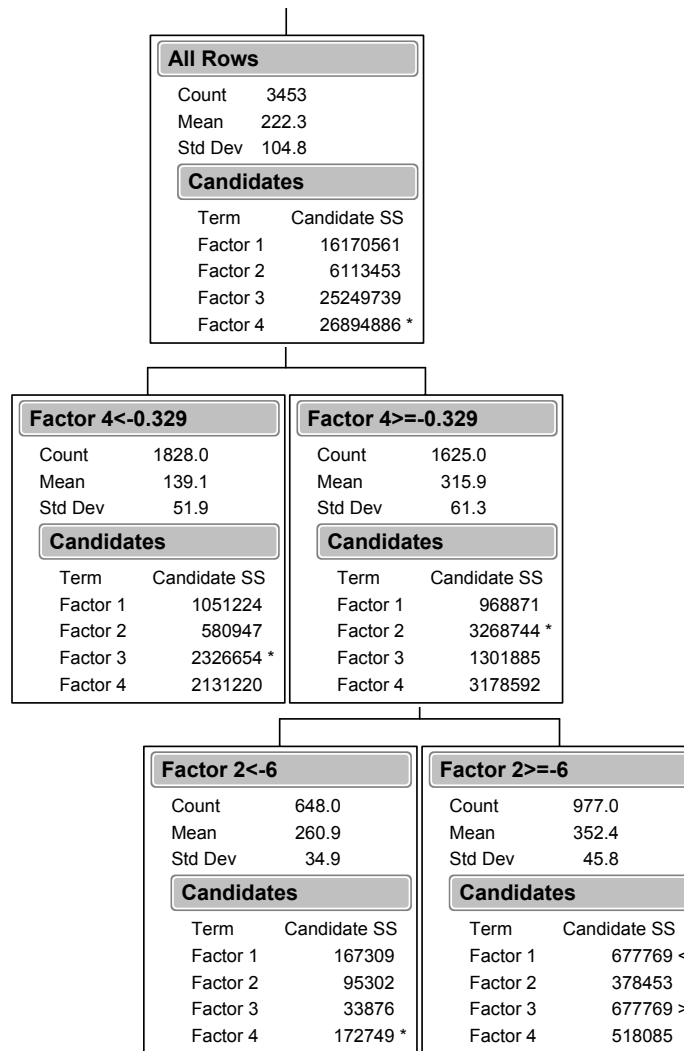


Figure 10. Example of two-split recursive partition tree from JMP IN output.

5.3 Model Bulk Density Analysis

Recursive partitioning was performed on groupings of data representing various combinations of data set size and type to create several models. For each of these models, assignRho was the response variable. Four effect variables were included in model construction: movAvgXpt5cm, movAvgYpt5cm, slopeTemp, and TGslope. Model outputs of predicted densities were recorded at five-split intervals, i.e. 5 splits, 10 splits, 15 splits, etc. This allowed an overview of relative model performance and identification of an optimum number of decision splits. Such optimization is done by identifying limited additional improvement evidenced by decreasing slopes between performance measures of subsequently more complex models.

Three, one-day model sets were constructed representing the first training-set day (23 February), the last training-set day (3 March), and the first test case day (5 March). The test case day model was built to allow comparison between the training-set and test-set values. Two model sets of two days each (one consecutive, one not) were constructed using the first and second training-set days (23 and 25

February) along with the last two training-set days (2 and 3 March). Two, three consecutive day model sets were also developed (26 to 28 February, 1 to 3 March). Different percentages (33.3, 50, and 66.6%) were randomly selected from measurements covering all eight training days and used in constructing another three model sets. Measurements from all eight training-set days were used for an additional model.

An example of output tree cutting values at 5, 10, 15 splits for the model constructed from the randomly selected 50% of measurements covering all eight training days is provided in Appendix F.

5.3.1 Model Precision

Models using Various Training-sets

A bivariate fit between the assignRho value representing the manually measured density at a probe measurement location and the model predicted density was plotted for each model output. A coefficient of determination (R^2) was calculated for the linear fit between the observed and predicted densities for each model. The coefficient of determination provides an index of how well a model fits (precision) without consideration of how well the model works (accuracy). Figure 11 illustrates the R^2 values for the fit between the various models described above and the manual density measurements. An example is provided in Appendix G illustrating the full complement of XY fit graphs for the 50% of all training days model.

The R^2 values for the three, one training-day model sets (23 February, 3 March, 5 March) can be seen close together from the 10th split on in the region above 0.98 (Figure 11). The R^2 values for the set representing all eight training-set days can be seen following the same trend as the other model sets from a value of 0.93 at 10 splits to 0.97 at 45 splits.

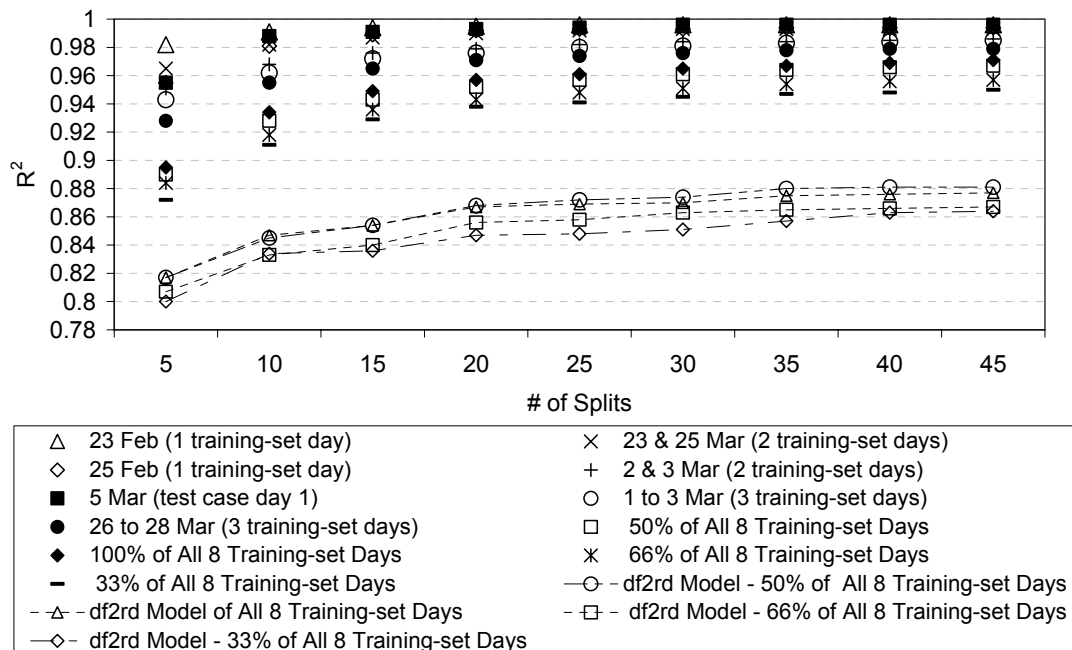


Figure 11. This graph shows the respective R^2 values calculated or precision for the bivariate fits between model predicted densities and the response variable used in creation of the various models.

Evident in the trend between split increments illustrated in Figure 11 are all models nearing a sill between 15 and 25 splits where little improvement in precision follows. This is evaluated further through residual analyses. A conservative conclusion is possible given the consistent patterns in the portion beyond 15 splits of Figure 11 that partitioning the four effect factors result in models with fits to the training-set data that accounts for over 93% of the variability in the manual density measurements.

Earlier work on dielectrics and density was done with sieved and near uniform grains (Kuroiwa, 1962; Takei and Maeno, 2003; Yosida et al., 1958). In an effort to explore the role that grain type and bonding might play in model predictions, four additional model sets were constructed in a similar manner as above. These were constructed using a partial data set, preened from all eight training-set days and represented a physical based model (df2rd). The df2rd models utilized only measurements where the identified grain type were non-rimed, decomposing fragments and non-rimed rounds to constrain the model as one solely based on slow growth metamorphism (rounding). One used all eight training-set days and the others represent randomly selected third, half, and two-thirds sets taken from all eight days.

Calculation of R^2 values for these df2rd models is also shown above in Figure 11. Their trend is similar to the all-grain models though clearly offset at a lower coefficient of determination. This is taken to indicate that in-situ snow structure possesses additional attributes related to the measured densities beyond the rounding and sintering characteristic of to the weak temperature gradient present in slow growth metamorphism.

Model Fit for Excluded Values from Selected Training-sets

In six of the models described above, the training-sets were subsets of the entire sample set. The portions not included in constructing the models were tested as validation-sets to gain an idea of relative classification error. The difference between precisions of predictions for each of the models against the training-set excluded values is shown in Figure 12. There are slight reductions and increases in precision from the model fit to the validation prediction evident. This general lack of difference supports the existence of the assumed strong relationship between the manually measured densities and the probe measurements. It also illustrates a general lack of over fitting for models based on multiple day training-sets. The model created from 50% of the entire eight training-set days exhibits the best performance when interpreting Figure 12. It is highlighted with a solid connecting line between square markers.

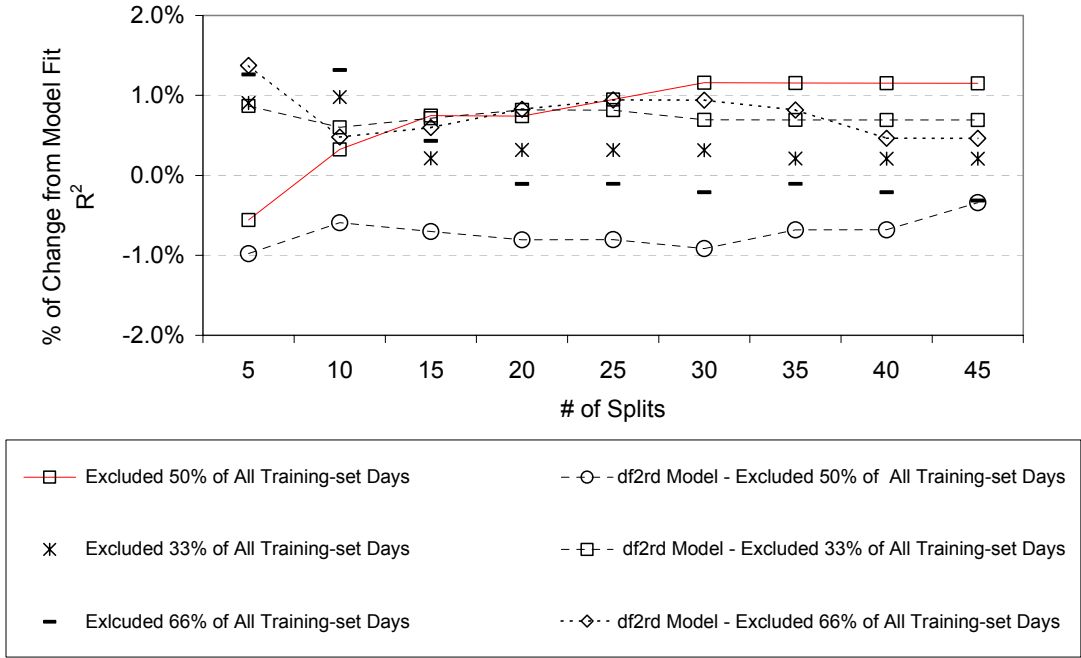


Figure 12. Comparison of precisions for selected models applied to excluded training-set data of the percentage of change between model fit to training-set data and model fit of predicted densities for training-set data excluded from model construction.

Training-set Size

To investigate the role training-set size affects model results, the last training-set day (March 3) was set aside as the validation-set. As before, assignRho served as the response variable with the four factors: movAvgXpt5cm, movAvgYpt5cm, slopeTemp, and TGslope, as effect variables. Prediction models were developed in the manner described earlier using incrementally larger training-sets sequentially incorporating earlier days. A seven-day set using all but the validation day, a six-day model including the six days prior to the validation day, a five-day model of the five prior days, and so forth.

The fit for five of the models (7, 6, 5, 4, and 3 cumulative days prior to 3 March) are almost uniform and nearly equal (Figure 13). This consistency supports the assumption of a strong correlation between the factors and the response variable. However, the application of such strong fitting models to the validation-set does not offer a similarly consistent pattern (Figure 14). The difference between the validation-set fit and the model fit is shown in Figure 14 as a percentage of change from the model fit. The results illustrate a cautionary conclusion that though model fits for the small training-sets are high, their validation values are the lowest tested. The greater number of days (7,6, and 5) in the training-set results in predictions with the least amount of negative change from the model fit (over fitting).

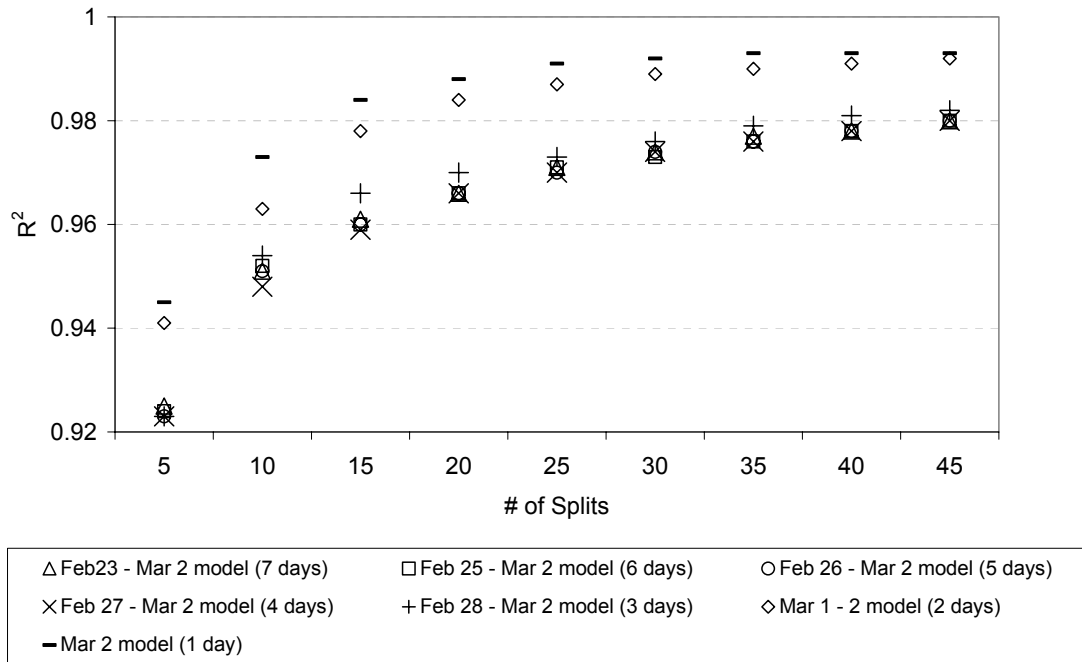


Figure 13. Coefficients of determination for density prediction results relative to training-set size.

When a curve is fitted to the points, there is a lack of symmetry to the trends for each model. Some models increase in precision at the early split outputs then decrease (seven and five day models). Generally, the precision of each set of predictions stabilizes in relation to the model fit between 20 and 30 splits. This suggests other influences resulting from combinations of specific days in the training-set.

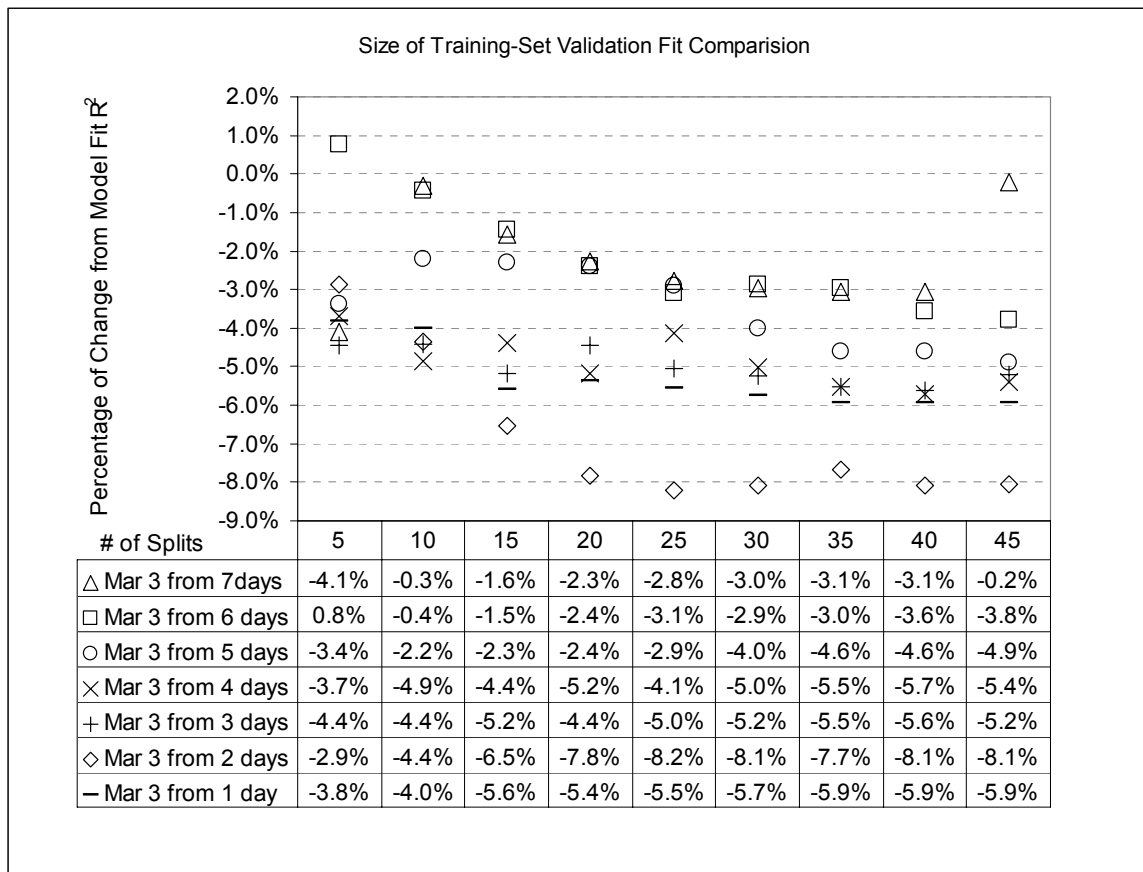


Figure 14. Summary of results for consecutively increasing sized training-sets shown as a percentage of change from the model fit to a single day validation-set.

Single-day Training-set Model Fits

Clearly if the probe is to be valuable in an operational application, a balance must be found between the number of training-set days and the length of time the predictive model is useful. It is unlikely that a user would spend seven days collecting a training-set to calibrate the probe for use in the same location. A single-day training-set would be ideal. A trend seen thus far are though, the least amount of over fitting of models occurs when they are created from a larger number of training-set days, smaller training-sets may produce results that fall in a useful range. The results may also point towards the concept that conditions may be present on specific days that influence the model if included.

The relationship resulting from use of a single-day model was explored by creating all-grain models for the individual days of 23, 25, and 26 February. As usual, assignRho served as the response variable with the four factors: movAvgXpt5cm, movAvgYpt5cm, slopeTemp, and TGslope, as effect variables. As previously observed, the single-day training-sets result in highly precise models with coefficients of determination ranging between 0.974 and 0.996 and reaching sills at 20 to 30 splits as shown below in Figure 16. The bivariate fits between assignRho and predicted densities from which the R^2 values were calculated are in Appendix H.

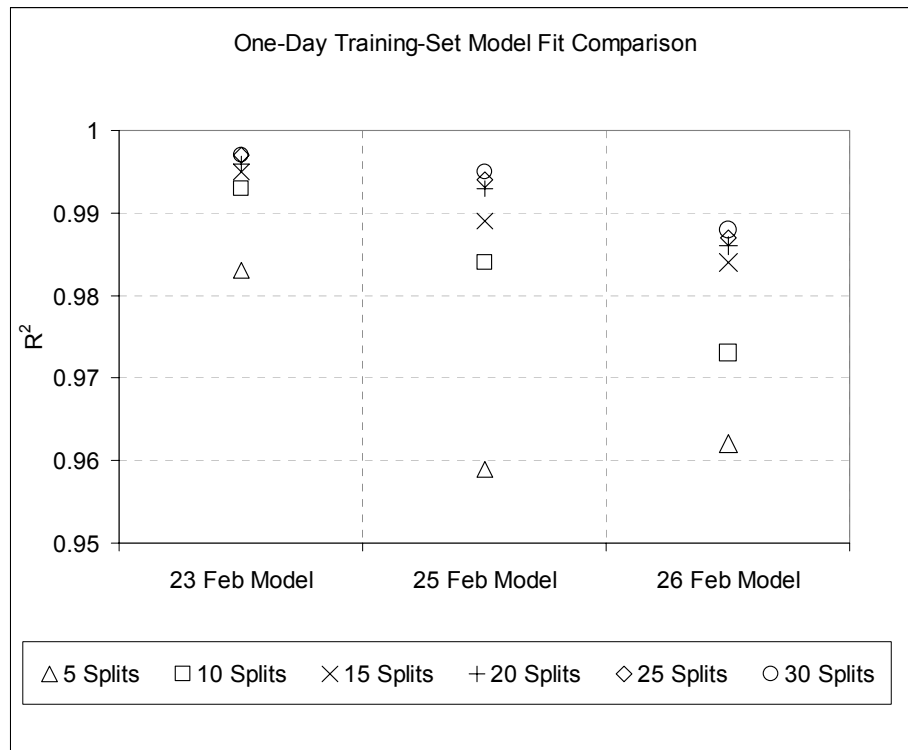


Figure 15. Comparison of selected one-day training-set model fits

The residuals of the three model sets shown in Figure 15 plotted against the predicted densities at each split output were analyzed. The standard deviation and Shapiro-Wilk statistic W for each fit is provided in Table 12. Interpretation of the results suggest that though the error decreases with the number of splits (over-fitting), the best performance gauged by normalcy of the model residuals is between 10 and 20 splits depending upon the model. Plots of these residuals are included in Appendix I. Figure 16 of the 15 split output for the 23 and 25 February models suggests that grain type might play a role in the errors associated with the density prediction based on probe measurements.

Model Split	23 Feb Model	25 Feb Model	26 Feb Model
5	12.7 / 0.96	21.1 / 0.97	17.2 / 0.95
10	8.1 / 0.93	13.1 / 0.94	11.9 / 0.90
15	6.6 / 0.87	10.8 / 0.87	8.6 / 0.92
20	5.9 / 0.84	9.0 / 0.82	6.3 / 0.79
25	5.5 / 0.82	7.9 / 0.81	5.6 / 0.62
30	5.4 / 0.83	7.5 / 0.73	5.1 / 0.49

Table 12. Residual analysis of the single training-set day models in Figure 15 summarizing the standard deviation and Shapiro-Wilk statistic W testing normal distribution of residuals.

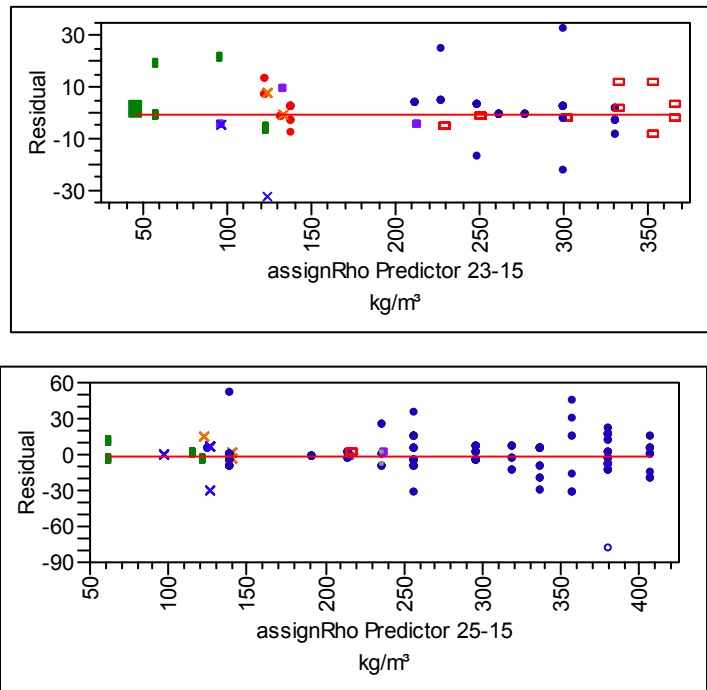


Figure 16. Residual plot examples suggesting grain type influence on model errors.

The three single-day models were applied to the subsequent days of the training-set. The results are presented from two perspectives. In Figure 17, the difference between the model fit R^2 values and the density prediction R^2 values on increasingly distant days from the model day are shown as a percentage of change from the model R^2 value. The three single-day models' predictions exhibit dissimilar precision. The model created from the 23 February training-set day is close to what one might expect if the precision decreases the further into the future one applies the model. The 25 February model provides a contrary example as does the 26 February model. Only predictions for 3 and 5 days out appear consistent though at a 10 to 15% lower precision than the model fit.

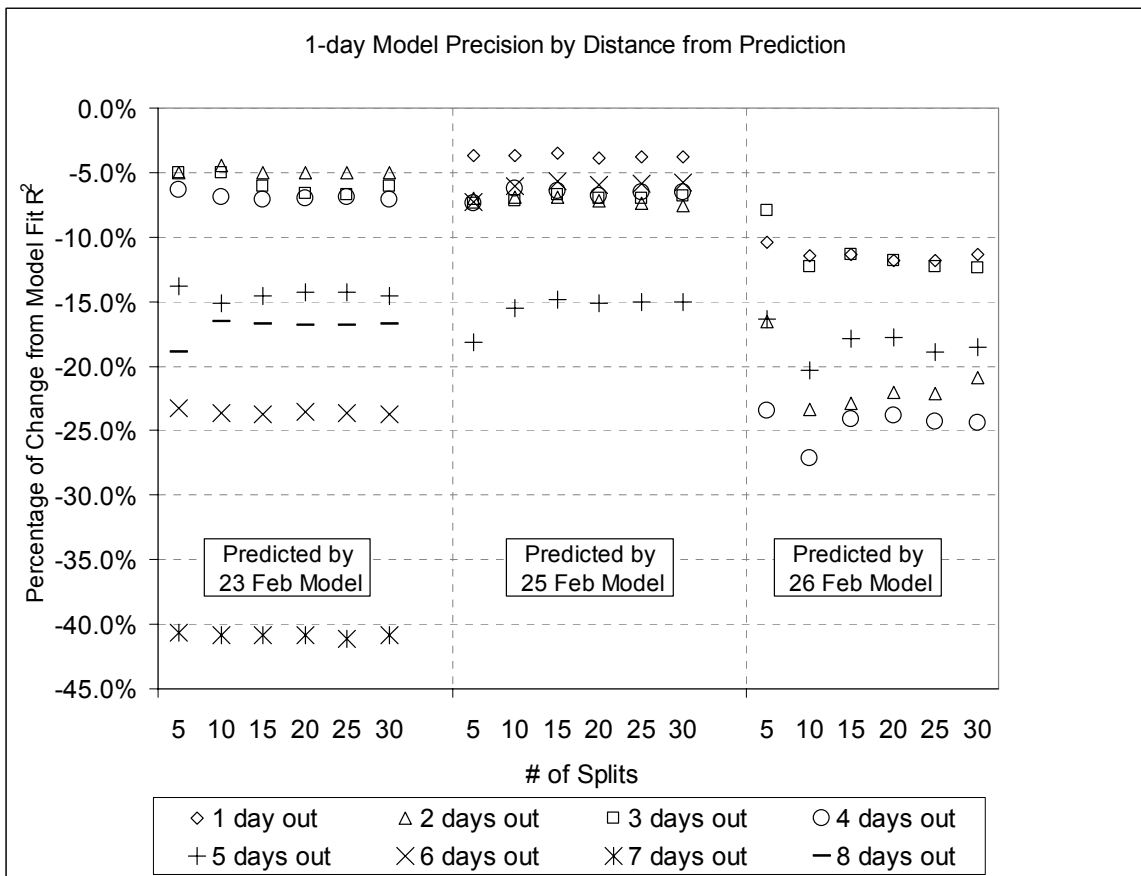


Figure 17. One-day model precisions by distance (days out) from prediction.

The same metric focused on the day predicted is illustrated in Figure 18. Clearly all three models exhibit difficulty in predicting values for 2 March since it has the largest difference from the model fit in all three applications. Predictions for 26 and 27 February are similar with little decrease in precision from the model fit.

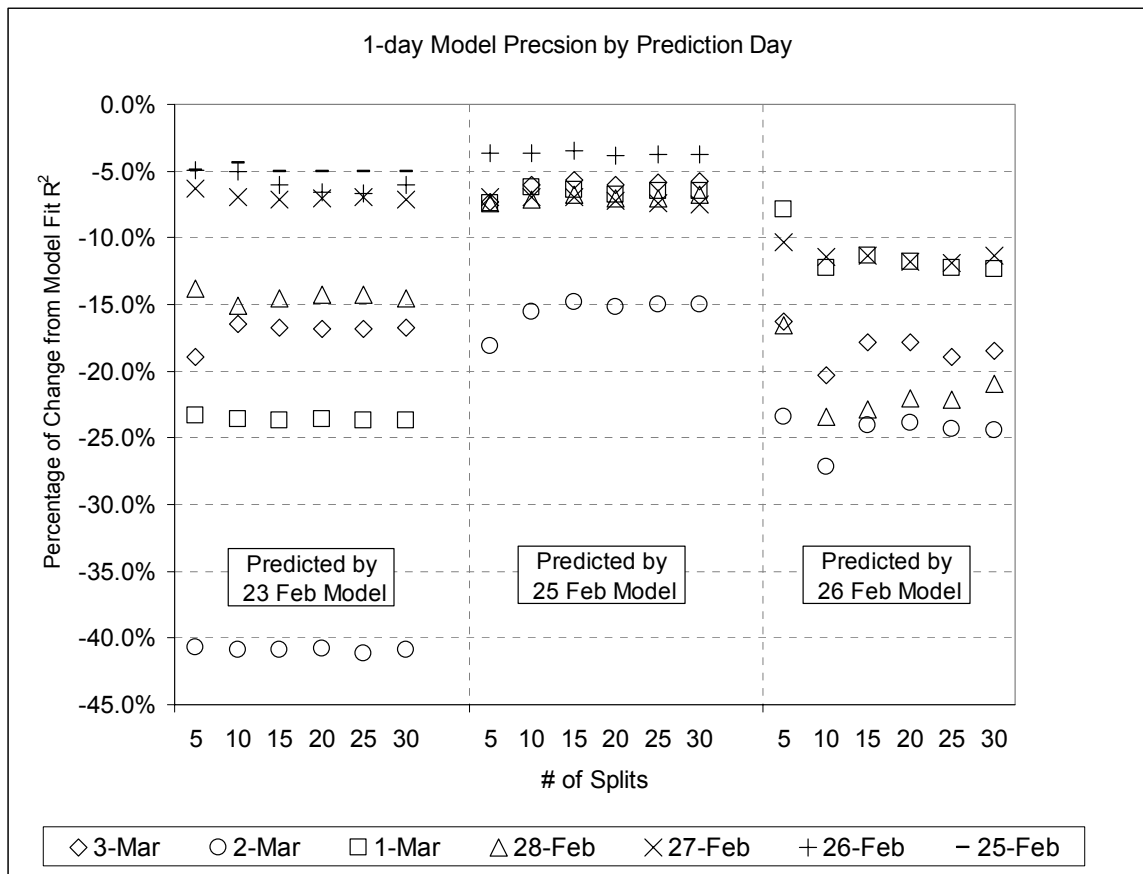


Figure 18. One-day model precisions organized by the prediction day.

Conclusions may be inferred from these two graphs:

- A precise model is possible that exhibits little influence of time (days) prior to application (25 February model),
- Single-day training-sets generally over fit by at least 5%, and
- The relationship between structure or characteristics of the training-set day and the prediction day plays a stronger role than the temporal distance between the days.

5.3.2 Model Accuracy

Model Fit and Cross-Validation for Selected Training-sets

The previous sections discussed sensitivity and apparent precision related to data type, amount, and time to model application but did not address accuracy of the evaluated models. Root Mean Square Error (RMSE) is an effective metric for such since it is in the same units as the measurements and represents an unbiased estimate of precision. RMSE values allow the comparison of prediction precision with the range of “accepted practice” described in section 4.2. The “accepted practice” value is illustrated relative to mean bulk density of the training-set, validation-set, or test case being describe in the following figures.

Additionally, the technique of cross validation is valuable in estimating miss-classification error of partitioning models. K-fold cross validations use a re-substitution method that is efficient and unbiased.

The all-grain and df2rd model sets described in the previous section (Figure 11) were analyzed in terms of the RMSE of their fit between measured and predicted densities. A ten-fold cross validation was calculated for each of the 5-split incremental output steps per model set. An RMSE value was calculated for both the model fit and the model's cross validation (Figure 19).

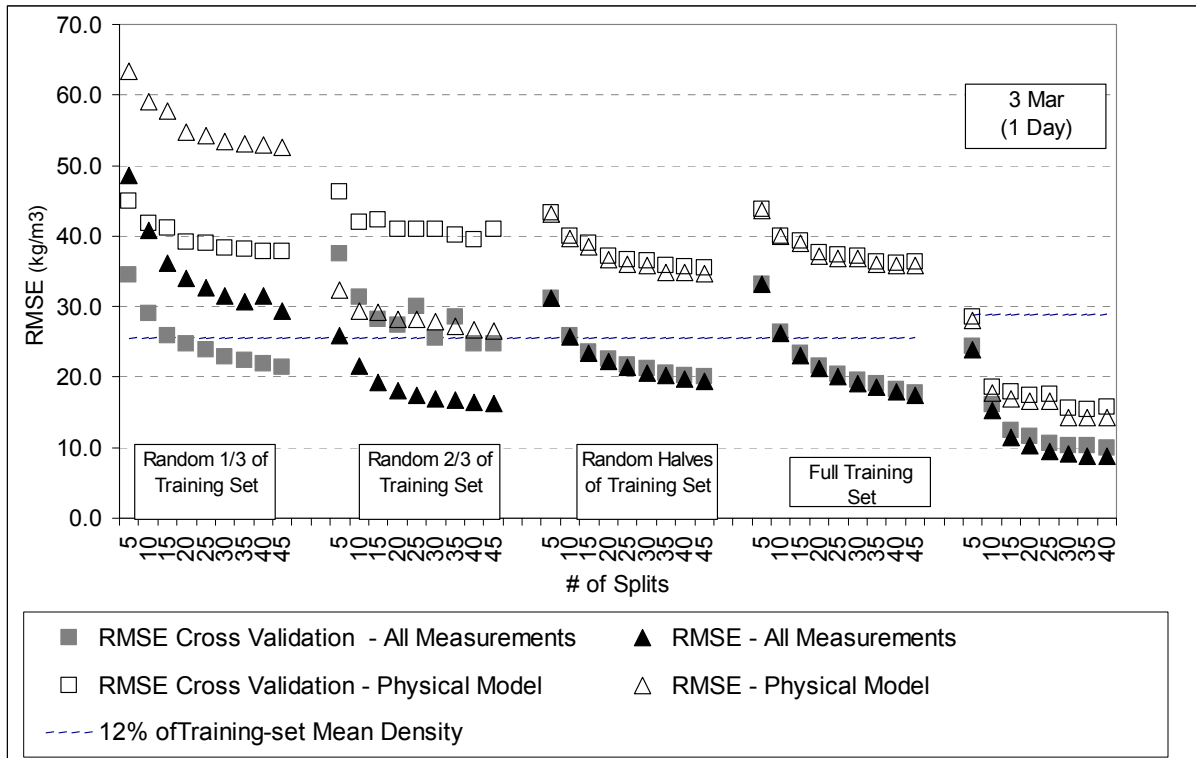


Figure 19. Comparison of fit accuracy for selected models as suggested by RMSE analysis.

Interpretations are possible based on the RMSE values illustrated above in Figure 19. A trend similar to one seen in the coefficient of determination analyses is present. In all cases, the df2rd physically based models do not perform as well as the all-grain models using all measurements for the given training-set. Though many of the values resulting from the all-grain training-sets are in the acceptable range for bulk density prediction at the higher splits, cross-validation indicates performance of the 1/3 and 2/3 partial training-sets failing to match the initial model run. The use of the full data or dividing it randomly in half, results in a cross validated models. The fit appears good and generally meets accepted practice values. The RMSE results support the sill for optimal decision tree size at 20 to 30 splits.

The seven incrementally larger training-sets described earlier in conjunction with Figure 13 were evaluated for their RMSE and cross validation. Each of the models fall within the accepted practice 12% mean bulk density with the exception of the 5 split output for the model constructed from five training-set days (Figure 20). Cross validation of the model fits consistently support the models except for the case of using the training-set for the one day prior to the 3 March validation-set. Generally for this selection of models, accuracy of fit decreases within the model at fewer number of splits and between models with increasing number of days in the training-sets. Models that incorporate measurements from the day

before the validation to three days earlier appear to be the most precise, i.e. lowest RMSE and with in the bulk density of the validation-set.

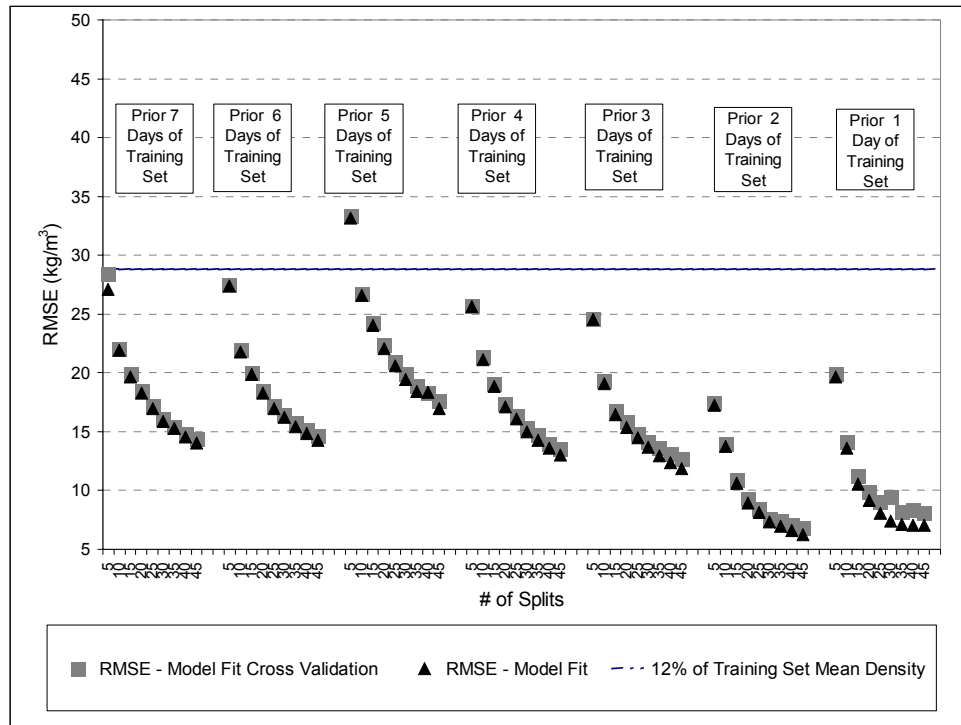


Figure 20. Accuracy comparison of increasing sized training-set models.

Prediction Accuracy for Selected Training-Sets

The accuracy of single-day models originally described in Figures 16 to 18 were investigated. RMSE values were calculated for the fit of the predictions of the 23, 25, and 26 February one-day models. Figure 21 highlights consistency in the 23 and 25 February models two to four days out. The RMSE values for these outputs are stable around 25 kg/m³. The outputs for the 26 February model fluctuate with the three-day out prediction paradoxically performing better than shorter prediction times. It is observed that the RMSE falls under accepted practice values only for models that prediction over fit was limited to approximately 5%. Figure 21 suggests that the variances of each one-day model are unequal. However, the sample sizes are small and therefore meaningful analysis of such is not appropriate.

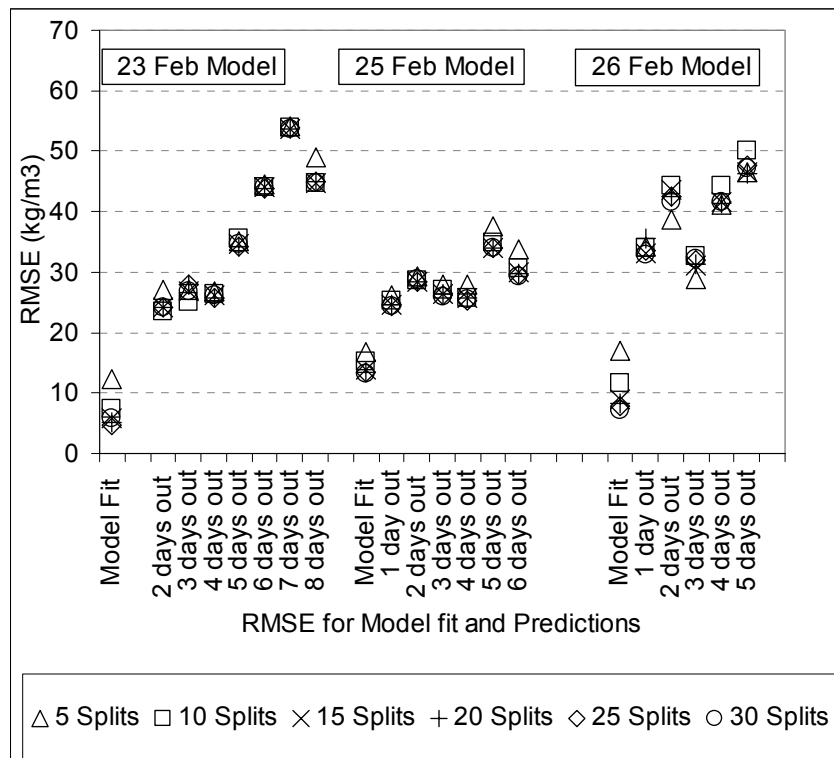


Figure 21. Accuracy of one-day training-set models applied to increasingly distant validation days.

5.3.3 Concluding Model Selection and Bulk Density Validation

The previous sections support the precept that construction of both accurate and precise bulk density models using various sized or aged training-sets is possible. In the final model analyses, I chose to use three individual days as validation-sets; the last training-set day and the two test case days. Two additional efforts were included to explore potential model improvements. The first was the manual intervention in splitting node selection by the statistical software. The second was use of a different effect variable as a factor.

Interactive versus Automated Construction Prediction Models

The previously discussed accurate and precise bulk density models were constructed by accepting the output of the JMP recursive partitioning platform without predetermining the choice of factor for various splits or pruning questionable splits. Interactive recursive partitioning of models is a method recommended to reduce the over-fitting that commonly occurs (Breiman et al., 1984; Davis et al., 1999; Friedman, 1977). This was undertaken for two iterations of three prediction models each applied to the last training-set day, 3 March.

For the first iteration of the three, the first split was made according to $movAvgYpt5cm$ values regardless of whether it resulted in creating the largest difference. This was tested based on an assumption that the $movAvgYpt5cm$ variable represents properties associated to the ice lattice structure relative to ϵ'' . Subsequent splits were according to the software's internal rules described earlier.

The procedure was followed to create prediction models for 3 March based on 2 March (one training-set day), 1-2 March (two training-set days), and 28 February – 2 March (three training-set days).

Each model was constructed to 40 splits and then the ten worst nodes were pruned. This pruning removed the splits that used the smallest discrimination cutting values.

Each model was 10-fold cross validated. The fits for model, cross validation, and prediction are shown in the following figures with accuracy (RMSE) and precision (R^2) as x and y-axes. Results are shown in Figure 22. The two-day model had the highest precision and accuracy followed by the three-day, then the one-day. Cross validation results were highest precision and accuracy for the three-day, followed by the two-day, then the one-day. Fit accuracy and precision for the 3 March validation-set followed suit with the cross validation ranking: three, two, then one-day models.

The mean density for the validation-set day was 240 kg/m^3 (accepted practice range: $<28.8 \text{ kg/m}^3$) placing the prediction results outside “accepted practice” values.

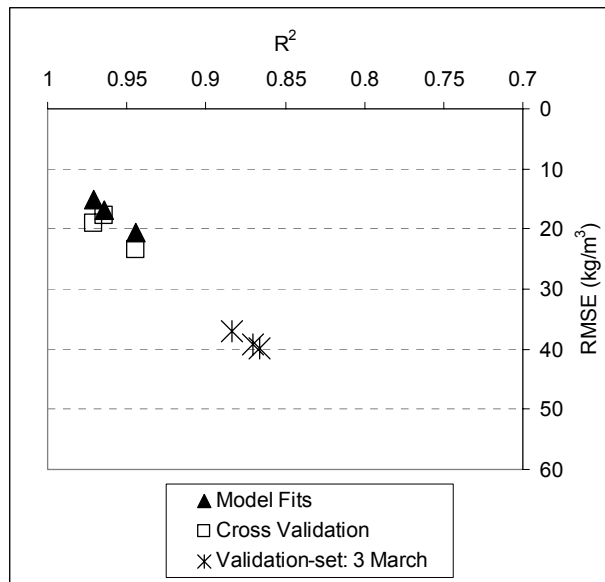


Figure 22. Overall fits for one, 2, and 3 consecutive training-set day, interactively constructed model applied to validation-set.

In the second iteration of one, two, and three-day models for validation against 3 March, no forcing of the first or any split was done. In allowing the automated choice of discrimination values, the model fits were better and improved predictions resulted. The single-day training-set model provided predictions very near the accepted practice limit, 29.7 versus 28.8 kg/m^3 (Figure 23). The one-day model had the highest precision and accuracy followed by the two-day, then the three-day. Cross validation results were highest precision and accuracy for the one and two-day, followed by the three-day. Fit accuracy and precision for the 3rd of March validation-set results ranked the two-day highest, one-day second, and the three-day lowest. Residual analysis of the model fits generated Shapiro-Wilk test statistic values (W) for the one, two, and three-day models of 0.970 , 0.956 , and 0.785 respectively. This suggests strong to moderate strength for the models. In this example, the one-day model is the overall better performer.

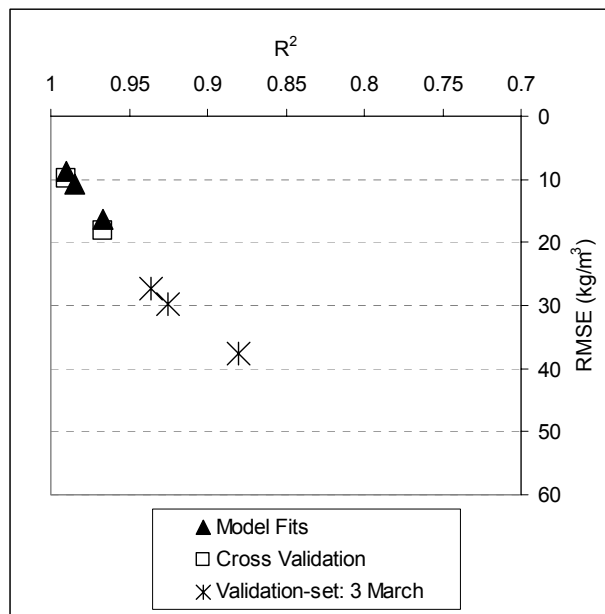


Figure 23. Fits for non-interactive one, two, and three consecutive day training-set model, model cross validation, and validation set.

The same procedure was followed to create two iterations of prediction models for the last three days of the training-set for application to the two test case days (Figure 24). Three models were constructed to make predictions for the test case days that consisted of one, two, and three consecutive training-set days (3 March, 2-3 March, and 1-3 March). Not evident in the graphic trend towards less accuracy and precision from the model fit to test case 2 is the ranking of the three. The three-day model predicted best, the one-day second, and the two-day third as shown in Table 13. Mean density for test case 1 was 263 kg/m³ and 285 kg/m³ for test case 2, 12% of which are 31.6 kg/m³ and 34.2 kg/m³ respectively. Only the one and three-day models applied to test case 1 fall within accepted practice range.

The one-day model had the highest precision and accuracy followed by the three-day, then the two-day. Cross validation results followed the same ranking. Fit accuracy and precision for the 5 March test case results ranked the three and one day highest and the two-day lowest. The same (3,1, 2-day) ranking was found for the 10th of March test case fit results. Residual analysis of the model fits generated Shapiro-Wilk test statistic values (W) for the one, two, and three-day models of 0.79, 0.801, and 0.861 respectively suggesting the accuracy and the precision of the predictions are related to the strength of the model.

Results of the models when applied to the test case days are contrariety; clearly there are conditions related to time and distance from the training-set that affect the model's ability to predict bulk densities. Application of non-interactively developed models generated overall fits at lower values for both test cases.

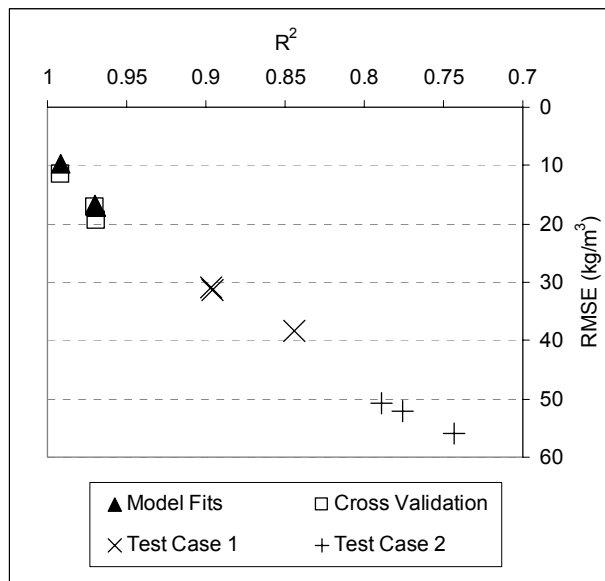


Figure 24. Overall fits for one, two, and three consecutive training-set day, interactively constructed model applied to the test cases.

R ² / RMSE	Model Fit	Test Case 1	Test Case 2
1-day	.992 / 9.8	.896 / 31.3	.776 / 52.2
2-day	.969 / 17.1	.844 / 38.3	.743 / 56.0
3-day	.970 / 16.6	.897 / 31.0	.789 / 50.8

Table 13. R² and RMSE values for model and test case fits of 1, 2, and 3 consecutive day models illustrated in Figure 24.

Unique Case Predictive Model Construction

Kuroiwa (1962) demonstrated large time-lapse dielectric measurement changes of snow. He attributed this ageing affect to the shortening of electrical paths due to ice bonding between grains. Without the ability to attach dates, and therefore age, to various snow pack layers a proxy was adopted for one round of model development. Distance from the surface (variable: locat) is assumed an ordinal metric representing the temporal sequence of the layers. The argument for use of this proxy can only be made when considering the flat, uniform conditions present in the study plot area. It would be inappropriate to use in extrapolating such a model to different locations or shaped stratigraphy on slope features and therefore is limited to this sole application and discussion. A one, two, and three-day training-set based model was constructed using movAvgXpt5cm, movAvgYpt5cm, locat, and TGslope in the same manner described in the previous section. The snow temperature was not used because it was strongly cross-correlated to the depth. This yielded a highly precise model with prediction accuracy better than “accepted practice”. The prediction R² and RMSE values of these models against the 3 March data set are illustrated in Figure 25.

The one-day model had the highest precision and accuracy followed in order by the two and three-day models. Cross validation results followed the same ranking. Fit accuracy and precision for the

unique model predictions for the 3 March validation-set were clustered extremely close with the three day highest ranked nearly identical the two-day, which was slightly higher than the one-day. Residual analysis of the model fits reflected the same tight cluster. The Shapiro-Wilk test statistic values (W) for the one, two, and three-day models of 0.952, 0.950, and 0.949 respectively suggests including the ageing proxy makes the model insensitive to the number of training-set days used in its construction.

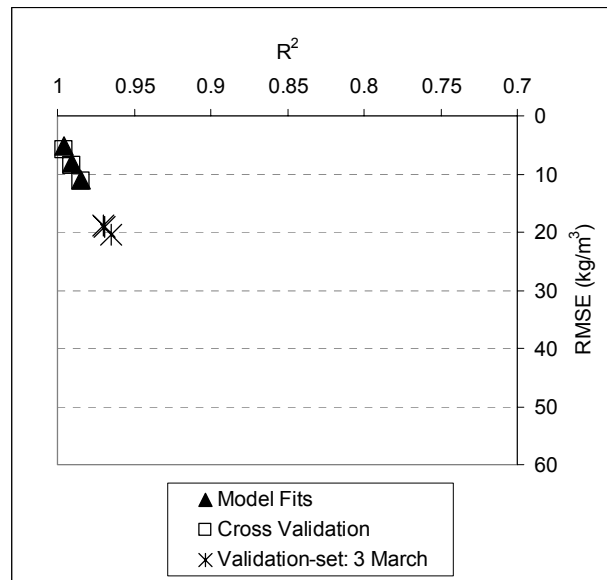


Figure 25. Exceptional overall fits for one, two, and three consecutive day training-set model, model cross validation, and validation set with inclusion of ageing proxy as an effect factor.

5.3.3 Bulk Density Conclusions

The use of accuracy (R^2) and precision (RMSE) values of the bulk density fit for predictions regressed over the length of the profile is consistent with other studies of snow profiling probes. The following conclusions are supported by the results presented in previous sections:

- Increases in time and space between training-set collection (calibration values) and application reduce the accuracy and precision of predictions made with probe measurements.
- Variations in processes dominant in the organization of local stratigraphy spatially limit application of predictions made with probe measurements.
- Physical process based models do not improve accuracy or precision of the results.
- Models are possible that provide bulk density predictions that account for 92% of the variability in the manual density measurements and are within “accepted practice” values (97% in a unique case).

The JMP scripts using the four factors (movAvgXpt5cm, movAvgYpt5cm, slopeTemp, and TGslope) for the models shown in Figures 23 and 24 are provided in Appendix J for reference. These prediction model scripts are unique to the samples taken due to local impurities and this study, however the modeling technique is valid and applicable to use of the probe.

5.4 Predicted Density Profile Analysis

The probe's ability to provide information with a strong relationship to the bulk density over the profile depth was shown in the previous sections. The manual density measurements were taken over discrete 3 cm intervals. The probe measurements, even though scaled to be comparable were taken at relatively random locations. This allowed statistical bulk density correlation but necessitates alternative method for comparison of manual density stratigraphy versus that described by the probe This section contains analysis of the relationship of the final three predictive models (Figures 23, 24, and 25) to the layered density profile.

Visual comparison of snow profiles for classification is not without precedent (de Quervain and Meister, 1986). I am confident that the relative accuracy between the probe profile and manual is such that visual fitting is acceptable for the following analysis based on the diligence exercised during data collection and preparation

5.4.1 Test Case 1: 5 March 2006

Test case 1 was the first of two sets of field day data gathered approximately 25 kilometres due north of the Mount Fidelity. It was collected below tree line near a backcountry ski lodge's sheltered weather observation plot. The lag between the last training-set day and the observation day was 2 days.

Figure 26 shows the profiles calculated for the test case based on the one, two, and three consecutive day training-set models. The interactively partitioned model was used because its overall accuracy and precision results were higher than the non-interactively generated ones. The three-day model approximates the manual density profile the nearest. Similar areas of visual fit can be seen for all three model applications. The fit is especially good in the top 40 cm where layer identification using the brush technique consistently represented the greatest variation as recent and storm snow is undergoing initial metamorphism. The fit is also good in the lower 60 cm of the profile. The most difference between the two is seen in the middle 40 cm of the profile around the first homogeneous layer and the density range of 200 to 300 kg/m³. The three modeled profiles are shown in conjunction with the manual profile in Figure 27. Though the profile shapes are close, the probe profile is not sufficiently close to the manual profile to replace it in representing the structure of the snow cover. This visual conclusion is in agreement with the R² and RMSE results for the same models.

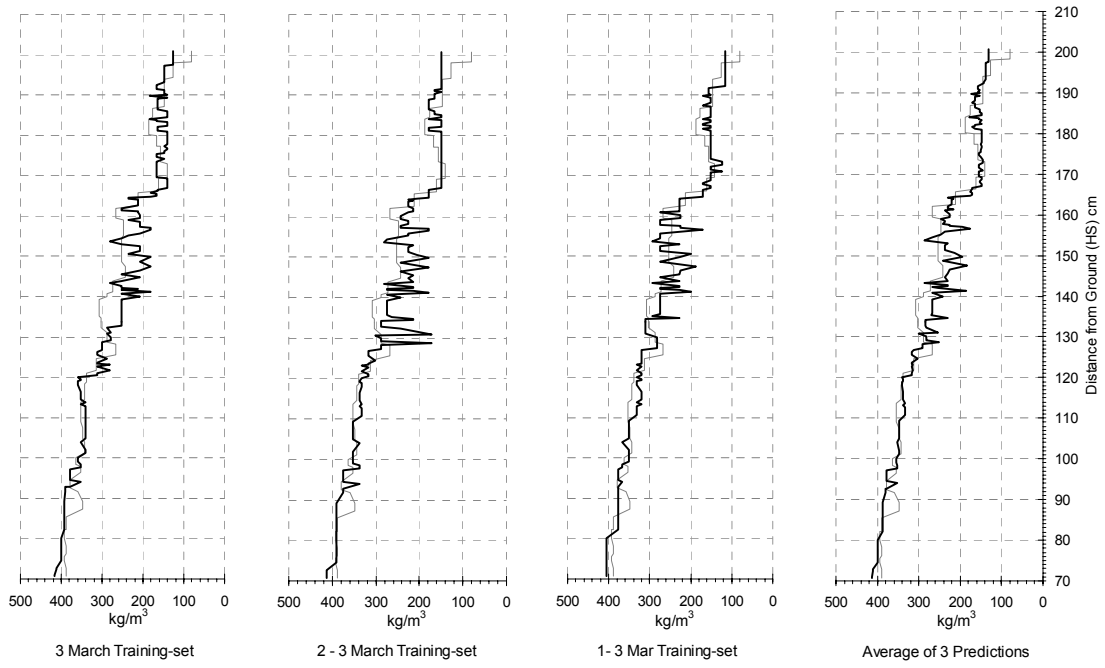


Figure 26. Predicted density profiles shown in relation to the measured density profile for test case 1 based on one, two, and three-day training-set models. The heavier and darker line represents the predicted profile while the lighter line is the manually measured density profile.

5.4.2 Test Case 2: 10 March 2006

Test case 2 was collected 400 m away at near the same elevation but in an open alpine valley bottom between two lateral moraines where the snowcover was exposed to regular winds and their effect to stratigraphy. The lag between the last training-set day and the observation day was 7 days and 5 days following test case 1.

Figure 28 shows the profiles calculated for test case 2 based on the one, two, and three consecutive day training-sets. The three-day model approximates the manual density profile the nearest. Again, similar areas of visual fit can be seen for all three model applications. The manual density and layer profile highlight the existence of dramatic differences in density and hardness, sometimes paradoxically as in the region from 160 to 175 cm above ground. Similar to test case 1, there is good agreement in the top 35 cm where layer identification using the brush technique indicates the most variation. The fit is also good in the lower 50 cm of the profile. The most difference between the two is seen in the middle of the profile in the transition of densities from 200 to just less than 400 kg/m³. The three modeled profiles are shown in conjunction with the manual profile in Figure 29. Empirically, the probe profile is not sufficiently close to the manual profile to replace it in representing the structure of the snow cover. This conclusion is supported by the earlier accuracy and precision analysis that placed all three models outside the accepted practice values for bulk density.

This test case represents a snow pack that is most different from the rest. A primary mechanism present is that of wind transport and wind packing of snow. Not only does the wind affect the shape of snow grains but also it is believed to organize the structure in a uniform relationship to the wind direction.

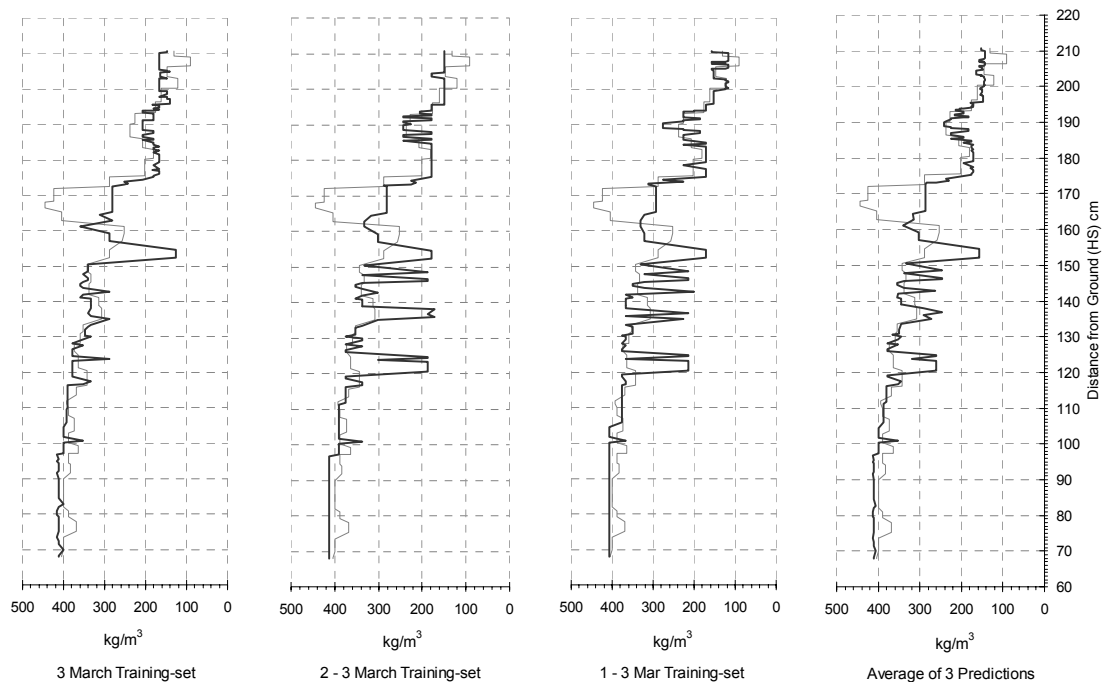


Figure 28. Predicted density profiles for Test Case 2 based on one, two, and three-day training-set models. The heavier and darker line represents the predicted profile while the lighter line is the manually measured density profile.



Snow Cover Profile

Location: Nordic Lake Date: 06 March 10
 Sky: ☁ Wind: calm Air Temperature: Time: 12:18
 Aspect: s Elevation: 2085 Incline: 3 Observer: SMC KE

HSW:

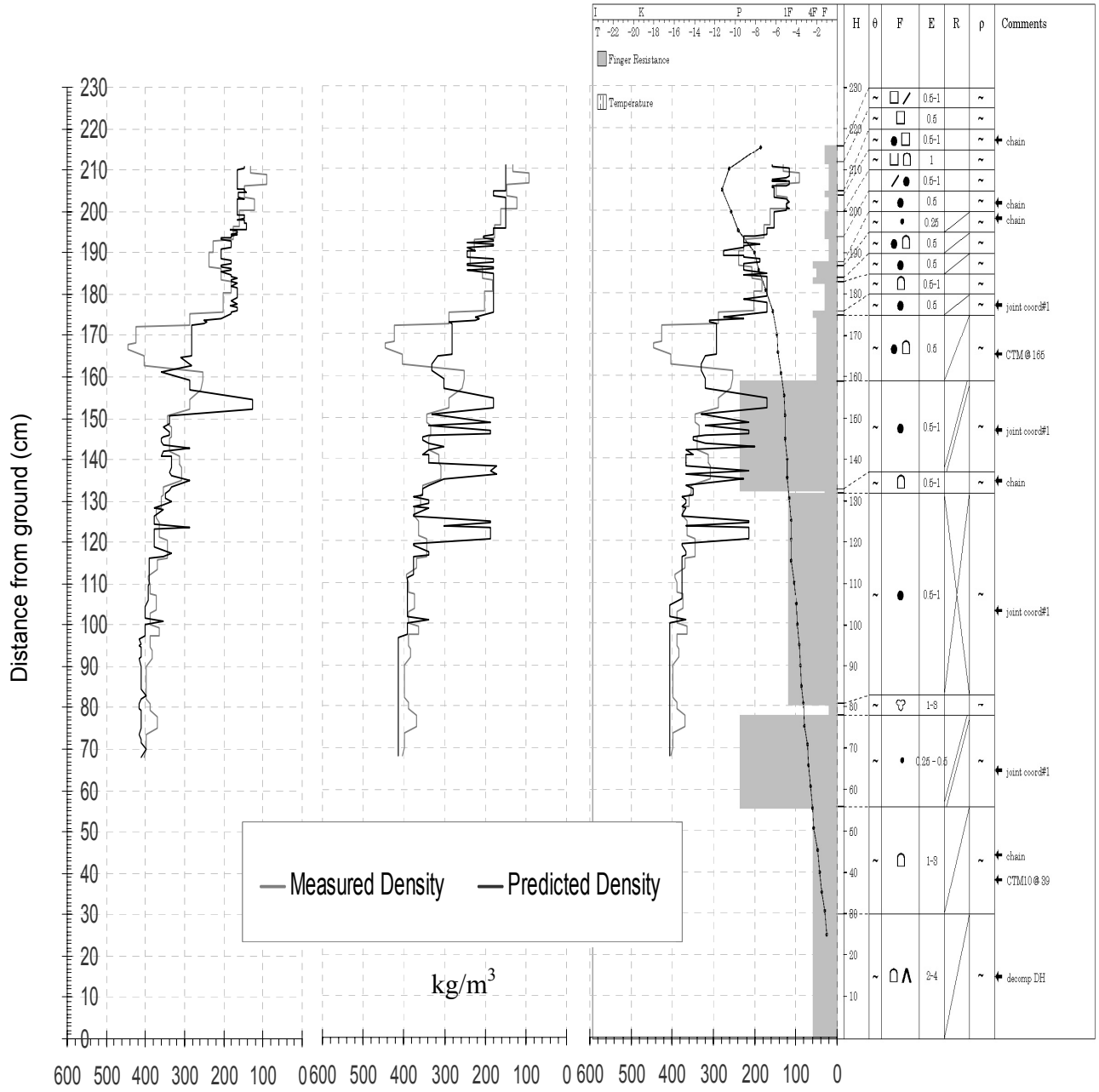


Figure 29. Modeled density profiles for test case 2 shown in conjunction with the manual snow profile. The heavier and darker line represents the predicted profile while the lighter line is the manually measured density profile. Left to right: 3 March training-set, 2-3 March training-set, and 1-3 March training set.

5.4.3 Validation-set: 3 March 2006

Two presentations are included of predicted profiles for the validation-set day immediately following the training-set days and in a location less than two meters away. The first includes the same model factors as presented in the test cases. The second uses the prediction model that included the ageing proxy, which proved most accurate and precise for bulk density.

Figure 30 shows the profiles calculated for the 3 March validation-set based on the one, two, and three consecutive day training-sets. Again, similarities of visual fit can be seen for all three model applications. The overall visual fit is better than each of the test cases in agreement with the better bulk accuracy described earlier. Variations between predicted and measured profiles tend to follow the trend of the measured profile, e.g. where the predicted is a greater density, it corresponds to the boundaries of a region of higher density such as 190 to 193 cm above ground. Unfortunately, the vertical position accuracy is not such that the negative spikes in the profile density can be definitively attached to the thin, low resistance layers identified in the manual profile such as at 193 cm and between 170 and 180 cm. The three modeled profiles are shown in conjunction with the manual profile in Figure 31. Empirically, the probe profile is not sufficiently close to the manual profile to replace it in representing the structure of the snow cover.

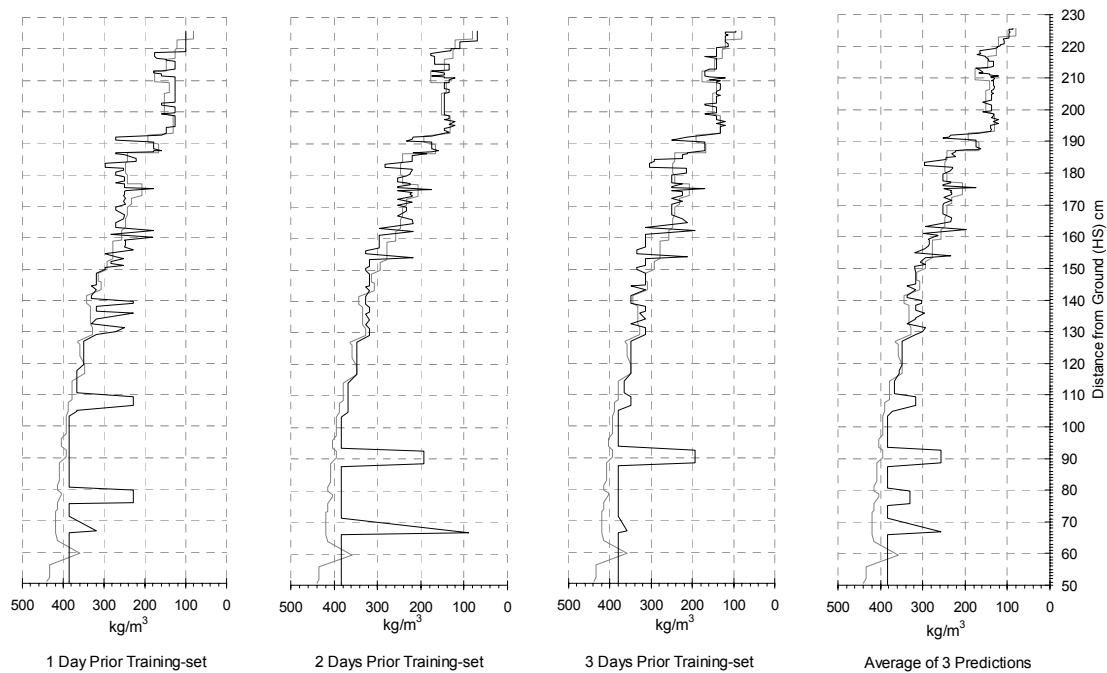


Figure 30. Predicted density profiles for 3 March validation-set based on one, two, and three-day training-set models. The heavier and darker line represents the predicted profile while the lighter line is the manually measured density profile.



Snow Cover Profile

Location: Fidelity Flats

Date: 06 Mar 3

Sky: ○

Wind: L-M@N

Time: 1123

Aspect: 0

Elevation: 1905

Incline: 0

Observer: SMC

HSW:

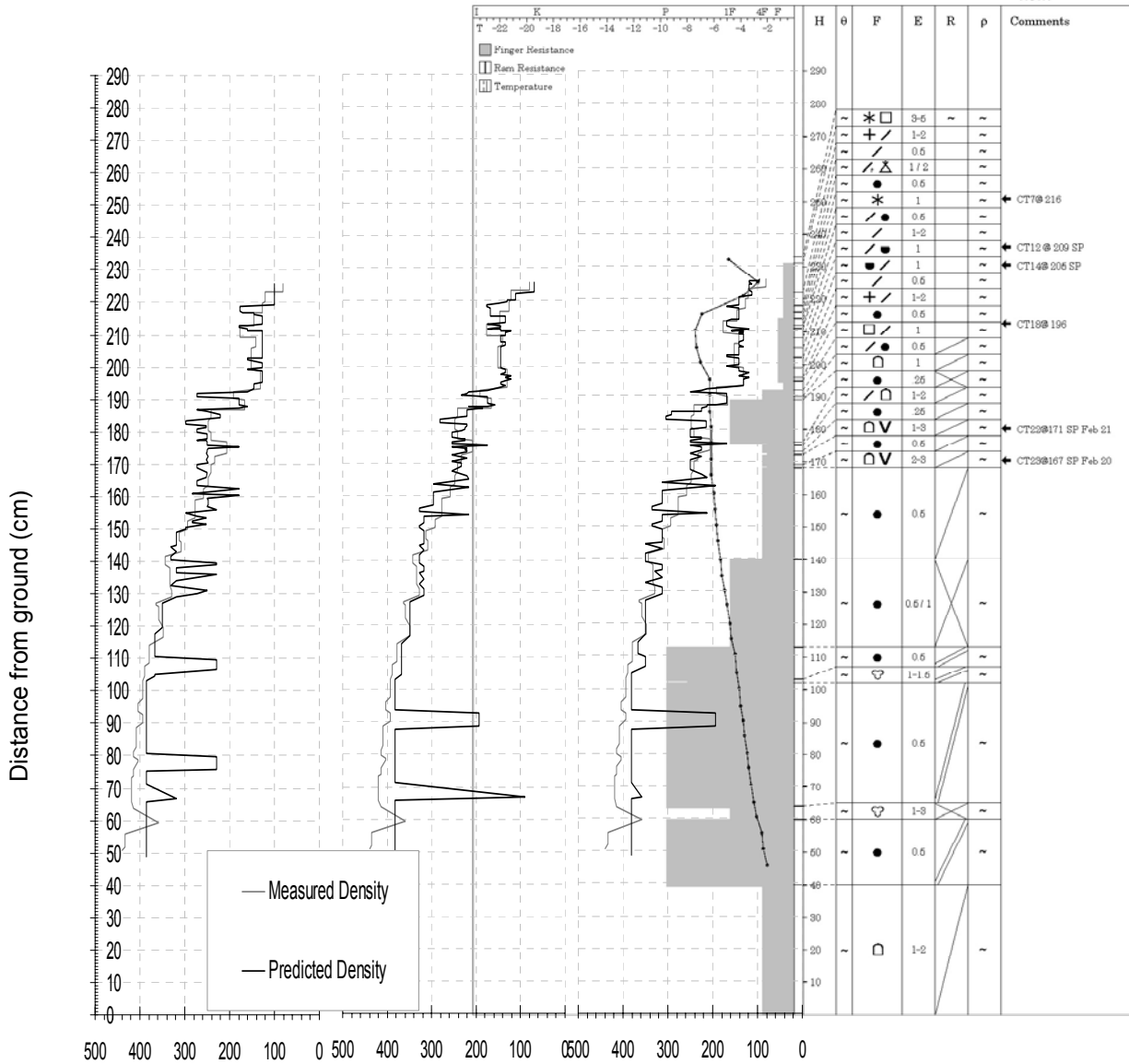


Figure 31. Modeled density profiles for 3 March validation-set shown in conjunction with the manual snow profile. Left to right, 2 March training-set, 1-2 March training-set, and 29 Feb – 2 March training-set.

Figure 32 shows the profiles calculated for the 3 March validation-set based on the one, two, and three consecutive day training-sets using the model that included the ageing proxy. There is less variation between the two density profiles and overall visual fit is better than the previous examples. The predicted profile closely mimics the measured density profile except in a few instances where comparison to the manual layer profile (Figure 33) suggests structure or distinct thin layers contained in the manual density sample may play a role. These are between 190 and 200 cm above the ground and between 170 and 180 cm. There is also more smoothing of the predicted density in the lower 100 cm of the profile than the models with out the ageing proxy shown earlier in Figure 30. The predicted density profiles in Figure 32 could replace the manual profile in representing the snow cover.

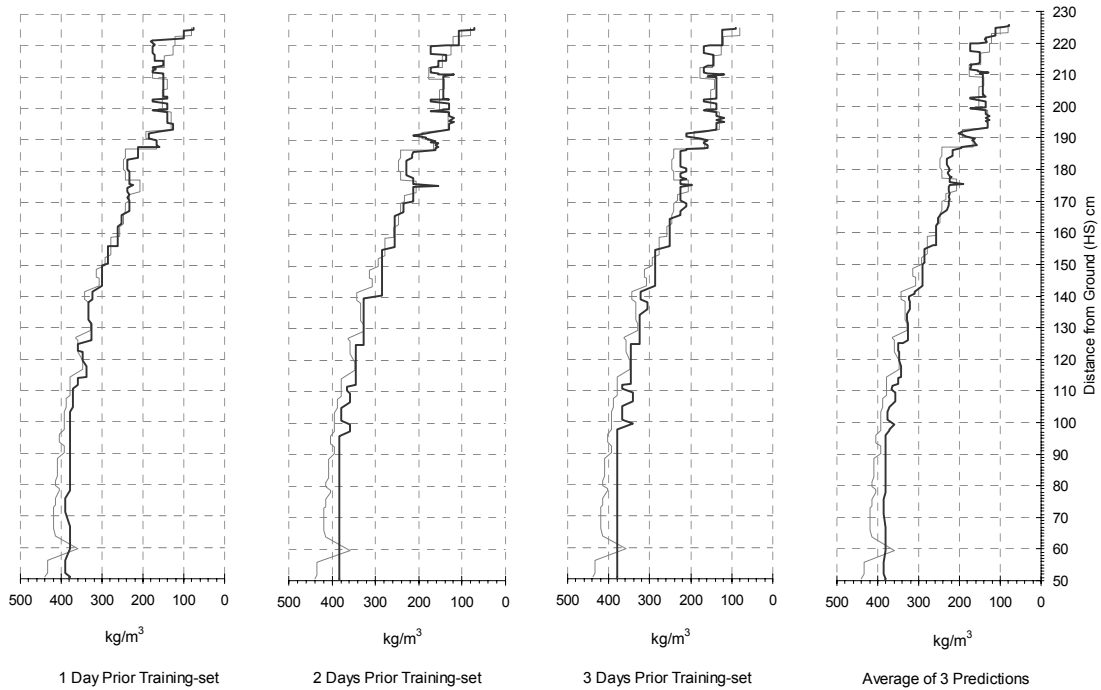


Figure 32. Predicted density profiles for 3 March validation-set based on one, two, and three-day training-set models including ageing proxy. The heavier and darker line represents the predicted profile while the lighter line is the manually measured density profile.

Chapter 6 CONCLUSIONS

6.1 Summary

In this study, I evaluated the performance of a probe designed to quickly gather vertically continuous snow density profiles relevant to avalanche forecasting and snow hydrology through measurement of dielectric properties. Such a validation is both valuable and difficult. A conundrum exists when evaluating new technology relative to avalanche forecasting. There must be far less uncertainty to the new method than the classic one if it is to be adopted. However, if the new technology or method is not replacing an existing one, it merely needs to illustrate a relation to empirical observations at a less rigorous level. Snow profiles are time consuming and limited to a specific location. Improvement to this activity would be in the form of faster information collection and more sampling sites over the time required for just one manual profile.

Snow profiles provide information of medium importance and uncertainty (Class II) about the characteristics of snow stratigraphy relative to patterns associated with avalanche formation and activity. Because avalanche forecasting already focuses on interpreting uncertainties, the practices of observing the snow stratigraphy and of the determination of snow profiles receive an inordinate amount attention since they are a tangible activity.

Early avalanche forecasting efforts included the use of both density and ram hardness profiles. Vertically continuous density profiles have not continued to be utilized in avalanche forecasting due to the substantial time required. The relative lack of additional information beyond the general shape interpretation of a ram profile, and the fact that other variables such as hardness seem more important. An exception is Conway and Wilbour's model (1999).

An apparent relationship has been described between hardness and the combination of microstructure and density. A relationship between snow's dielectric properties and its density has been shown in prior work by others. It has also been suggested (by others) that the dielectric properties of snow might relate to its structure (grain shape, size, and bonds).

I investigated three hypotheses. The first tested whether bulk snow density measured by the probe is equal to or better than currently accepted practice. A supporting study determined that the range of values for "accepted practice" includes under sampling errors of 1 to 2%, variation within individual cutters of 0.8 to 6.2%, and variation between cutters of 3 to 12%. The results of a statistical analysis suggest that snow density measurements taken by various density cutters might be significantly different from each other. Given the mean of all samples is the accepted true value of the measured density, variation solely in cutter types provides "accepted practice" measurements that are within 12% of the true density.

Methods consistent with other studies of snow profiling probes provided results that supported the following conclusions. These conclusions are limited to training-set values collected one day prior and application of the prediction model to near-by terrain with similar history of weather events and snow accumulation.

- It is possible to create models from single-day training-set measurements accounting for 92% (97% in a unique case) of the variability between bulk density predictions and manual density measurements and that are within “accepted practice” values.
- Increases in time and space between training-set collection (calibration values) and application reduce the accuracy and precision of predictions made with probe measurements.
- Physically based process models did not improve accuracy or precision of the results.
- Variations in processes dominant in the organization of local stratigraphy or the presence of contaminants appear to limit application of predictions made with probe measurements.

I have confidence in the reproducibility of these conclusions based on field experience with the probe, the method of analysis, and trends evident throughout the results. The modeling technique is valid and applicable to future, similar use of the probe.

Failure to reject the null hypothesis here does not validate its use in avalanche forecasting though it does validate the probe’s intended design of measuring snow densities. It does however strongly support the probe’s use in snow hydrology applications for dry snow. Manual, bulk density measurements using tools such as the Mount Rose snow sampler have error ranges of -9.1 to $+18.5\%$ with a mean error of 10.0 to 10.3% (Goodison et al., 1981).

In applied use, the predicted measurements of mass per volume would allow gathering useful load or snow water equivalent values over a small area. This study suggests inconsequential scaling issues in up-scaling the support scale measurements from the probe to the support of small density cutters. Patterned consistency in the validation of the models suggests extrapolation along the extent scale decreases as time and space increase.

The second hypothesis explored whether a density profile as estimated by the probe is equal to or better than currently accepted practice. Mechanical problems with the probe prevented numerical comparison of predicted and manual profiles. Visual analysis ascertained that though predicted and measured density profile shapes were close, the probe profiles were generally not sufficiently close to the manual profile to replace it in representing the structure of the snow cover. One case utilizing an ageing proxy did fit close enough for practical use. This model is constrained to use in areas that possess the same weather event and accumulation history such as a study plot or possibly a small slope (limited extent).

The third hypothesis investigated whether characteristics associated with structure and stratigraphy in the snowpack could be identified in the information provided by the probe. The results of this study were inconclusive primarily due to the mechanical problems with the encoder. The manually identified layer boundaries were located relative to the scale attached to the probe at a resolution of 0.25 cm with an estimated accuracy ± 0.1 cm. The vertical accuracy of probe measurements ± 0.7 cm associated with the location of manual measurements precluded analyses matching density measurement boundaries. Without the ability to know with appropriate accuracy the location of probe measurements relative to a reference such as the surface, the measurements could not be analyzed against careful observations and measurements of grain type, size, and test failure locations. However, even without high accuracy in the location of probe measurements, one can compare or gain information

from the shape of profiles. My experience with the probe output and with the manual observations suggests the nature of grain bonding plays a noticeable role in the properties measured. This is can be interpreted from the smoothing of densities predicted by the probe at higher densities that include rounding facets (mixed forms) lower in the snowpack along with visible signal and prediction changes at the new snow or storm snow interface to old snow.

6.2 Study Limitations

The most glaring limitations of this study are those resulting from equipment constraints and problems. One limitation manifested in the study is that only the top 190 cm of the pack is addressed on any given test day. The results and conclusions might be different if the lower portion of the snow pack was considered. However, most training and validation-set profiles included higher densities e.g. 400+ kg/m³ and examples of faceted grains. Variations may be expected when considering depth hoar. Another limitation is the inability to know the vertical location of the probe measurements at accuracy equivalent to the manual measurements. Confidence is high that they are relatively close (within 1 cm) due to the use of the probe left in-situ as the measuring device and careful manual measurements.

Another limitation is the inability to compare outcomes of this study with other published work due to the lack of ability to calculate dielectric values from the probe measured voltages. Fortunately, the voltages appear to represent a response equivalent to the dielectric properties for the physical properties being measured.

6.3 Future Work

6.3.1 Investigations and Analyses

This study has established a baseline for accurate use of the probe. The next step is evaluation of the probe measurements in relation to specific structure and texture. There is ample evidence in the information collected during this study that points towards the probes ability to differentiate areas of similar bonding. A field method of identifying bonding structure will be necessary to accomplish this as will improvement of the vertical accuracy of the probe as described in the next subsection.

Preliminary investigation of the spatial consistency of the probe measurements indicated good correlation between parallel plunges. The movAvgXpt5cm values for the plunges made on 17 March are shown in Figure 34. Table 14 presents the correlation matrix of the various plunges.

	Plunge 1	Plunge 2	Plunge 3	Plunge 4	Plunge 5	Plunge 11	Plunge 10	Plunge 9	Plunge 8	Plunge 7	Plunge 6
Plunge 1	1.000	0.936	0.945	0.942	0.950	0.904	0.952	0.942	0.941	0.865	0.908
Plunge 2	0.936	1.000	0.934	0.920	0.944	0.879	0.938	0.922	0.915	0.814	0.883
Plunge 3	0.945	0.934	1.000	0.947	0.926	0.907	0.935	0.918	0.916	0.837	0.876
Plunge 4	0.942	0.920	0.947	1.000	0.935	0.904	0.937	0.930	0.932	0.887	0.897
Plunge 5	0.950	0.944	0.926	0.935	1.000	0.882	0.954	0.938	0.923	0.874	0.899
Plunge 11	0.904	0.879	0.907	0.904	0.882	1.000	0.899	0.906	0.930	0.854	0.929
Plunge 10	0.952	0.938	0.935	0.937	0.954	0.899	1.000	0.954	0.931	0.862	0.927
Plunge 9	0.942	0.922	0.918	0.930	0.938	0.906	0.954	1.000	0.951	0.881	0.921
Plunge 8	0.941	0.915	0.916	0.932	0.923	0.930	0.931	0.951	1.000	0.895	0.926
Plunge 7	0.865	0.814	0.837	0.887	0.874	0.854	0.862	0.881	0.895	1.000	0.876
Plunge 6	0.908	0.883	0.876	0.897	0.899	0.929	0.927	0.921	0.926	0.876	1.000

Table 14. Correlation matrix for parallel plunge variable movAvgXpt5cm values.

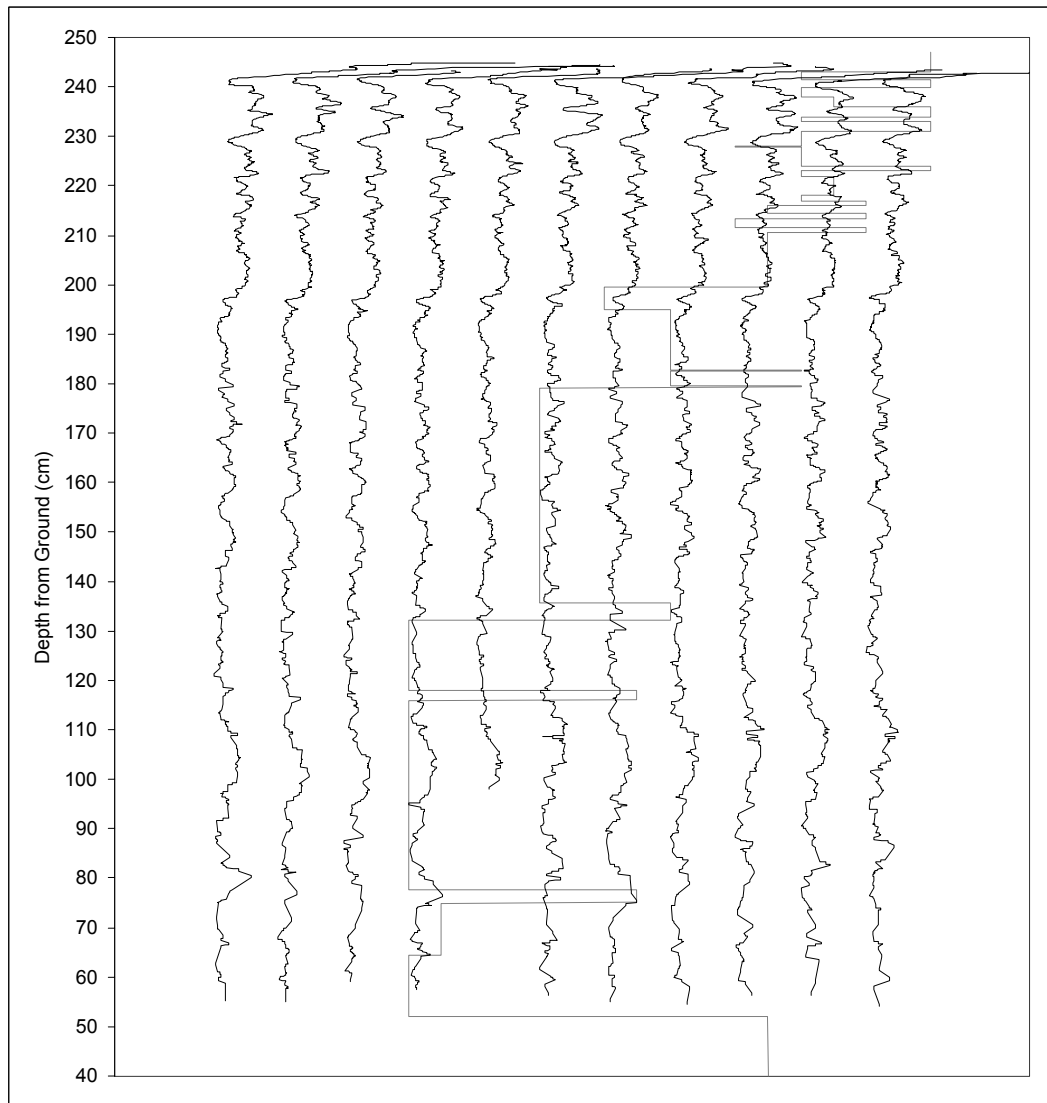


Figure 34. Traces of movAvgXpt5cm variable for parallel plunges 30 cm apart. The order of the plunges left to right are 1, 2, 3, 4, 5, 11, 10, 9, 8, 7, 6 that correspond to the plunge numbers in Table 5. Relative hand hardness layering is shown for reference in grey.

6.3.2 Probe Improvements

Suggestions for several improvements to the probe resulted from its use and evaluation. A key and primary improvement would be sample recording triggered at specific vertical increments rather than governed by a temporal cycle. The spacing that the current encoder is capable of (0.48 mm) is more than adequate. The addition of a second set of sensors at an optimal distance apart would allow simple field averaging and quality control of measurements. If possible, a set of sensors that sampled along the vertical axis of the probe might provide information that recognized a lack of bonding between layers.

General usefulness would be improved if the unit were to be better adapted to rugged fieldwork with the appropriate display screen, cabling, and connections for the winter environment. Incorporation of a set of capacitance sensors identical to those on the probe in a box-type density cutter would allow efficient and potentially more accurate calibration to a training-set. The ability for field visualization of the collected profile will ultimately change the instrument from research focused to operationally viable.

6.3.3 Other Recommendations

An outcome of this study is the recommendation that observation guidelines and recording standards include descriptions of density cutter technique. The wedge and tube cutters are prone to higher variances if used on one axis versus another. A wedge shaped density cutter when inserted horizontally (top of wedge sloping from the top at the front to the bottom at the back and the bottom parallel to the layering), 75% of the measured volume is in the lower half of the measurement (Figure 35) providing a vertically biased sample. When it is rotated 90° and inserted with the bottom and top of the wedge plumb, any layering bias is removed. This is reflected in the description by the current manufacture of wedge cutters.

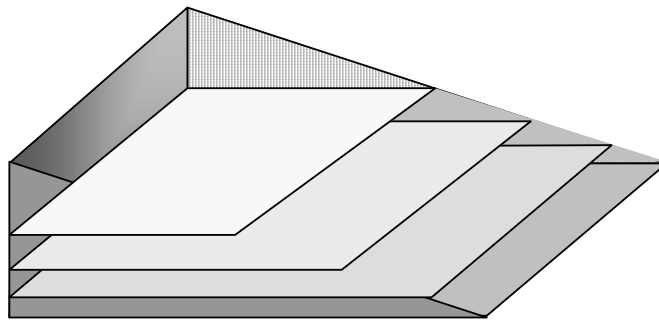


Figure 35. Illustration of varying vertically segregated volume percentages sampled by a wedge-type density cutter when inserted horizontally.

A similar condition exists when using tube density cutters. They should be inserted with the cylinder axis vertical, cutting down through the layer to a pre-placed metal spatula or snow crystal card. This will provide a sample with less variance than inserting horizontally. This effectively limits the thickness of layers that these two types can sample based on the length of the tube or width of the wedge.

BIBLIOGRAPHY

- Abe, O., Sato, H., Chiba, M. and Tanasawa, S., 1998. The advanced digital snow sonde. *Proceedings: International Snow Science Workshop 1998*, Sunriver, Oregon. 300 - 304.
- American Society for Testing and Materials (ASTM), 2002. *D5301-92 Standard Practice for Physical Characterization of Paint Brushes*. ASTM International, West Conshohocken.
- Andersen, V.H., 1960. A technique for photographing snow-pit stratigraphy. *Journal of Geophysical Research*, 65(3): 1080-1082.
- Armstrong, R.L., 1976. The application of isotopic profiling snow gauge data to avalanche research. In: *Avalanche Release and Snow Characteristics, San Juan Mountains Colorado - Final Report 1971-1975*. R.L. Armstrong and J.D. Ives (Eds), Institute of Arctic and Alpine Research, Boulder, 131 - 143.
- Armstrong, R.L., 1985. Metamorphism in a subfreezing, seasonal snow cover. The role of thermal and vapor pressure conditions. (Ph.D. Thesis, University of Colorado, Boulder). 175.
- Arons, E.M. and Colbeck, S.C., 1995. Geometry of heat and mass transfer in dry snow: A review of theory and experiment. *Reviews of Geophysics*, 33(4): 463 - 493.
- Associate Committee on Geotechnical Research, 1982. *Guidelines for Weather, Snowpack, and Avalanche Observations, Technical Memorandum No. 132*. National Research Council.
- Atwater, M., 1968. *The Avalanche Hunters*. Macrae Smith, Philadelphia.
- Atwater, M. and Koziol, F.C., 1952. *Avalanche Handbook*. U. S. Dept. of Agriculture, Forest Service, Washington.
- Auty, R.P. and Cole, R.H., 1952. Dielectric properties of Ice and Solid D2O. *The Journal of Chemical Physics*, 20(8): 1309-1314.
- Bader, H., 1954. Mineralogy and structural characterization of snow and its metamorphism. In: *Der Schnee und Seine Metamorphose*. H. Bader, R. Haefeli, E. Bucher, J. Neher, O. Eckel, C. Thams and P. Niggli (Eds), Beitrage zur Geologie der Schweiz, Bern, 1-56.
- Bader, H., 1962. *The Physics and Mechanics of Snow as a Material*. II-B, US Army CRREL, Hanover. 79.
- Bader, H., Haefeli, R., Bucher, E., Neher, J., Eckel, O., Thams, C. and Niggli, P., 1954. *Snow and its Metamorphism*. Snow, Ice and Permafrost Research Establishment, Wilmette.
- Bartelt, P. and Lehning, M., 2002. A physical SNOWPACK model for the Swiss avalanche warning Part I: Numerical model. *Cold Regions Science and Technology*, 65: 123-145.
- Birkeland, K.W., Hansen, K.J. and Brown, R.L., 1995. The spatial variability of snow resistance on potential avalanche slopes. 41(137): 183-190.
- Blöschl, G., 1996. Scale and scaling in hydrology. *Wiener Mitteilungen: Wasser, Abwasser und Gewässer*, 132: 70-99.
- Bovis, M.J., 1976. Statistical analysis. In: *Avalanche Release and Snow Characteristics, San Juan Mountains Colorado - Final Report 1971-1975*. R.L. Armstrong and J.D. Ives (Eds), Institute of Arctic and Alpine Research, Boulder, 83-130.
- Bovis, M.J., 1977. Statistical forecasting of snow avalanches, San Juan Mountains, southern Colorado, U.S.A. *Journal of Glaciology*, 18(78): 87.
- Bradley, C.C., 1965. The snow resistograph and slab avalanche investigations. *Proceedings: International Symposium on Scientific Aspects of Snow and Ice Avalanches*, Davos. 251-260.
- Breiman, L., Friedman, J.H., Olshen, R.A. and Stone, C.J., 1984. *Classification and Regression Trees*. Wadsworth, Belmont.
- British Columbia Natural Resources Conference, 1956. *British Columbia Atlas of Resources*. Smith Lithograph, Vancouver.
- Brown, R.L., 1980. A volumetric constitutive law for snow based on a neck growth model. *Journal of Applied Physics*, 51(1): 161-165.
- Brown, R.L. and Birkeland, K., 1990. A comparison of the digital resistograph with the ram penetrometer. *Proceedings: International Snow Science Workshop*, Bigfork, Montana. 19-30.
- Brun, E., David, P., Sudul, M. and Brunot, G., 1992. A numerical model to simulate snow cover stratigraphy for operational avalanche forecasting. *Journal of Glaciology*, 38(128): 13-22.
- Canadian Avalanche Association, 2002. *Observation Guidelines and Recording Standards for Weather, Snowpack and Avalanches*. Canadian Avalanche Association, Revelstoke.
- Carroll, T., 1977. A comparison of the CRREL 500 cc tube and the ILTS 200 and 100 cc box cutters used for determining snow densities. *Journal of Glaciology*, 18(79): 334-337.
- Coelho, R., 1979. *Physics of Dielectrics for the Engineer*. Elsevier Scientific, Amsterdam.
- Colbeck, S.C., 1991. The layered character of snow covers. *Reviews of Geophysics*, 29(1): 81-96.

- Colbeck, S.C., Akitaya, E., Armstrong, R., Gubler, H., Lafeuille, L., Lied, K., McClung, D. and Morris, E., 1990. *The International Classification of Snow on the Ground*. International Commission on Snow and Ice.
- Conger, S.M., 1980. *Snow Study Weatherproof Field Book*. Snow Knowledge, Park City.
- Conway, H. and Wilbour, C., 1999. Evolution of snow slope stability during storms. *Cold Regions Science and Technology*, 30(1-3): 67-77.
- Cumming, W.A., 1952. The dielectric properties of ice and snow at 3.2 centimeters. *Journal of Applied Physics*, 23(7): 768 - 773.
- Davis, R.E., Elder, K., Howlett, D. and Bouzaglou, E., 1999. Relating storm and weather factors to dry slab avalanche activity at Alta, Utah, and Mammoth Mountain, California, using classification and regression trees. *Cold Regions Science and Technology*, 30(1-3): 79-89.
- de Quervain, M.R. and Meister, R., 1986. 50 years of snow profiles on the Weissfluhjoch and relations to the surrounding avalanche activity. in *Proceedings: Avalanche Formation, Movement and Effects*, Davos. 161-181.
- Denoth, A., 1982. Effect of grain geometry on electrical properties of snow at frequencies up to 100 MHz. *Journal of Applied Physics*, 53(11): 7496 - 7501.
- Dowd, T.F., 1984. A New instrument for determining strength and temperature profiles in snowpack, (M.Sc. Thesis, Montana State University, Bozeman). 42.
- DuPont Filaments, 1999. *How to Evaluate a Paint Brush*. du Pont de Nemours and Company, Wilmington.
- Durand, Y., Giraud, G., Brun, E., Merindol, L. and Martin, E., 1999. A computer-based system simulating snowpack structures as a tool for regional avalanche forecasting. *Journal of Glaciology*, 45(151): 469-484.
- Ellerbruch, D.A. and Boyne, H.S., 1980. Snow stratigraphy and water equivalence measured with an active microwave system. *Journal of Glaciology*, 26(94): 225-233.
- Evans, S., 1965. Dielectric properties of ice and snow - a review. *Journal of Glaciology*, 5(42): 773-792.
- Ferguson, S.A., 1984. The role of snowpack structure in avalanching. (Ph.D. Thesis, University of Washington, Seattle). 150.
- Floyer, J. and Jamieson, B., 2006. Empirical analysis of snow deformation below penetrometer tips. *Proceedings: International Snow Science Workshop*, Telluride, Colorado. 555-561.
- Fraser, C., 1966. *The Avalanche Enigma*. Rand McNally, New York.
- Fredston, J.A. and Fesler, D., 1984. *Snow Sense - A Guide to Evaluating Avalanche Hazard*. Alaska Department of Natural Resources Division of Parks and Outdoor Recreation, Anchorage.
- Friedman, J.H., 1977. A recursive partitioning decision rule for nonparametric classification. *IEEE Transactions on Computers*, 26: 404-408.
- Goodison, B.E., Ferguson, H.L. and McKay, G.A., 1981. Measurement and data analysis. In: *Handbook of Snow*. D.M. Gray and D.H. Male (Eds), Pergamon Press, Ontario, 776.
- Green, R.H., 1987. *They Followed the Glory Trail*. Roberta Green, Challis.
- Greene, E., Birkeland, K., Elder, K., Johnson, G., Landry, C., McCammon, I., Moore, M., Sharaf, D., Sterbenz, C. and Williams, K., 2004. *Snow, Weather, and Avalanches: Observational Guidelines for Avalanche Programs in the United States*. American Avalanche Association, Pagosa Springs.
- Gubler, H., 1975. On the rammsonde hardness equation: A review of basic snow mechanics. *Proceedings: International Symposium on Snow Mechanics*, Grindelwald, IAHS Publication 114, Switzerland. 110-121.
- Gubler, H. and Hiller, M., 1984. Use of microwave FMCW radar in snow and avalanche research. *Cold Regions Science and Technology*, 9(2): 109 - 119.
- Häfeli, R., 1954. Snow mechanics with references to soil mechanics. In: *Der Schnee und Seine Metamorphose*. H. Bader, R. Häfeli, E. Bucher, J. Neher, O. Eckel, C. Thams and P. Niggli (Eds), Beitrage zur Geologie der Schweiz, Bern, 59-218.
- Häfeli, R., Bader, H. and Bucher, E., 1954. The time profile, a graphic representation of the development of a snow cover. In: *Der Schnee und Seine Metamorphose*. H. Bader, R. Häfeli, H. Bader, J. Neher, O. Eckel, C. Thams and P. Niggli (Eds), Beitrage zur Geologie der Schweiz, Bern, 220 - 230.
- Hägeli, P., 2005. Canadian Avalanche Association Markup Language. Canadian Avalanche Association. (accessed 20 July 2006). <<http://www.avalancheinfo.net/caaml/schema/3.0.3/>>.
- Hägeli, P. and Atkins, R., 2002. Storage and visualization of relevant avalanche information at different scales. *Proceedings: International Snow Science Workshop*, Penticton, BC. 32-38.
- Hägeli, P. and McClung, D., 2000. A new perspective on computer-aided avalanche forecasting: scale and scale issues. *Proceedings: International Snow Science Workshop*, Big Sky, Montana.

- Hägeli, P. and McClung, D.M., 2003. Avalanche characteristics of a transitional snow climate--Columbia Mountains, British Columbia, Canada. *Cold Regions Science and Technology*, 37(3): 255-276.
- Harper, J.T. and Bradford, J.H., 2003. Snow stratigraphy over a uniform depositional surface: spatial variability and measurement tools. *Cold Regions Science & Technology*, 37(3): 289-298.
- Harrison, W.L., 1982. *Snowpack profile analysis using extracted thin sections*. Cold Regions Research & Engineering Laboratory.
- International Union of Geodesy and Geophysics Commission for the Cryospheric Sciences, 2005. Minutes: Bureau meeting of the IUGG (CCS), 3 and 4 Nov., 2005, UNESCO Paris. (accessed 31 October 2006).
<www.glaciologi.su.se/ICSI/docs/paris_2005/IUGG_CCS_Bureau_Meeting_Paris_2005_MINUTE_S.pdf>.
- Jones, P.A., 1968. *Field Work in Geography*. Longmans, Harlow.
- Kahrl, M. 2003. Snowpilot. Vers. Computer software. <<http://www.snowpilot.org/>>.
- Kelly, J. 2005. Pro-File. Vers. 1.8.2. Computer software. Cedar Waxwing.
- Kendra, J.R., Ulaby, F.T. and Sarabandi, K., 1994. Snow probe for in situ determination of wetness and density. *IEEE Transactions on Geoscience and Remote Sensing*, 32(6): 1152.
- Kronholm, K., 2004. Spatial variability of snow mechanical properties with regard to avalanche formation, Universität Zürich, Zürich). 187.
- Kuroiwa, D., 1962. Electrical Properties of Snow. In: *The Physics and Mechanics of Snow as a Material*. F.J. Sanger (Editor), Cold Regions Research and Engineering Laboratory, Hanover, 63-79.
- LaChapelle, E., 1961. *Snow Layer Densification*, Alta Avalanche Study Center, USFS, Alta. 14.
- LaChapelle, E., 1974. Review of operational, in-house forecasting procedures. In: *Development of methodology for evaluation and prediction of avalanche hazard in the San Juan Mountains of southwestern Colorado*. R.L. Armstrong (Editor), Institute of Arctic and Alpine Research, Boulder, 141.
- LaChapelle, E.R., 1980. The fundamental processes in conventional avalanche forecasting. *Journal of Glaciology*, 26(94): 75-84.
- LaChapelle, E.R., 1985. *The ABC of Avalanche Safety, 2nd edition*. Mountaineers, Seattle.
- LaChapelle, E.R. and Ferguson, S.A., 1980. Snow-pack structure: stability analyzed by pattern-recognition techniques. *Journal of Glaciology*, 26(94): 506 -11.
- Landry, C.C., 2001. Avalanche processes 'space-time' in spatial variation in snow stability, earth-surface systems, and sampling system states. Center for Snow & Avalanche Studies, Silverton.
- Lehning, M., Bartelt, P. and Brown, B., 1998. Operational use of a snowpack model for the avalanche warning service in Switzerland: model development and first experiences. *Publikasjon - Norges geotekniske institutt*, 203: 169-174.
- Louge, M.Y., 2006. [personal communication: 10 October 2006, address: myl3@cornell.edu].
- Louge, M.Y., Foster, R.L., Clifford, K. and Manning, B., 2002. *Final Report A Multi-Parameter Snow Sounding Probe*, Capacitec, Ayer. 61.
- Louge, M.Y., Foster, R.L., Jensen, N. and Patterson, R., 1998a. A portable capacitance snow sounding instrument. *Cold Regions Science and Technology*, 28(2): 73.
- Louge, M.Y., Foster, R.L., Jensen, N. and Patterson, R., 1998b. A portable capacitance snow sounding instrument. in *Proceedings: International Snow Science Workshop*, Sunriver, Oregon. 202 - 207.
- Mackenzie, R. and Payten, W., 2002. A portable, variable-speed, penetrometer for snow pit evaluation. *Proceedings: International Snow Science Workshop*, Penticton, BC. 294 - 300.
- McClung, D., 1995. Use of expert knowledge in avalanche forecasting. *Defence Science Journal*, 45(2): 117-123.
- McClung, D. and Schaerer, P., 2006. *The Avalanche Handbook, 3rd Edition*. The Mountaineers, Inc, Seattle.
- McClung, D. and Schaerer, P.A., 1993. *The Avalanche Handbook*. The Mountaineers, Seattle.
- McMurdo Dry Valley LTER, 2000. Glacier snow densities. (accessed 20 July 2006).
<<http://huey.colorado.edu/LTER/datatets/glaciers/glsnwdns.html>>.
- Mellor, M., 1964. *Properties of Snow*, III-A1. Cold Regions Research & Engineering Laboratory, Hanover.
- Mock, C.J. and Birkeland, K.W., 2000. Snow Avalanche Climatology of the Western United States Mountain Ranges. *Bulletin of the American Meteorological Society*, 81(10): 2367 - 2392.
- Nakaya, U., Tada, M., Sekido, Y. and Takano, T., 1936. The physics of skiing, the preliminary and general survey. *Journal of the Faculty of Science*, 1(Investigations on snow, no. 9. series II): 265-287.
- Niggli, P., 1954. Introduction. In: *Der Schnee und Seine Metamorphose*. H. Bader, R. Häfeli, E. Bucher, J. Neher, O. Eckel, C. Thams and P. Niggli (Eds), Bern, ix - xix.

- Perla, R.I., 1970. On contributory factors in avalanche hazard evaluation. *Canadian Geotechnical Journal*, 7: 414 - 419.
- Peterson, N.R. and Brown, A.J., 1975. Accuracy of snow measurements. *Proceedings: Western Snow Conference, 43rd Annual Meeting*. 1 - 5.
- Pielmeier, C. and Schneebeli, M., 2003a. Developments in the stratigraphy of snow. *Surveys in Geophysics*, 24: 389-416.
- Pielmeier, C. and Schneebeli, M., 2003b. Stratigraphy and changes in hardness of snow measured by hand, rammsonde and snow micro penetrometer: A comparison with planar sections. *Cold Regions Science & Technology*, 37(3): 393-405.
- Pielmeier, C., Schneebeli, M. and Stucki, T., 2001. Snow texture: A comparison of empirical versus simulated texture index for Alpine snow. *Annals of Glaciology*, 32: 7-13.
- Randolph, P.D., Coates, R.A., Killian, E.W., Johnson, L.O. and Heath, R.L., 1972. A network of telemetered profiling isotopic snow gauges. *Proceedings: Role of Snow and Ice in Hydrology*, Banff. 688 - 701.
- Robinson, J.L., 1987. Sorting out all the mountains in British Columbia. *Canadian Geographic*(Feb): 42-53.
- Sall, J., Creighton, L. and Lehman, A., 2005. *JMP Start Statistics, Third Edition*. Brooks/Cole, Belmont.
- Sall, J., Ng, K., Hecht, M., Potter, R., Corcoran, B., Zangi, A., Jones, B., Hales, C., Nelson, P., Gotwalt, C. and Gregg, X. 2003. JMP IN. Version. 5.1. Computer software. SAS Institute, Inc.
- Schaefer, V.J., Klein, G.J. and de Quervain, M.R., 1954. *The International Classification for Snow (with special reference to snow on the ground)*. Technical Memorandum No. 31, National Research Council, Ottawa. 17.
- Schleiss, V.G.F., 1990. *Rogers Pass Snow Avalanche Control - A Summary, Glacier National Park, British Columbia, Canada*. Canadian Parks Service, Revelstoke.
- Schneebeli, M. and Johnson, J.B., 1998. A constant speed penetrometer for high resolution stratigraphy. *Annals of Glaciology*, 26: 107 - 111.
- Schneebeli, M., Pielmeier, C. and Johnson, J., B., 1998. Measuring snow microstructure and hardness using a high resolution penetrometer. *Proceedings: International Snow Science Workshop*, Sunriver, Oregon. 305 - 311.
- Schweizer, J. and Jamieson, J.B., 2001. Snow cover properties for skier triggering of avalanches. *Cold Regions Science and Technology*, 33(2-3): 207-221.
- Schweizer, J., Jamieson, J.B. and Skjonsberg, D., 1998. Avalanche forecasting for transportation corridor and backcountry in Glacier National Park (BC, Canada). *Proceedings of the Anniversary Conference 25 Years of Snow Avalanche Research*, Voss, Norway, Norwegian Geotechnical Institute, (203): 238-244.
- Seligman, G., 1936. *Snow Structure and Ski Fields*. R & R Clark, Limited, Edinburgh.
- Shapiro, L.H., Johnson, J.B., Sturm, M. and Blaisdell, G.L., 1997. *Snow Mechanics - Review of the state of knowledge and applications*. 97-3, CRREL. 40.
- Sihvola, A. and Tiuri, M., 1986. Snow fork for field determination of the density and wetness profiles of a snow pack. *IEEE Transactions on Geoscience and Remote Sensing*, GE-24(5): 717 - 721.
- Sims, G. 2005. Snowpro. Version 2005.11.17. Computer software. Gasman. <<http://www.gasman.com>>.
- Takei, I. and Maeno, N., 2003. Dielectric and mechanical alterations of snow properties near the melting temperature. *Canadian Journal of Physics*, 81: 233-239.
- Tiuri, M., Sihvola, A., Nyfors, E. and Hallikaiken, M., 1984. The complex dielectric constant of snow at microwave frequencies. *IEEE Journal of Oceanic Engineering*, 9(5): 377-382.
- Tokka Oy, 2005. Snow fork. (accessed 31 October 2006). <<http://www.toikkaoy.com/>>.
- Tremper, B., 1992. Of computers and dirtbags, part 1. *The Avalanche Review*, 10(3): 1,3-6.
- Tyndal, J., 1861. *Glaciers of the Alps*. Everyman's Library Science. J.M. Dent, London.
- USDA Forest Service, 1961. *Snow avalanches: a handbook of forecasting and control measures*. 84.
- Walker, D.A. and Walker, M.D., 1991. History and pattern in Alaskan arctic terrestrial ecosystems: A hierarchical approach to analysing landscape change. *Journal of Applied Ecology*, 28(1): 244 - 276.
- Wells, M.W., 1964. *Gold Camps & Silver Cities, Nineteenth Century Mining in Central and Southern Idaho*, Bulletin 22. Idaho Bureau of Mining and Geology, Boise.
- Yosida, Z., Oura, H., Kuroiwa, D., Huzioka, T. and Kojima, K., 1955. *Physical Studies on Deposited Snow I. Thermal Properties*. Contribution No. 279, Institute of Low Temperature Science, Sapporo. 74.
- Yosida, Z., Oura, H., Kuroiwa, D., Huzioka, T., Kojima, K. and Kinoshita, S., 1958. *Physical Studies on Deposited Snow: V. Electrical Properties*, Institute of Low Temperature Science, Sapporo. 33.

Young, G.J., 1976. Portable profiling snow gauge results of field tests on glaciers. *Proceedings: Western Snow Conference 44th Annual Meeting*, Calgary. 7 - 11.

APPENDICES

Appendix A Training-set Day Weather Observations

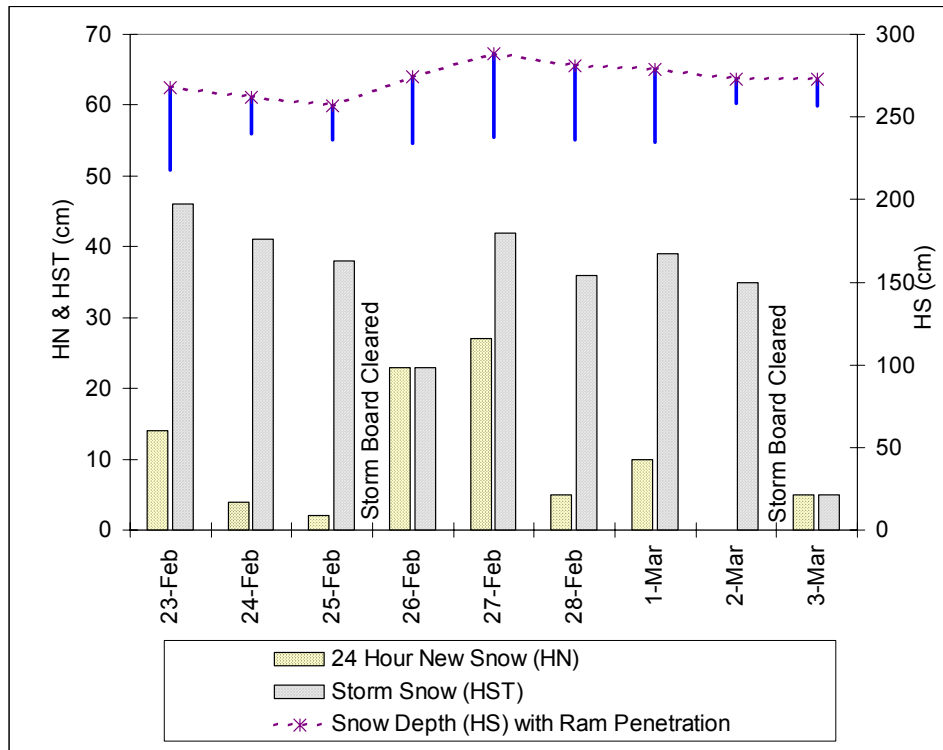


Figure 36. New snow and height at Fidelity 23 February through 3 March 2006.

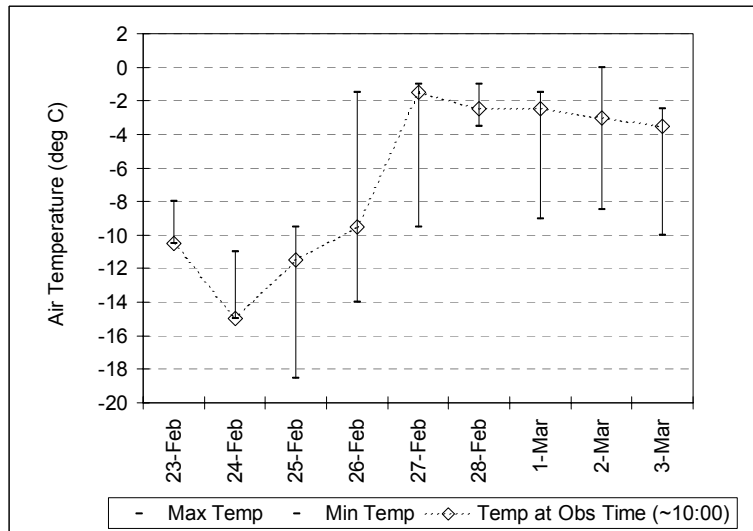


Figure 37. Air temperatures at Fidelity 23 February through March 3 2006.

Appendix B Grain Notation

		Grain Description / Classification
■	bl	“Bread Loaf” Mixed forms Facets *
+	bl/ibx	“Bread Loaf / Ibex” Mixed forms Facets / Decomposing SH **
×	mf	Rounded Polycrystals
□	df	Decomposing & Fragmented Precipitation Particles
◇	dfr	Decomposing & Fragmented Precipitation Particles - rimed
△	fc	Facets
Y	fc/pp	Facets / Precipitation Particles
z	ibx	“Ibex” Decomposing Surface Hoar **
○	pp	Precipitation Particles
◻	ppr	Precipitation Particles - rimed
□	rg	Rounded Grains
*	rgr	Rounded Grains - rimed
●	sh	Surface Hoar
■	tc	“Tea Cups” Mixed forms Rounded Grains *
■	~	Grain classification not assigned to probe measurement location

* Common field practitioner classification vernacular was used in recording ICSI grains 3c RGMx as “Tea Cups”, 4c FCmx as “Bread Loaves” .

** Non-ICSI classified form of decomposing SH was recorded as “Ibex”.

Table 15. Description of grain notation used in field recording and study graphics.

Appendix C Brush Comparison Summary and Test Results

Brush ID	Style	Supplier	Weight (g)	Material	Width (mm)	Thickness (mm)	Length (mm)	Pressure Test Area (mm ²)	% of length flexed in Pressure Test	Pressure index (Pa)
A	Wallpaper Brush	Paint Sundry Products	229	bristle	180	20	50	6960	40.0%	975
B	Stain	Simms	151.5	polyester	101.6	20	80	3200	25.0%	2445
C	Wall	Simms	62	bristle	101.6	10	47	2920	42.6%	1056
D	Stain	Simms	127	bristle	101.6	17	70	3840	28.6%	689
E	Sash	HydroTech	21.5	bristle	37	7	42	1040	47.6%	880
F	Wax	Swix	21	polyester	50	8	37	1480	54.1%	1464
G	Sash	Generic	25.5	polyester	50.8	9	45	1040	44.4%	1839
H	Sash	Rona	37	bristle	30	14	65	1200	30.8%	1101
I	Drafting	Staeder	65.5	mixture	200	6	53	2640	37.7%	1218
J	Sash	Simms	16	bristle	12	round	50	640	40.0%	1024

Test was done with a standard amount (20 mm) of the tip displaced

Table 16. Summary of brush characteristics and specifications.

Brush Test Results

Brush ID	Test 1	Test 2	Test 3	Test 4	Test 5	Test 6	Overall Rating	General test with denser pack						
	30-Jan-06	30-Jan-06	19-Feb-06	19-Feb-06	19-Feb-06	25-Feb-06			8-Mar-06					
	1 sweep L to R with light pressure	5 sweeps (3 to right/2 to left)	1 pass L to R	rating	One pass both directions	rating	# of passes	Counted number of passes to remove F to 1/2 of brush clear length	rating	# of passes	Counted number of passes to remove F to 1/2 of brush clear length	rating		
A	1st pass 1st brush, generally ok	Not very good at the bottom of the pack in facets	Too stiff, displaces top 20 cm	4	Exaggerated relief between F- & F, visible relief in F	2	6	Exaggerated relief between F- & F	3	8	Difficult with low relief	3	8	Did not test
B	Better than A at F-	Visible relief in new snow	No relief	9	F- / layers in all else	3	5	Exaggerated relief, thin layer evident	2	8	Easy with exaggerated relief, brought out loose snow under crust 43 down	2	7	Fairly evenly displaces F and F-snow, shows stiffening below new snow
C	Too short and stiff for this snow	No difference from Test 1	No relief	9	F-	6	10	Visible relief	2	5	Challenging with light relief, didn't do as well as B	2.5	10.5	Too soft, no relief
D	Consistent visible relief	2nd best visible relief	No relief	9	F-	6	10	Visible relief	2	6	Easy with exaggerated relief, didn't bring out layer 43 down but did for layer 40 down	1.5	9.5	Too soft, no relief
E	No relief	No difference from Test 1	No relief	9	F-	6	10	Exaggerated relief, good disaggregation	2	7	Easy with light relief, brought out layers in HST but not below	2.5	10.5	Too soft, no relief
F	Visible relief in F-	No difference from Test 1	No relief	9	F-	6	7	Exaggerated relief, good disaggregation	2	5	No relief	9	17	Requires cleaning each stroke, obliterates most layers

	Test 1	Test 2	Test 3	Test 4	Test 5	Test 6	Test 7							
	30-Jan-06	30-Jan-06	19-Feb-06	19-Feb-06	19-Feb-06	25-Feb-06	8-Mar-06							
Brush ID	1 sweep L to R with light pressure	5 sweeps (3 to right/2 to left)	1 pass L to R	rating	One pass both directions	rating	# of passes	Counted number of passes to remove F to 1/2 of brush clear length	rating	# of passes	Counted number of passes to remove F to 1/2 of brush clear length	rating	Overall Rating	General test with denser pack
G	Visible relief	No difference from Test 1	Visible relief in F	1.5		2	5	Exaggerated relief, good disaggregation	2.5	5	No relief	9	13.5	Cleaned each pass, good relief but doesn't correspond to CT location
H	No relief	No difference from Test 1	Exaggerated relief between F- & F, visible relief in F	1.5	F-	1.5	6	Challenging with visible relief	2	5	Easy with light relief, good in low density, layer down 40 comes out well	1	4.5	No comments
I	Consistent visible relief	No difference from Test 1	No relief except highlighting crust	9	NC in slab	1.5	12	Easy, visible relief in all layers >=4F	1	5	Easy with light relief, good at 40 down	1	3.5	Brings out stiff layer in F-/F/- where CT PC is located
J	Visible relief F-/F/+	No difference from Test 1	Exaggerated relief between F- & F, visible relief in F	2	NC in slab	1.5	8	Challenging with visible relief	2	5	Same as H, a little difficult at 40 down layer, variation in stiffness in upper 20 is evident, grains visible	1.5	5	Became bent in bag which seemed to make a difference
			Inconclusive test and not very interesting Not included in overall rating								H & J best in low density, B best in high density. Layer 40 down was facets and surface hoar			

Table 17. Brush test results.

Appendix D

Training-set Manual Snow Profiles



Snow Cover Profile

Location: Fidelity Flats

Date: 06-02-23

Sky: Wind: nil Air Temperature: -10.3 Time: 1215
 Aspect: 0 Elevation: 1905 Incline: 0 Observer: smc

HSW:

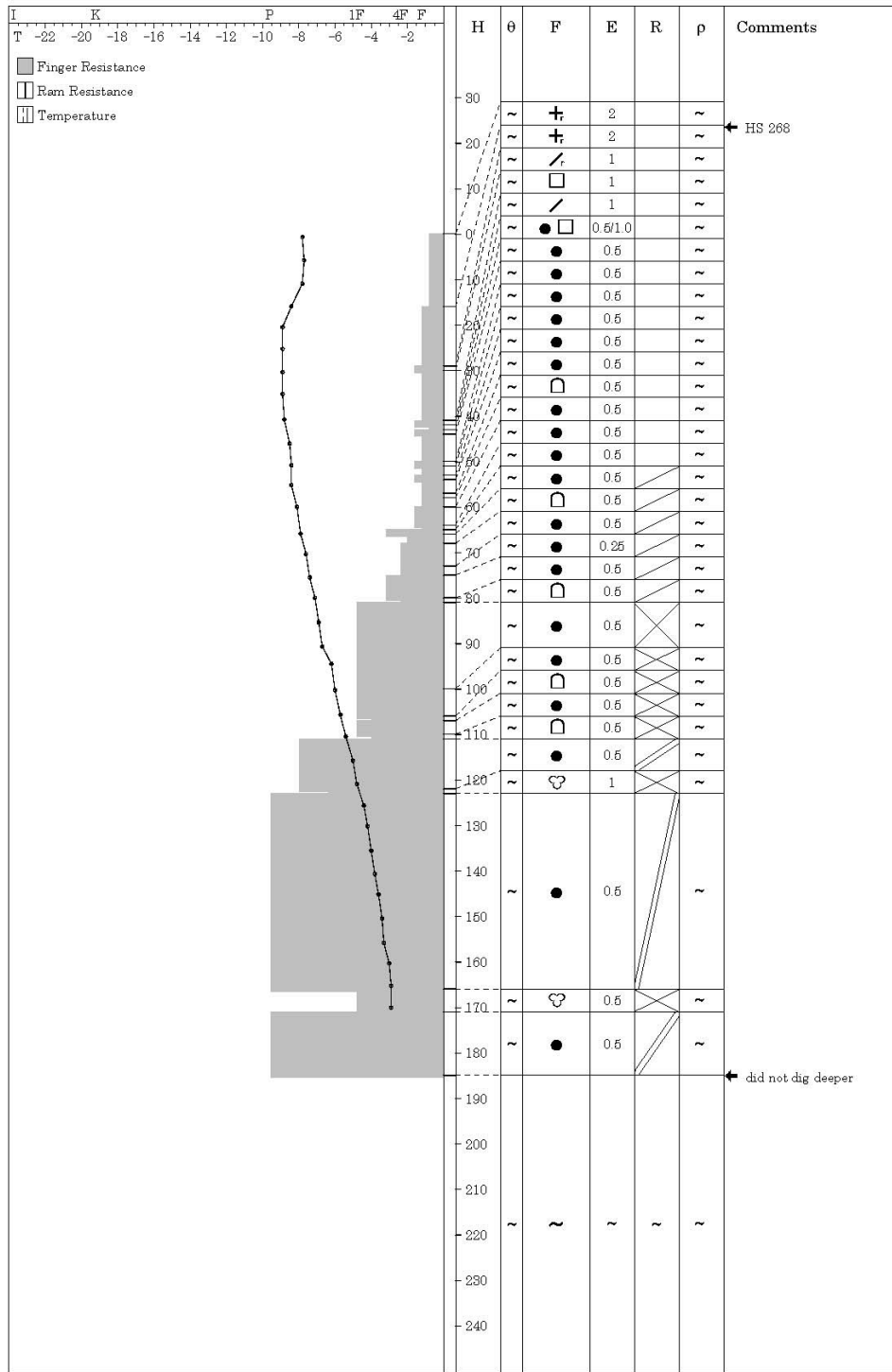
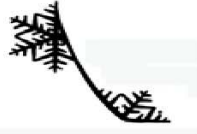


Figure 38. Snow profile for 23 February 2006.



Snow Cover Profile

Location: Fidelity Flats

Date: 07-02-25

Sky: ☉

Wind: nil

Air Temperature: -9.2

Time: 1223

Aspect: 0

Elevation: 1905

Incline: 0

Observer: smc

HSW:

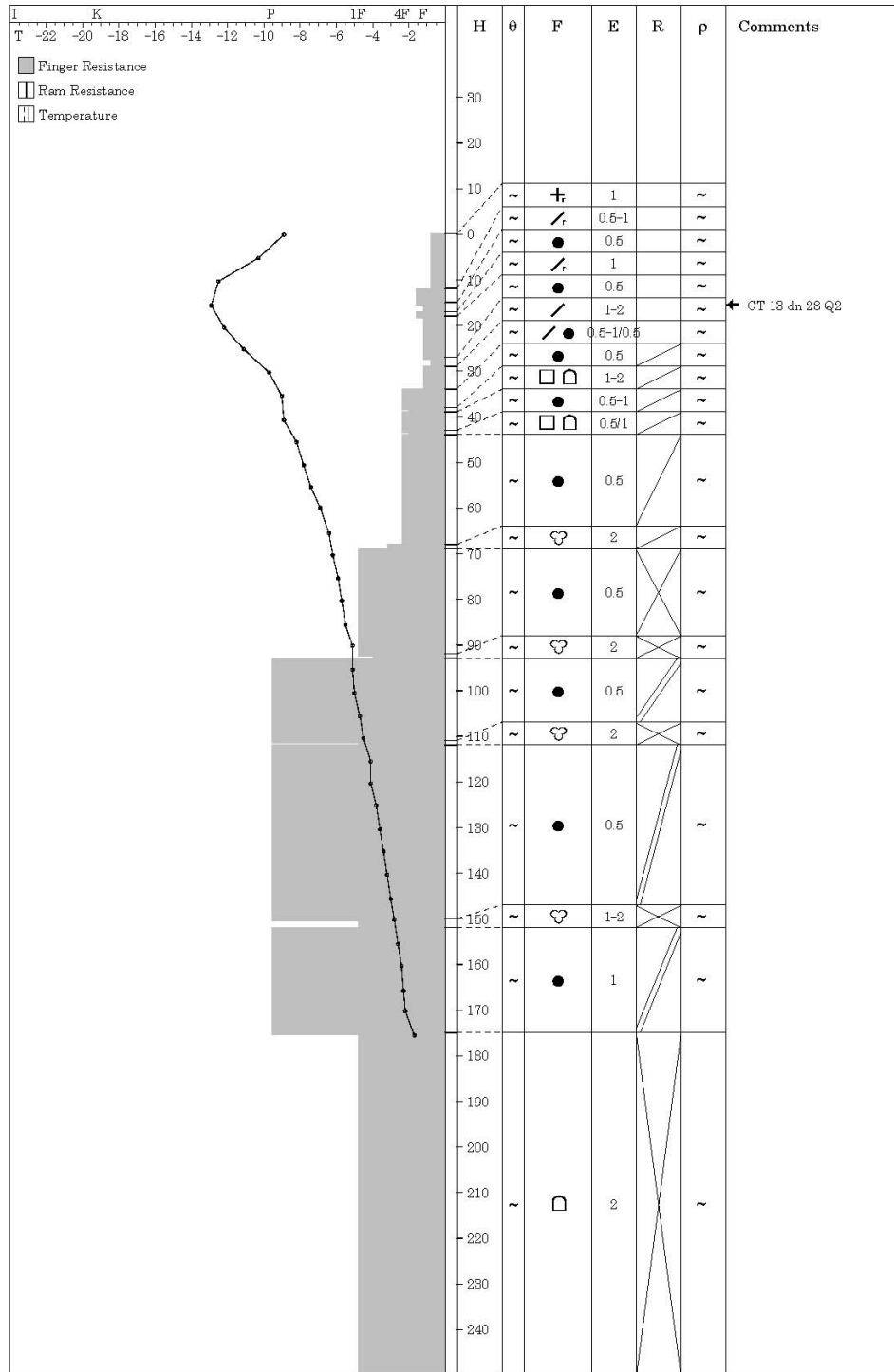
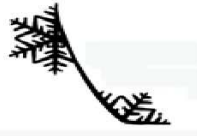


Figure 39. Snow profile for 25 February 2006.



Snow Cover Profile

Location: Fidelity Flats

Date: 06-02-26

Sky: ☒

Wind: calm

Air Temperature: -5.8

Time: 1142

Aspect: 0

Elevation: 1905

Incline: 0

Observer: SMC

HSW:

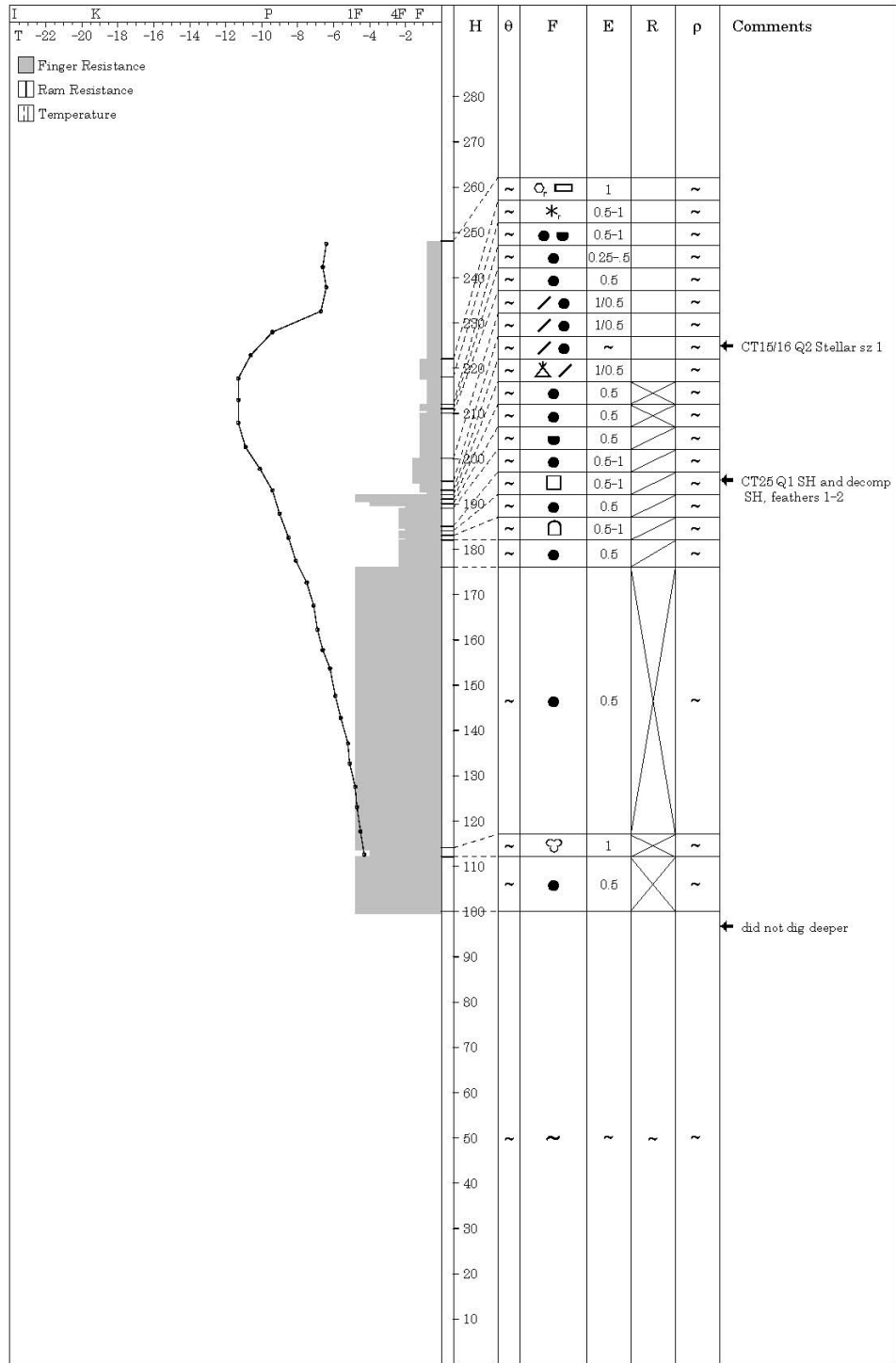


Figure 40. Snow profile for 26 February 2006.



Snow Cover Profile

Location: Fidelity Flats

Date: 06-02-27

Sky:

Wind:

Air Temperature: -1.3

Time: 1437

Aspect: 0

Elevation: 1905

Incline: 0

Observer: SMC

HSW:

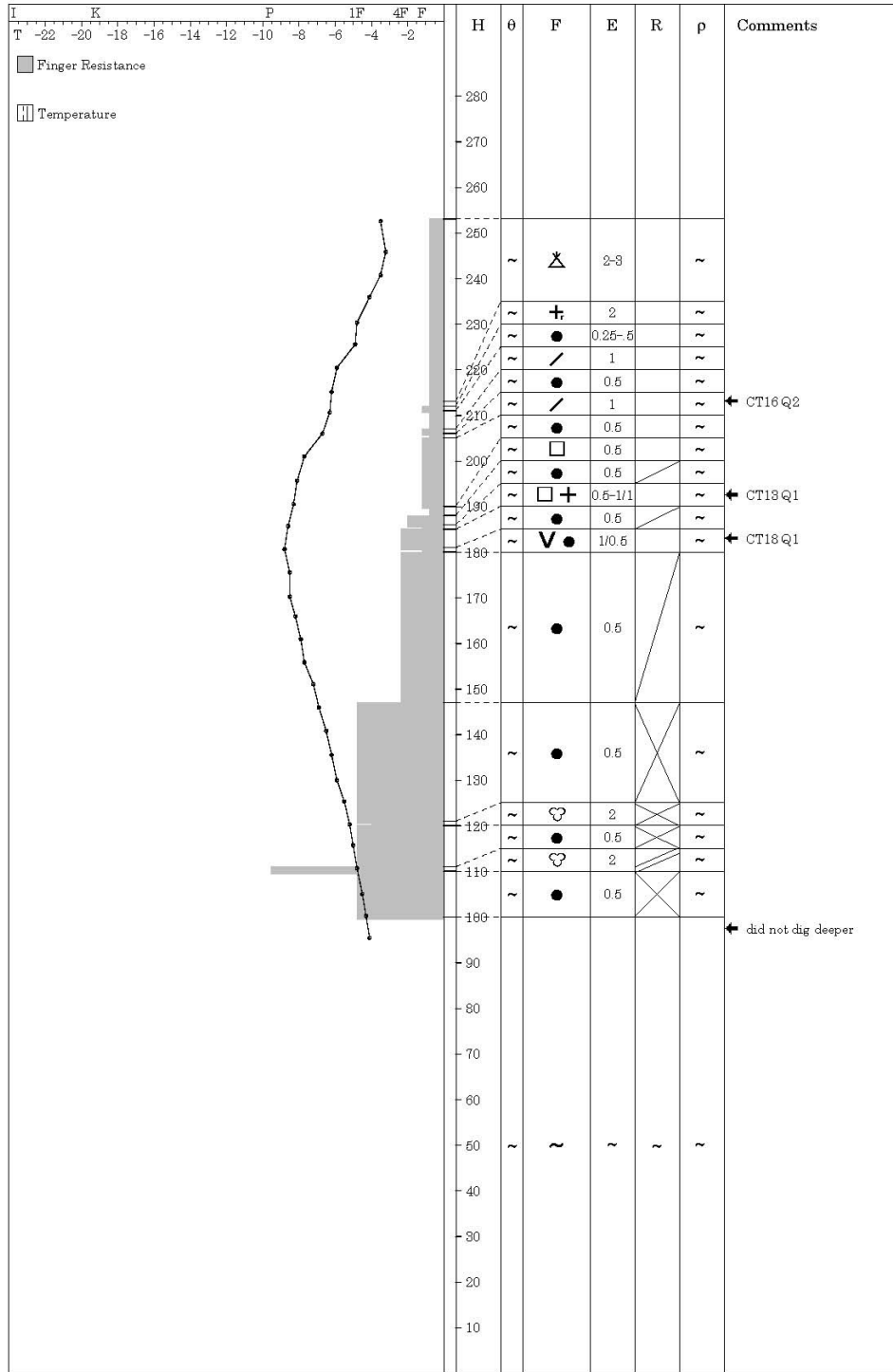


Figure 41. Snow profile for 27 February 2006.



Snow Cover Profile

Location: Fidelity Study Flats

Date: 06 Feb 28

Sky: ☒

Wind: mod NW Air Temperature: -1.8

Time: 1234

Aspect: 0

Elevation: 1905

Incline: 0

Observer: SMC

HSW:

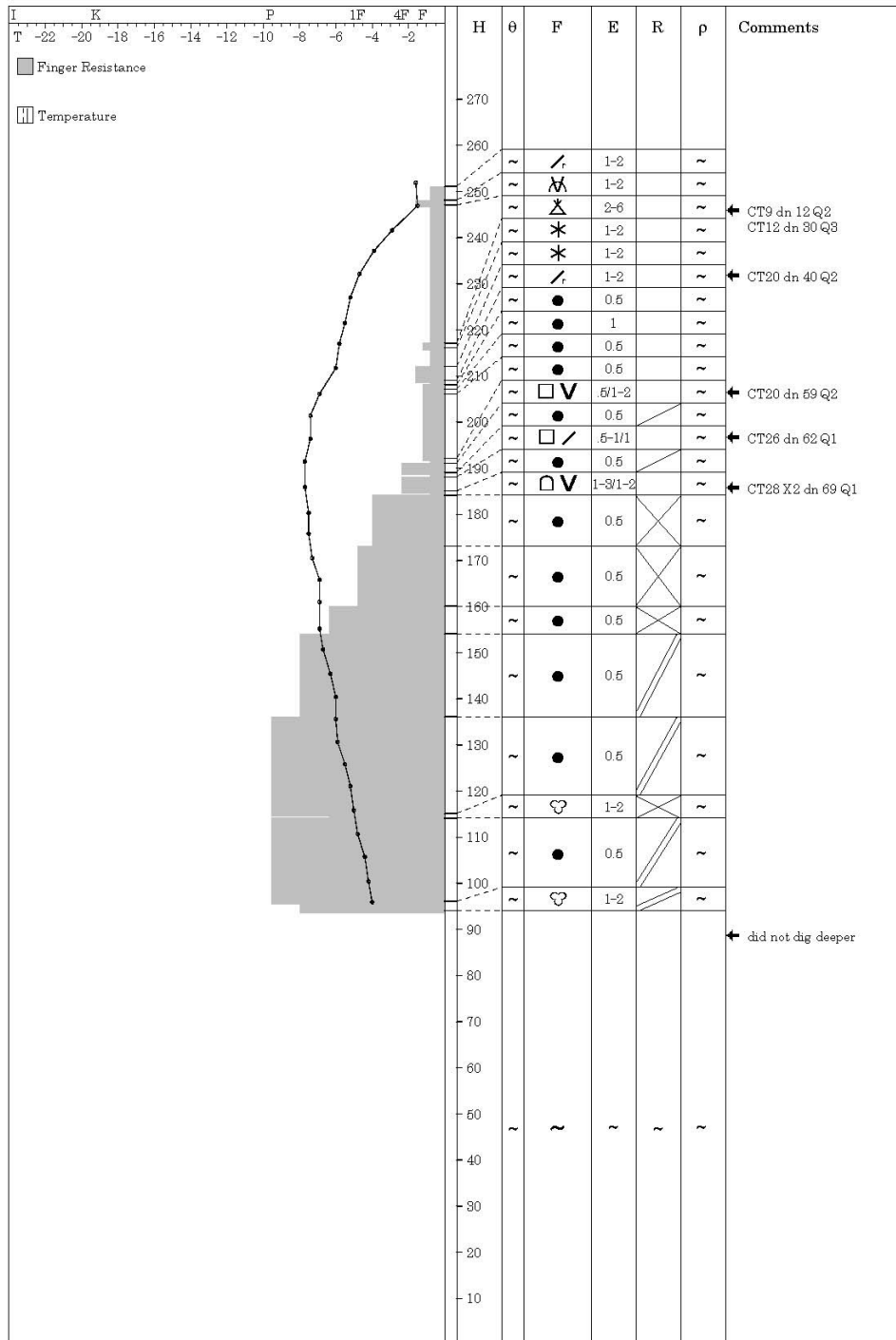


Figure 42. Snow profile for 28 February 2006.



Snow Cover Profile

Location: Fidelity Flats

Date: 07 Mar 1

Sky: ☉

Wind: nil

Air Temperature: -3.8

Time: 1102

Aspect: 0

Elevation: 1905

Incline: 0

Observer: SMC

HSW:

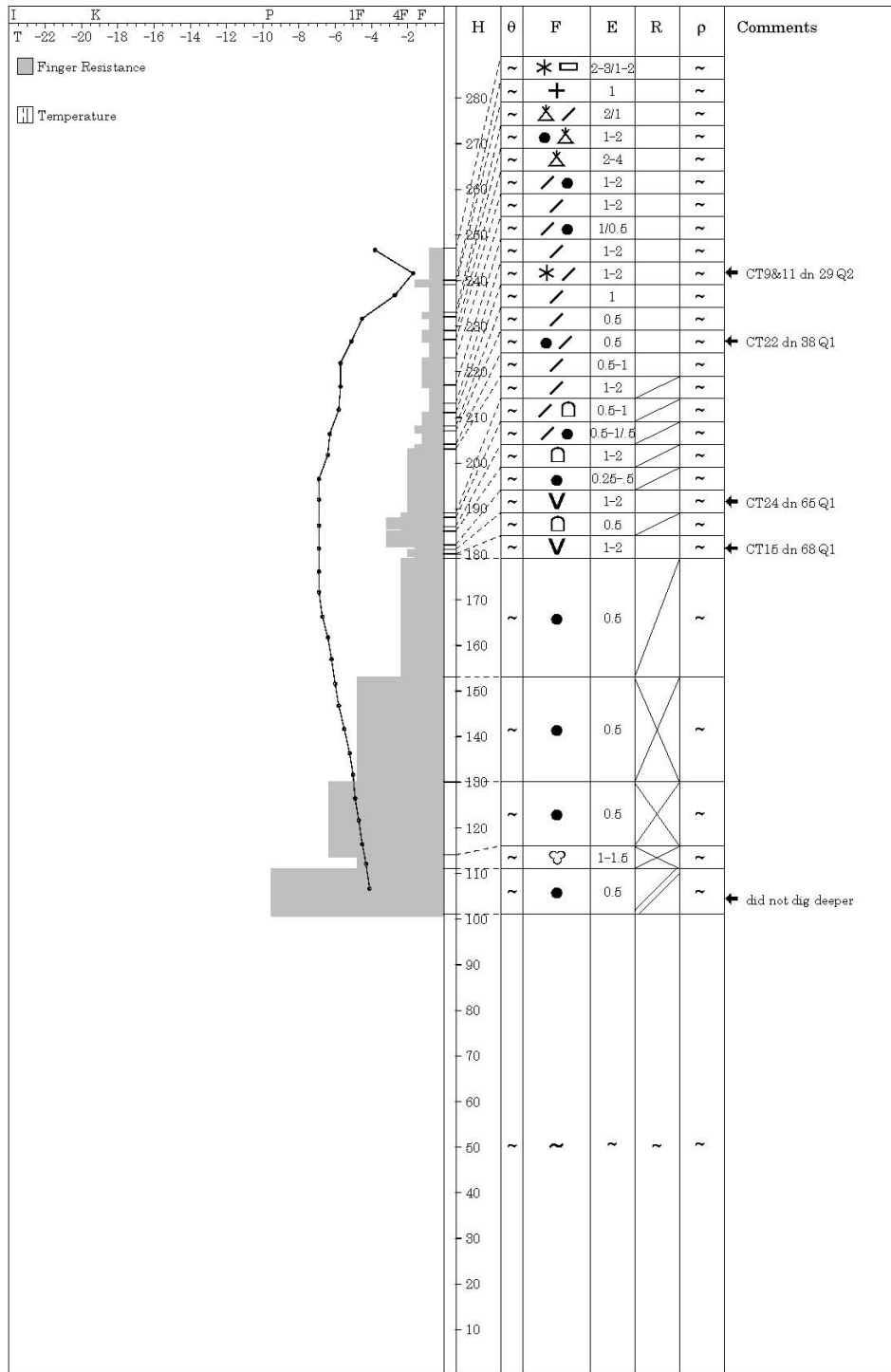


Figure 43. Snow profile for 1 March 2006.



Snow Cover Profile

Location: Fidelity Flats

Date: 06-03-02

Sky: ☁

Wind: It N

Air Temperature: -0.6

Time: 1339

Aspect: 0

Elevation: 1905

Incline: 0

Observer: SMC

HSW:

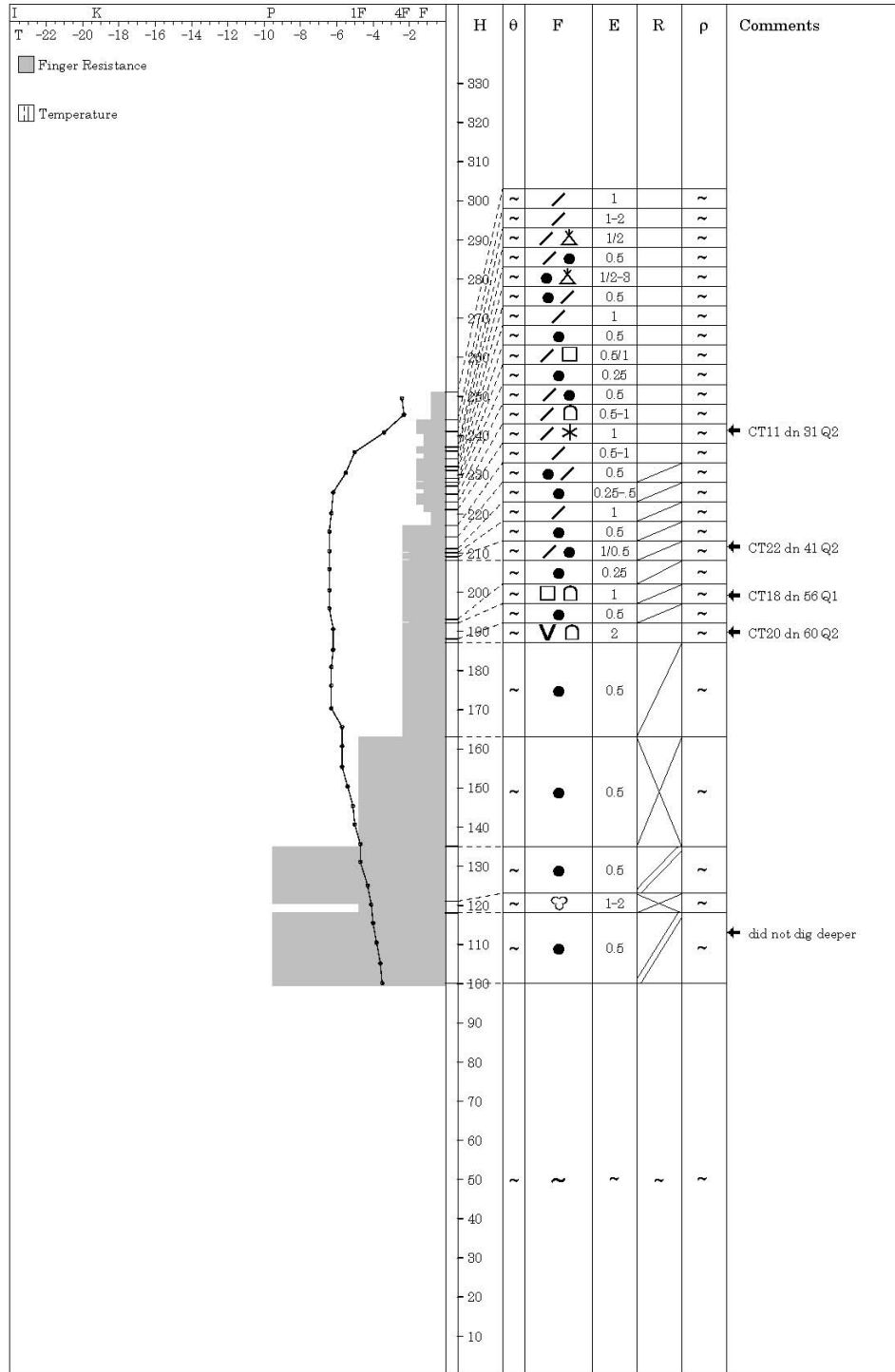
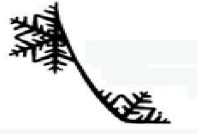


Figure 44. Snow profile for 2 March 2006.



Snow Cover Profile

Location: Fidelity Flats

Date: 06 Mar 3

Sky: ○

Wind: L-M@N Air Temperature:

Time: 1123

Aspect: 0

Elevation: 1905

Incline: 0

Observer: SMC

HSW:

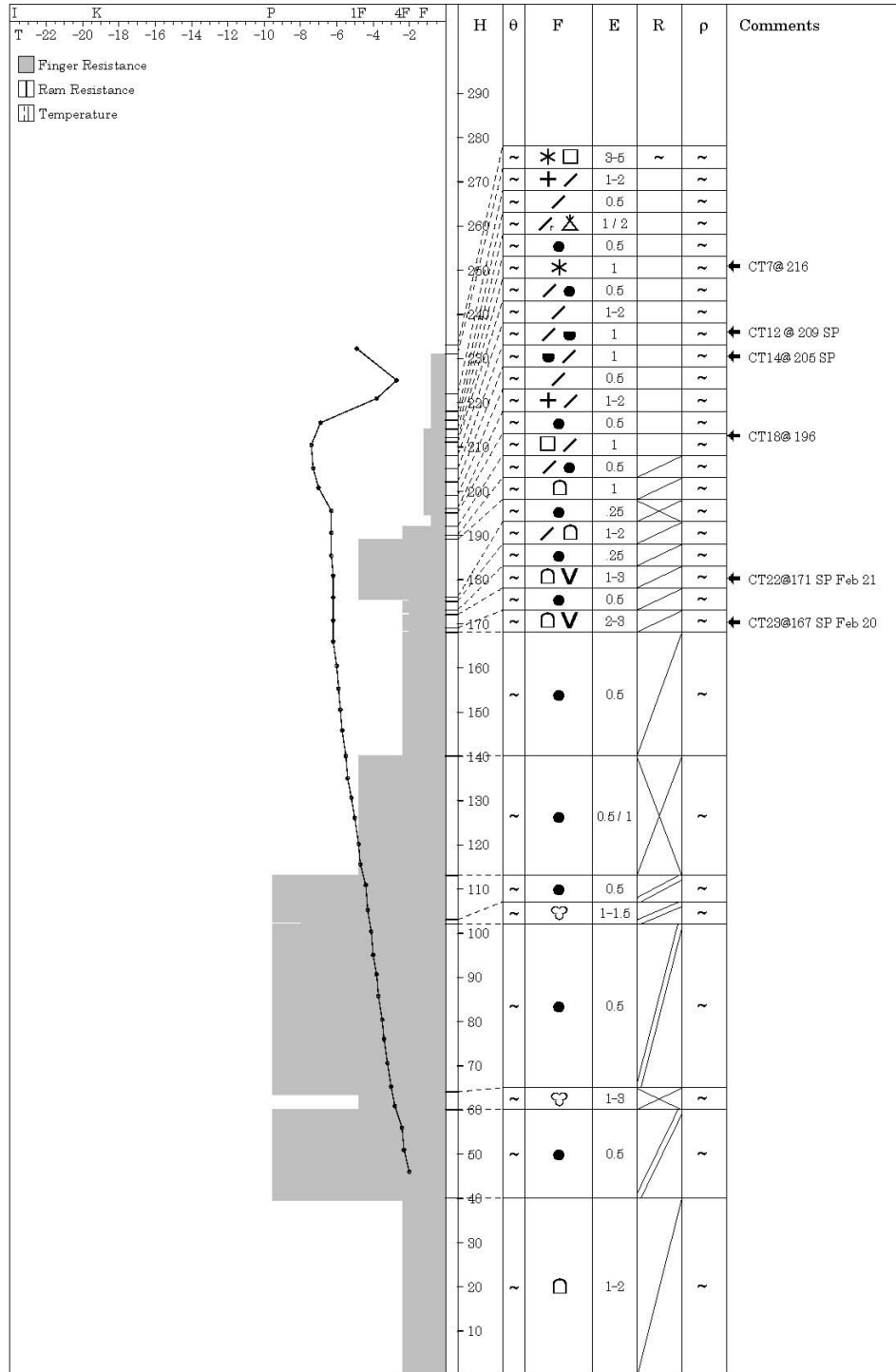


Figure 45. Snow profile for 3 March 2006.



Snow Cover Profile

Location: Sorcerer Lodge - Weather Plot

Date: 06 Mar 5

Sky: ☁

Wind: calm

Air Temperature: -5

Time: 1047

Aspect: 0

Elevation: 2030

Incline: 0

Observer: SMC KE

HSW:

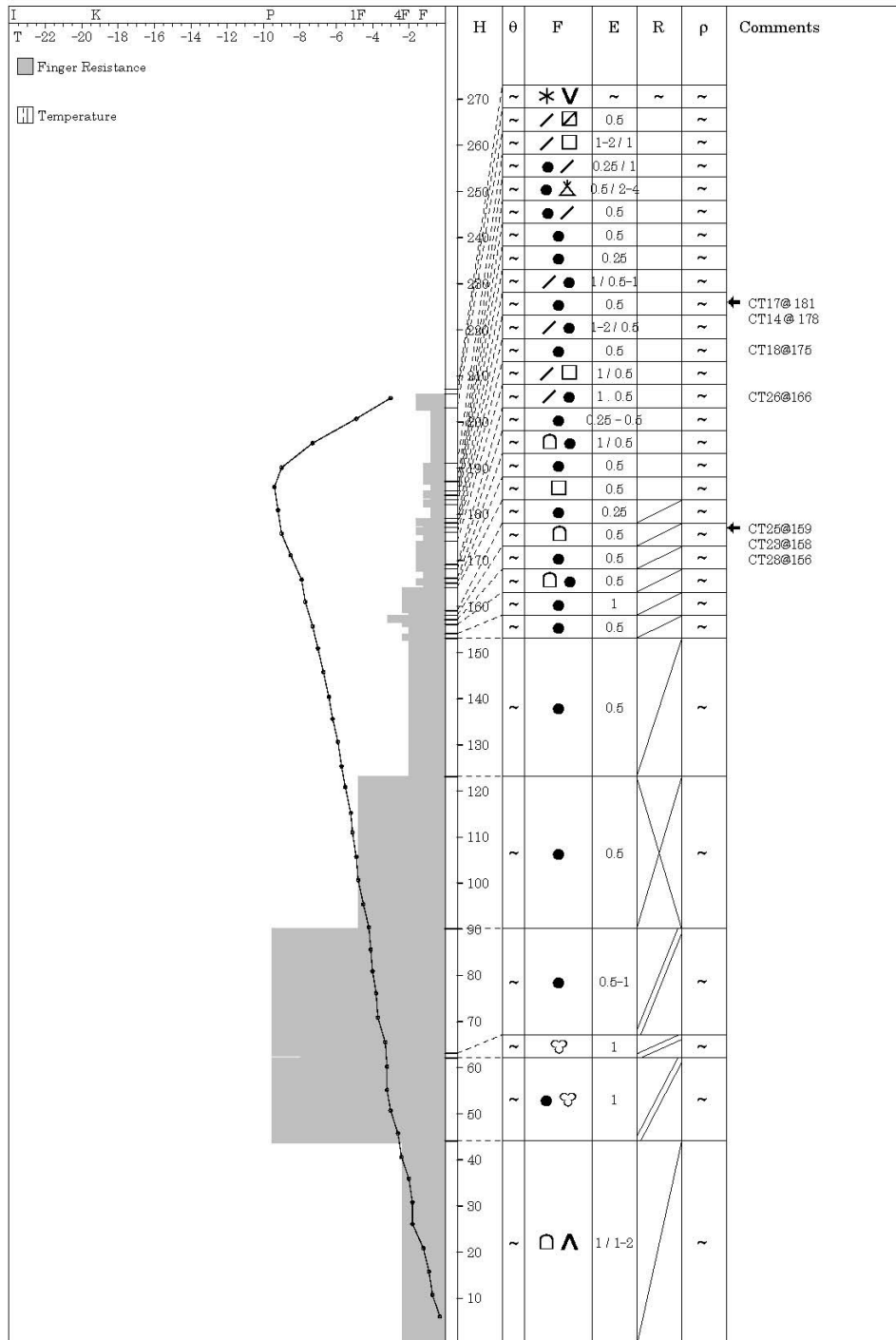


Figure 46. Snow profile for 5 March 2006.



Snow Cover Profile

Location: Nordic Lake

Date: 06 March 10

Sky: ☁

Wind: calm

Air Temperature:

Time: 1218

Aspect: s

Elevation: 2085

Incline: 3

Observer: SMC KE

HSW:

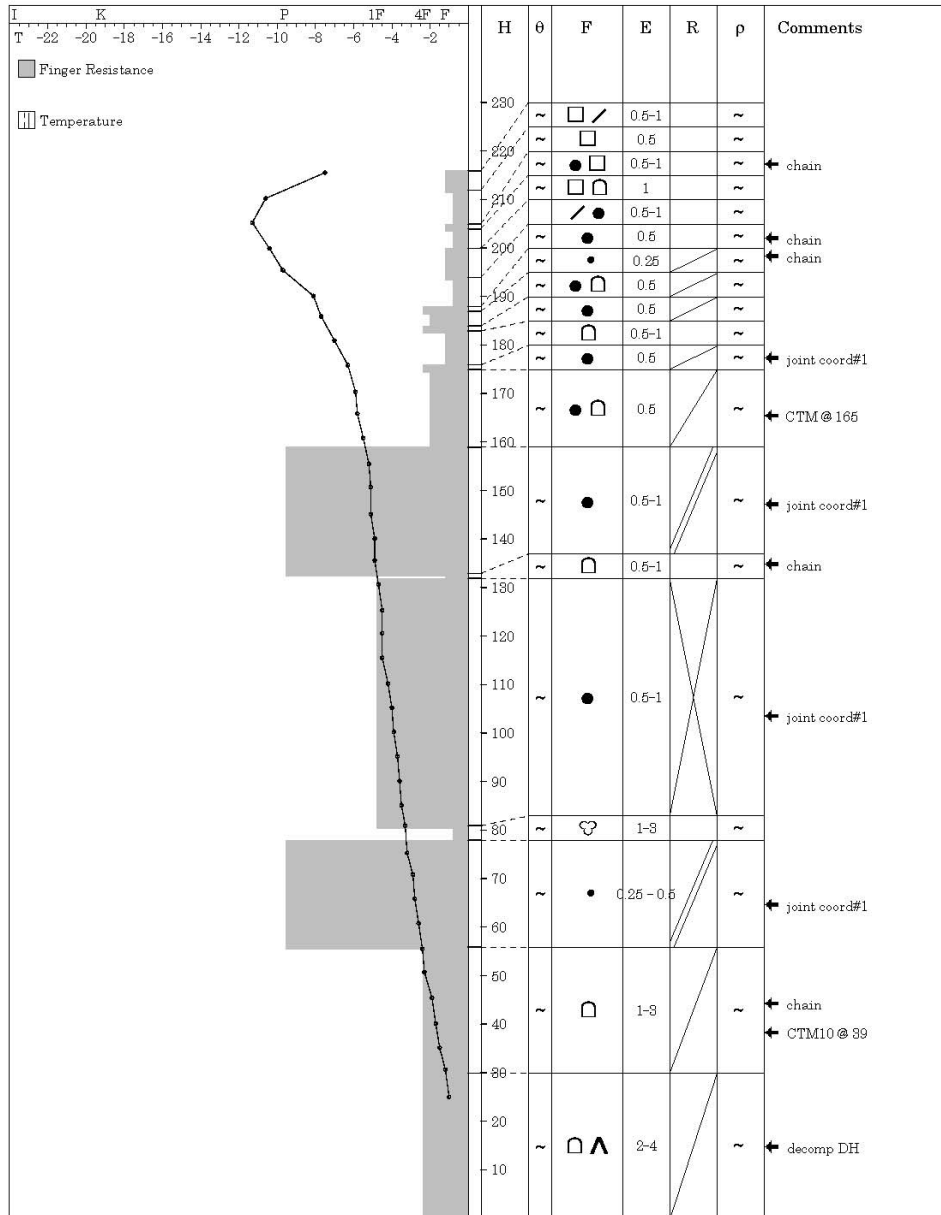
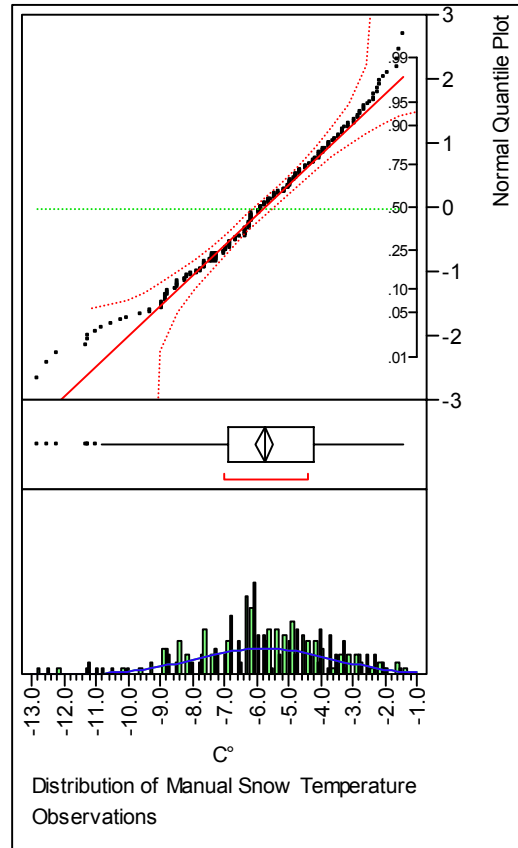
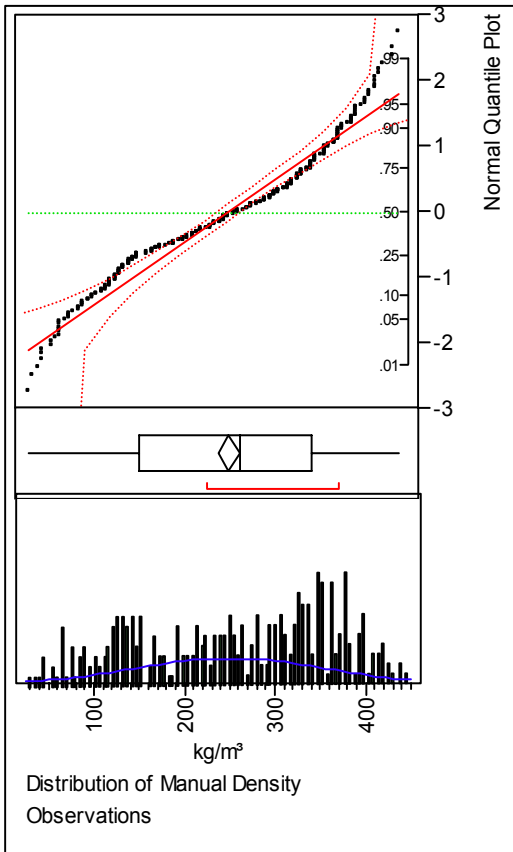
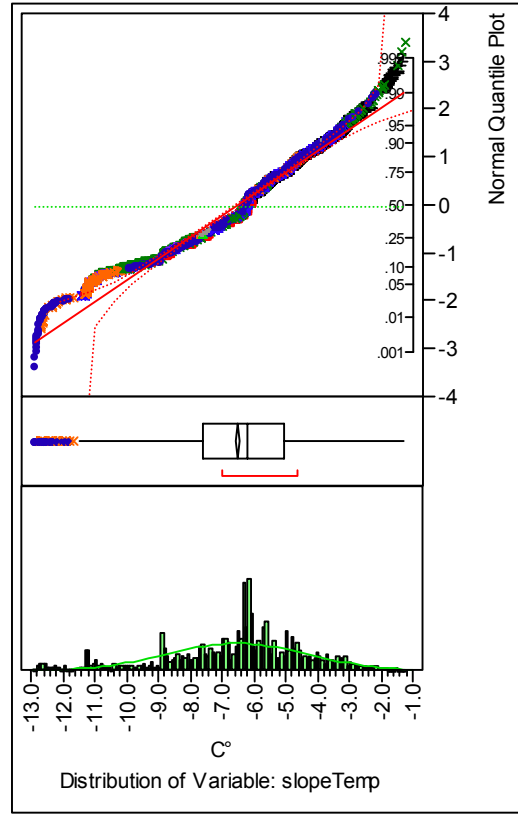
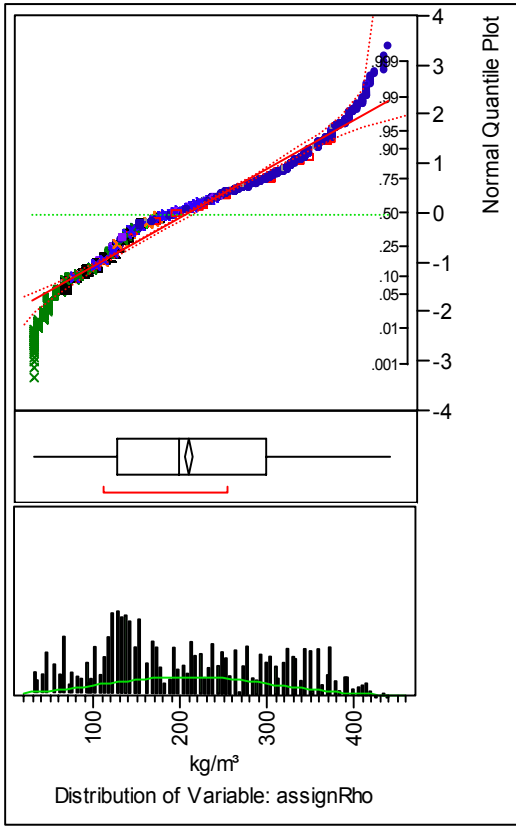


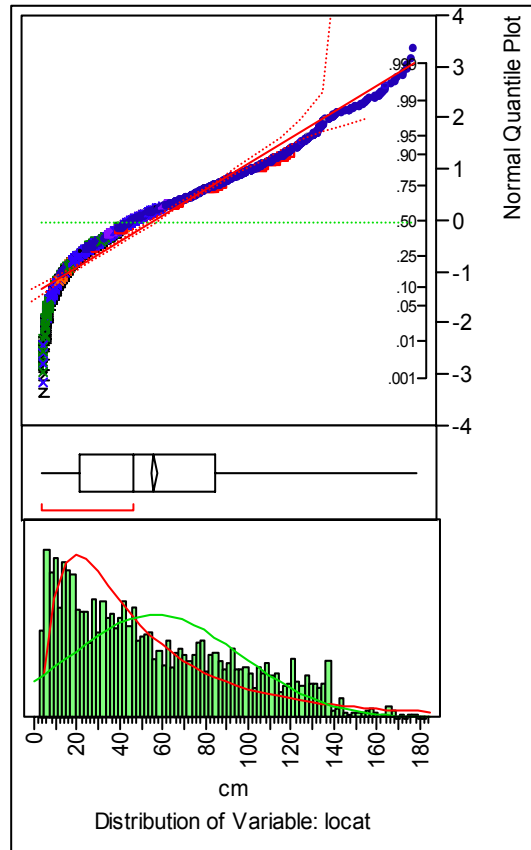
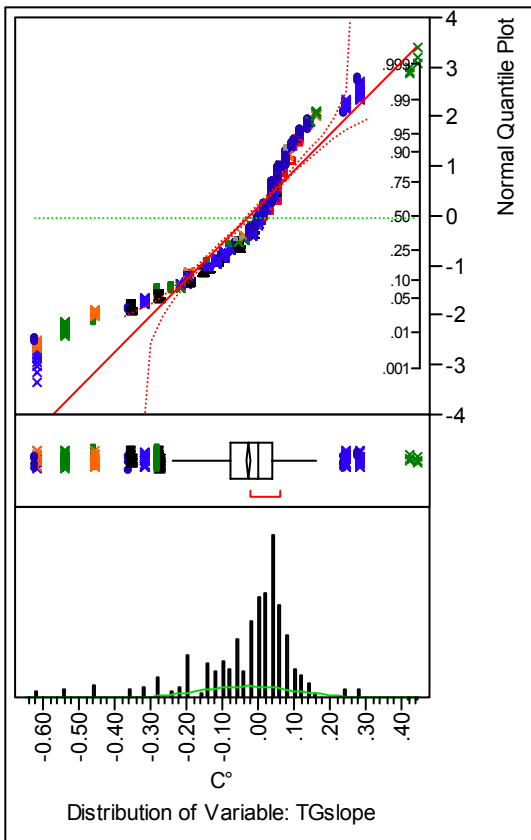
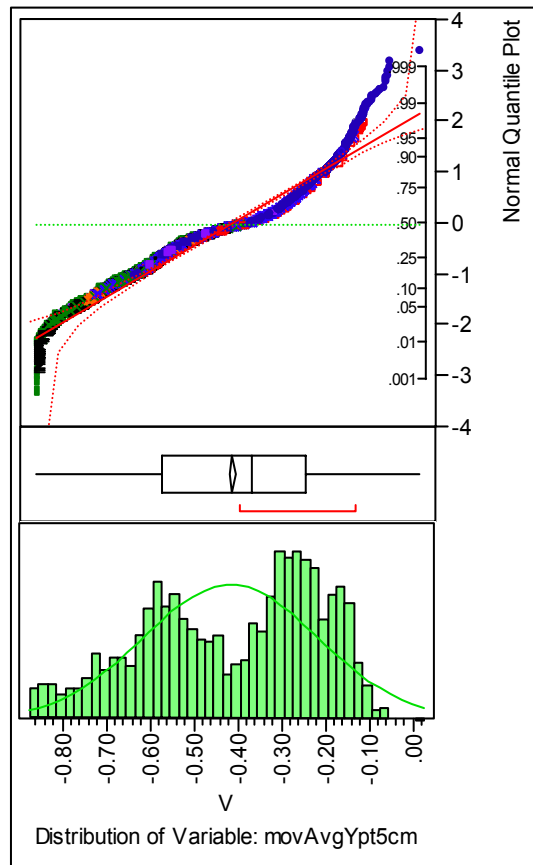
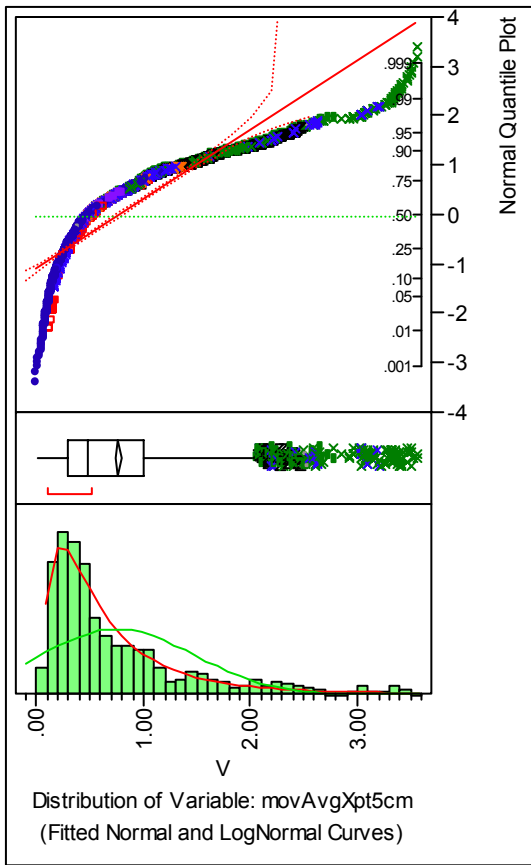
Figure 47. Snow profile for 10 March 2006.

Appendix E

Observation and Variable Distributions







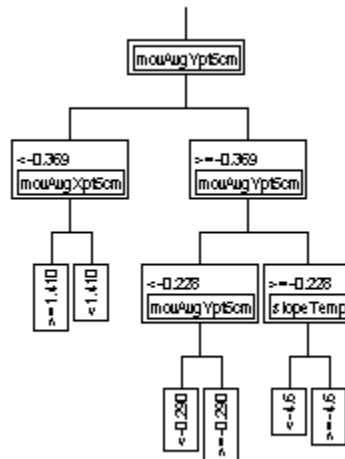


Figure 48. Recursive partitioning tree for density prediction model based on 50% of training-set days at 5 splits.

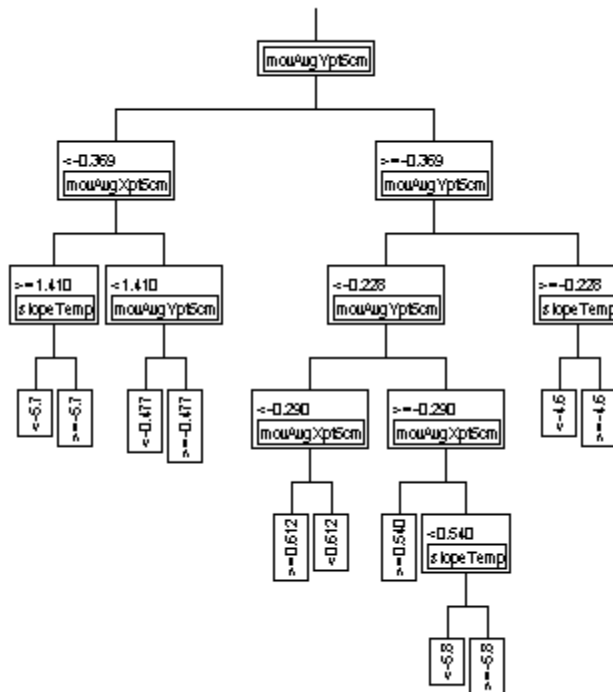


Figure 49. Recursive partitioning tree for density prediction model based on 50% of training-set days at 10 splits.

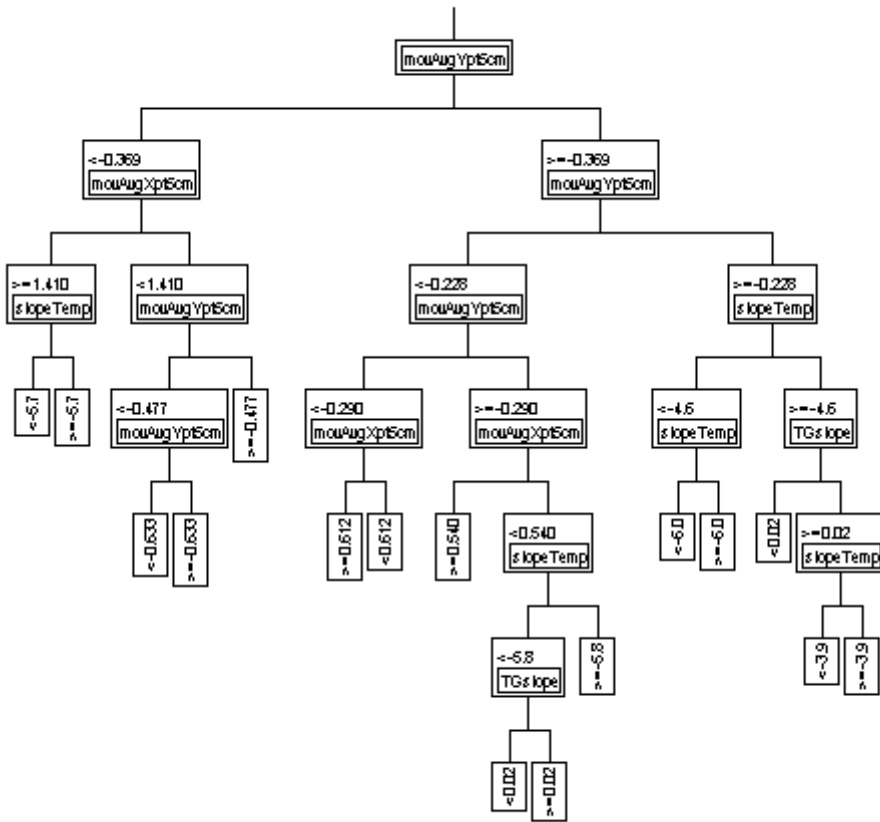


Figure 50. Recursive partitioning tree for density prediction model based on 50% of training-set days at 15 splits.

Appendix G

Bivariate Fits for 50% Training-set Day Models and Validations

of
Splits
at
Model
Output

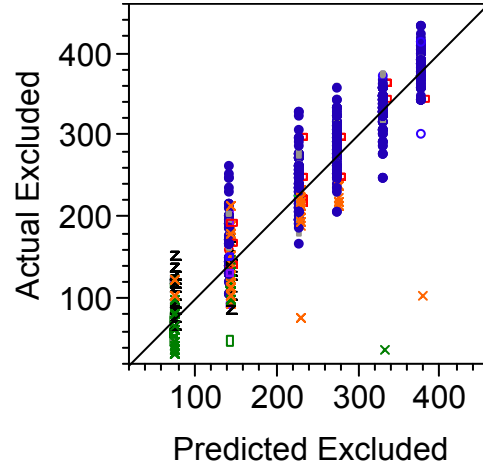
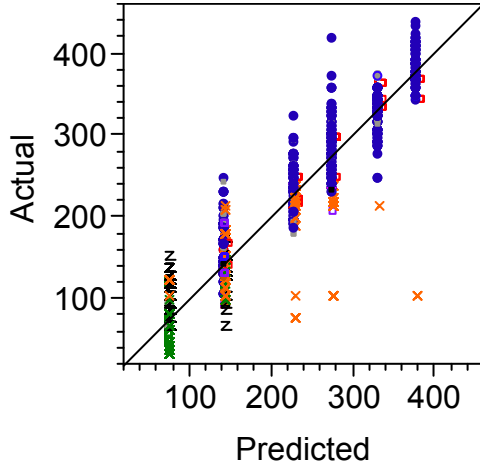
Model predicted densities fitted against manual
densities at assigned probe measurement
location. (kg/m^3)

N = 1371

Model predicted densities for training-set
excluded values fitted against manual
densities at assigned probe measurement
location. (kg/m^3)

N = 1370

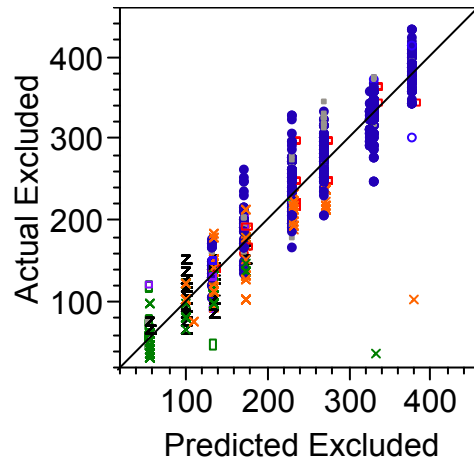
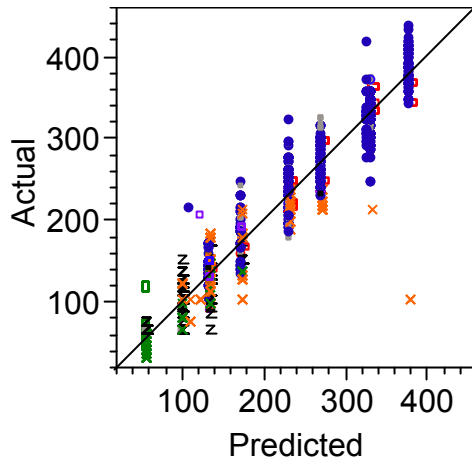
5



R^2
Model
0.890

R^2
Predicted
Excluded
0.895

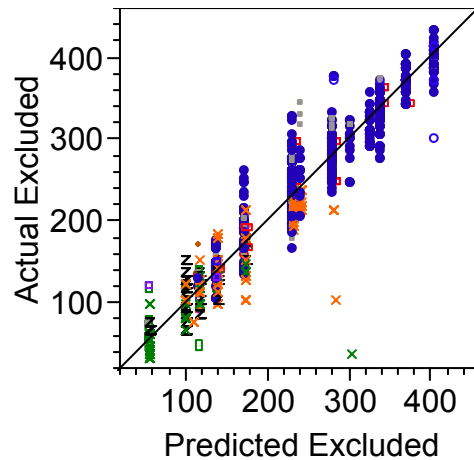
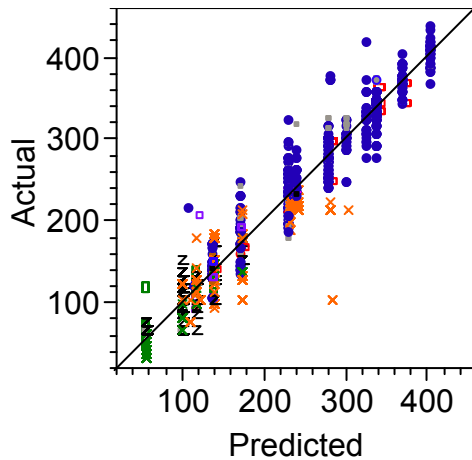
10



R^2 Model
0.928

R^2
Predicted
Excluded
0.925

15



R^2 Model
0.943

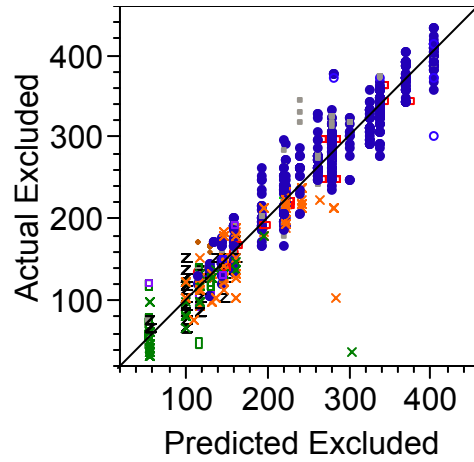
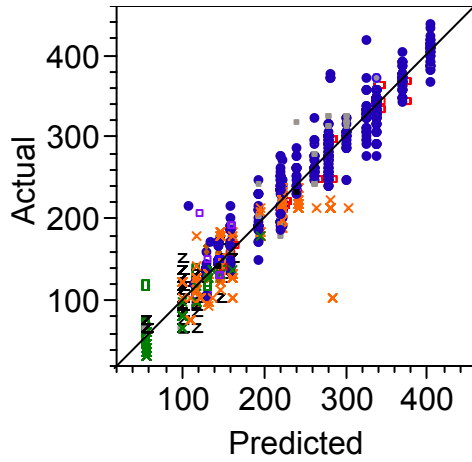
R^2
Predicted
Excluded
0.936

of
Splits
at
Model
Output

Model predicted densities fitted against manual
densities at assigned probe measurement
location. (kg/m³)
N = 1371

Model predicted densities for training-set
excluded values fitted against manual
densities at assigned probe measurement
location. (kg/m³)
N = 1370

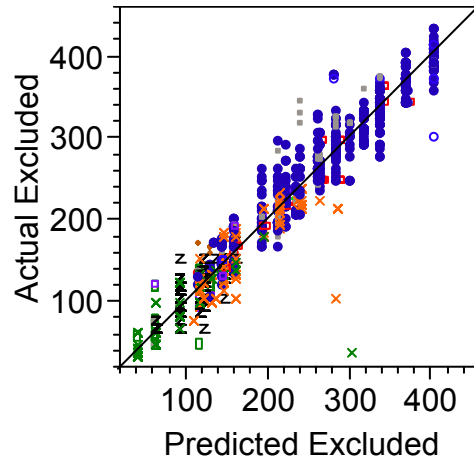
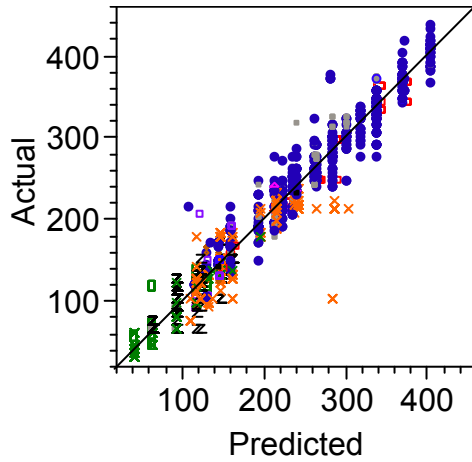
20



R² Model
0.952

R²
Predicted
Excluded
0.945

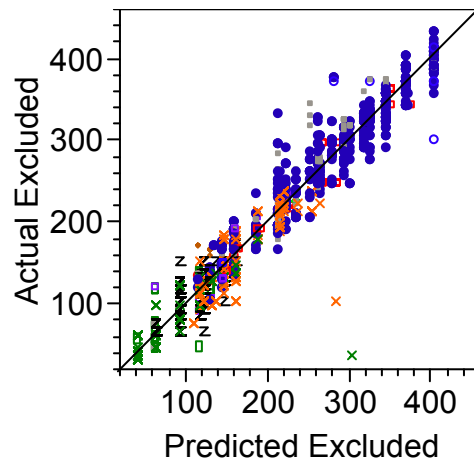
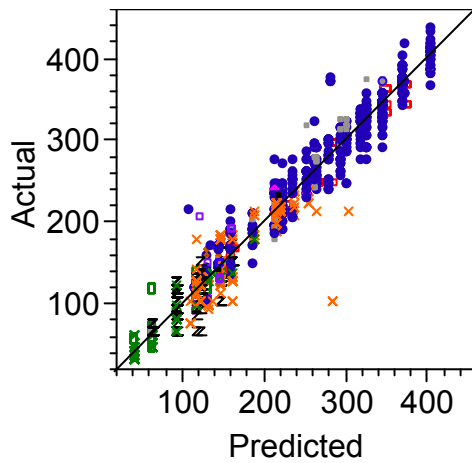
25



R² Model
0.957

R²
Predicted
Excluded
0.948

30



R²
Model
0.961

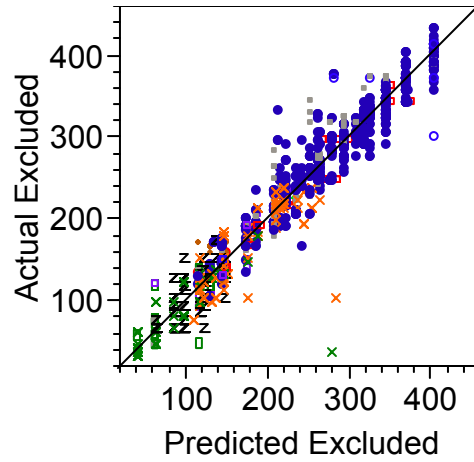
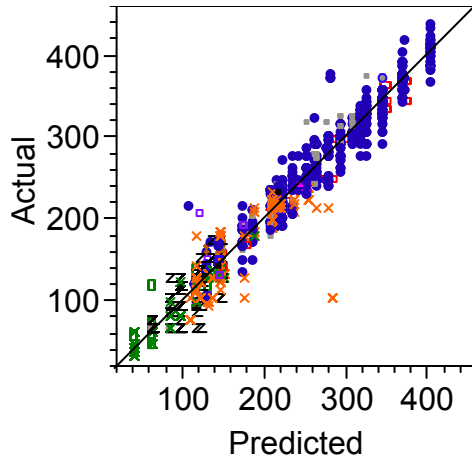
R²
Predicted
Excluded
0.950

of
Splits
at
Model
Output

Model predicted densities fitted against manual
densities at assigned probe measurement
location. (kg/m³)
N = 1371

Model predicted densities for training-set
excluded values fitted against manual
densities at assigned probe measurement
location. (kg/m³)
N = 1370

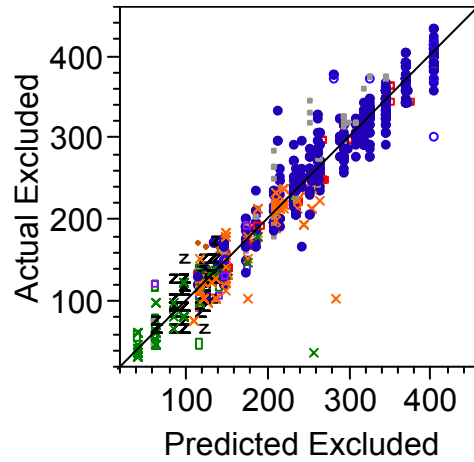
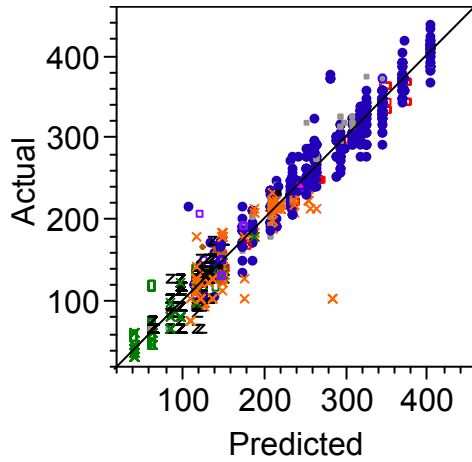
35



R² Model
0.964

R²
Predicted
Excluded
0.953

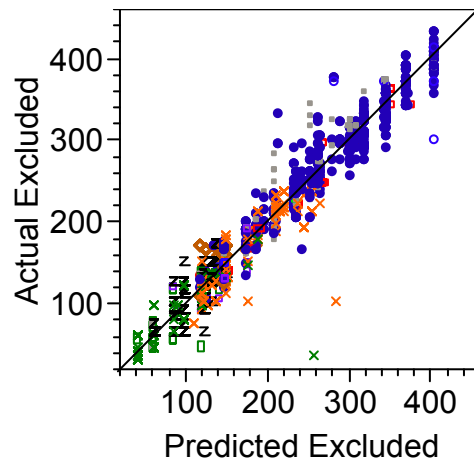
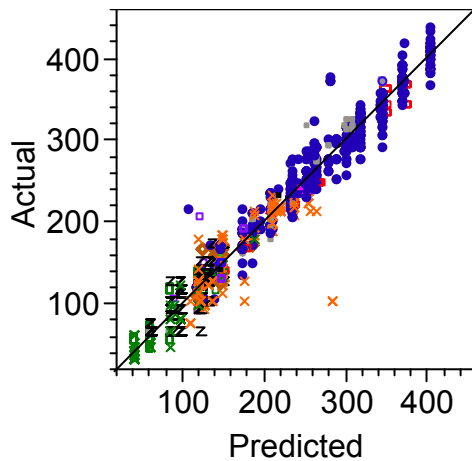
40



R² Model
0.966

R²
Predicted
Excluded
0.955

45



R² Model
0.967

R²
Predicted
Excluded
0.956

Appendix H

Bivariate Fits for 1 Training-set day Model Examples

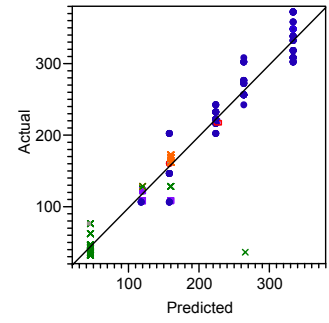
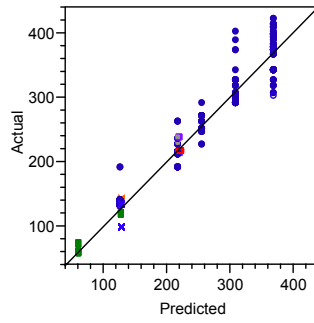
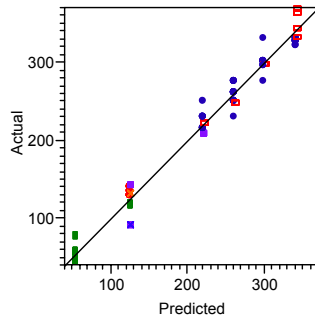
of Splits

23 Feb

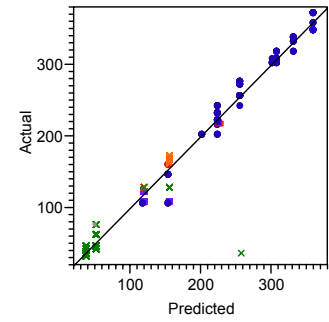
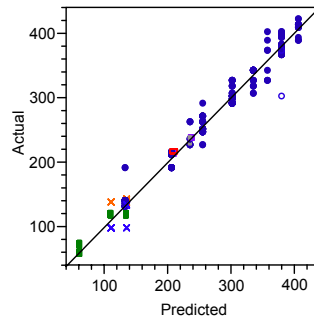
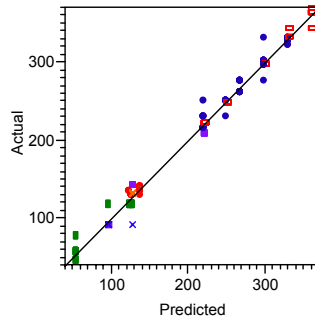
25 Feb

26 Feb

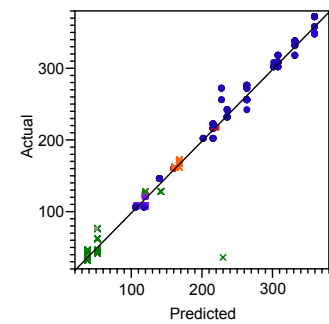
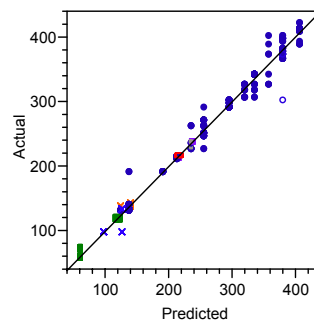
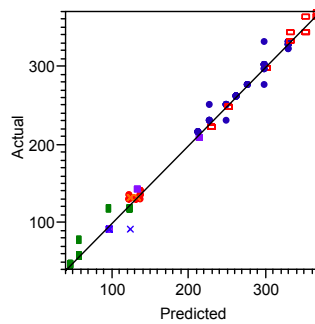
5



10



15



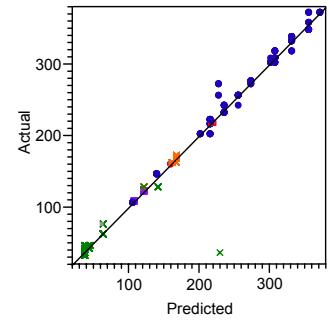
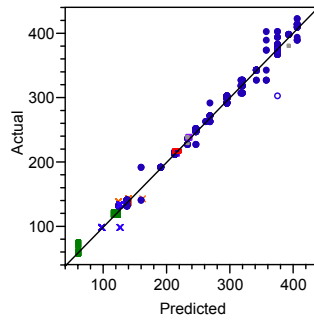
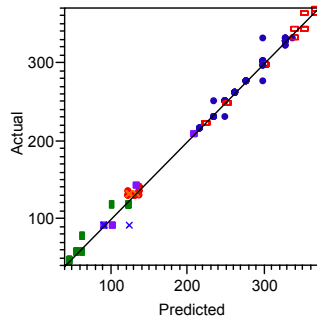
of Splits

23 Feb

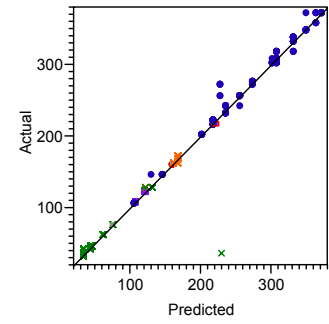
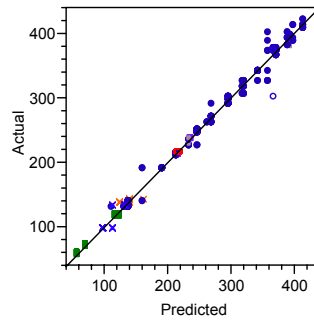
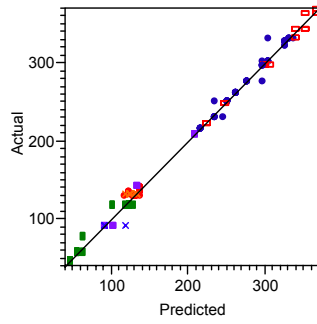
25 Feb

26 Feb

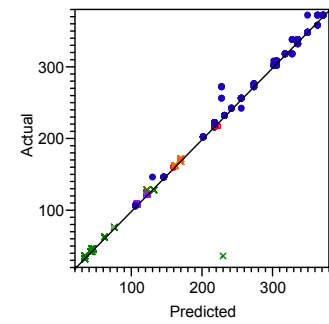
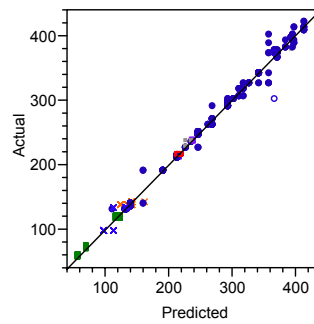
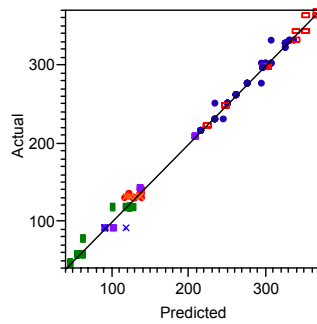
20



25



30



Appendix I Residual Plots for 1 Training-set day Model Examples

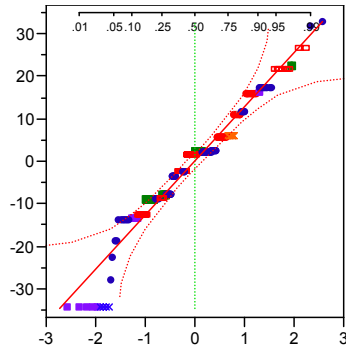
of Splits

23 Feb

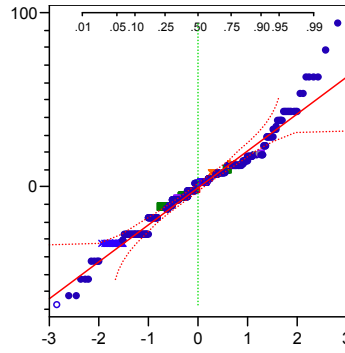
25 Feb

26 Feb

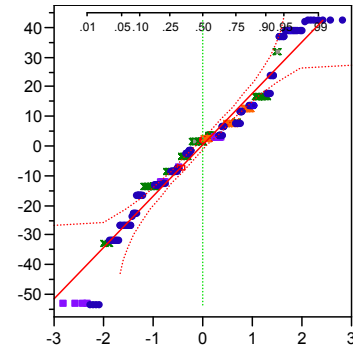
5



Normal Quantile Plot

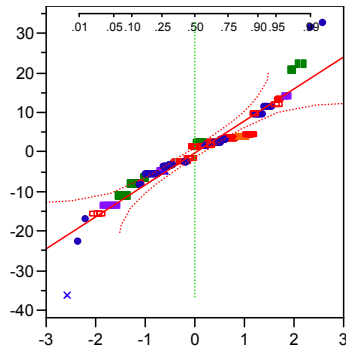


Normal Quantile Plot

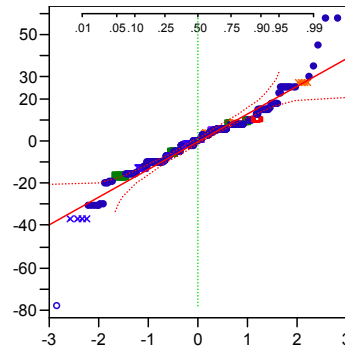


Normal Quantile Plot

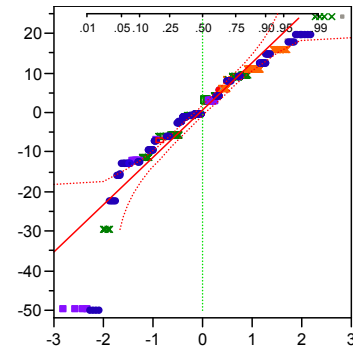
10



Normal Quantile Plot

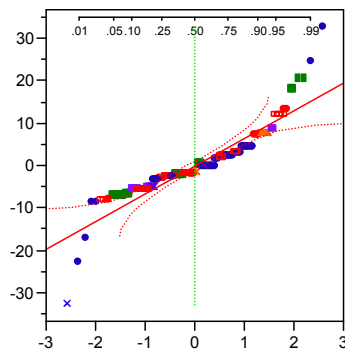


Normal Quantile Plot

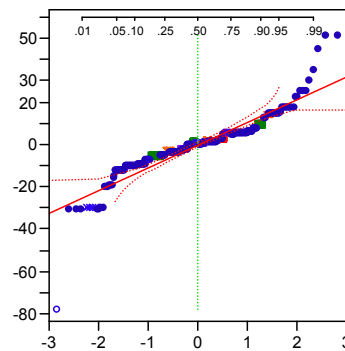


Normal Quantile Plot

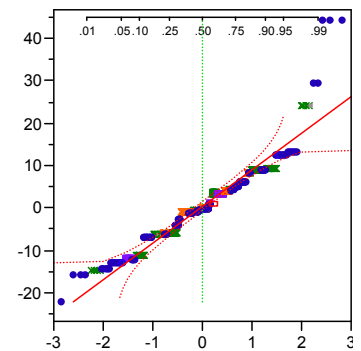
15



Normal Quantile Plot



Normal Quantile Plot



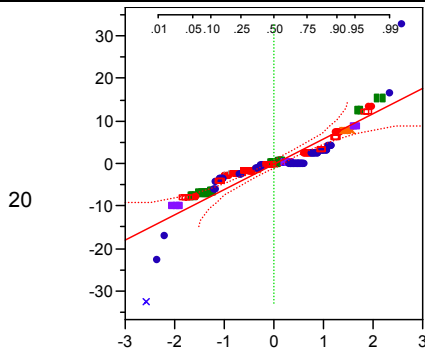
Normal Quantile Plot

of Splits

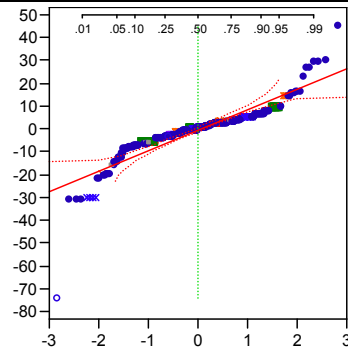
23 Feb

25 Feb

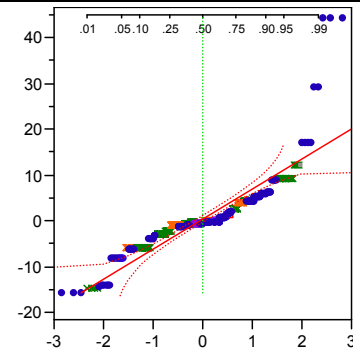
26 Feb



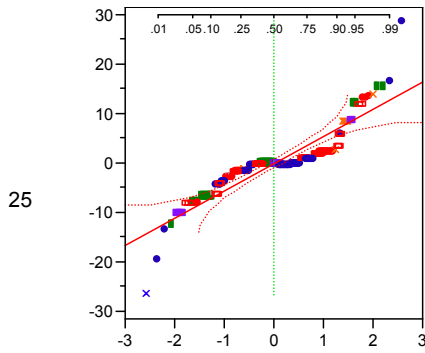
Normal Quantile Plot



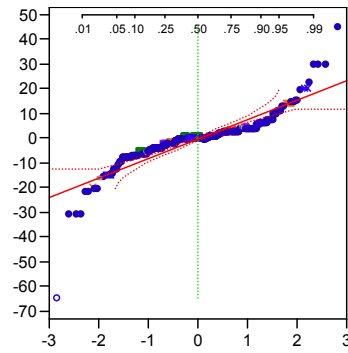
Normal Quantile Plot



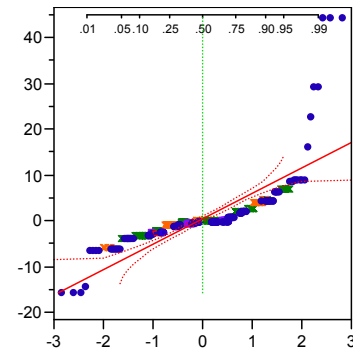
Normal Quantile Plot



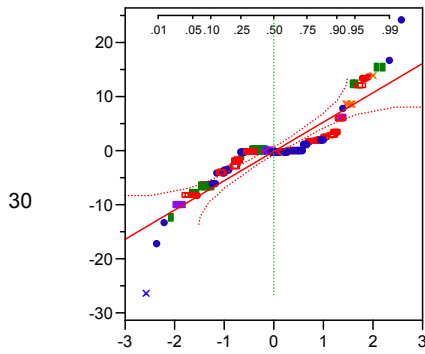
Normal Quantile Plot



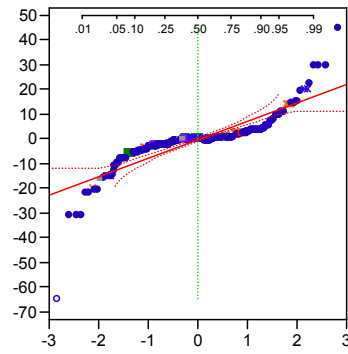
Normal Quantile Plot



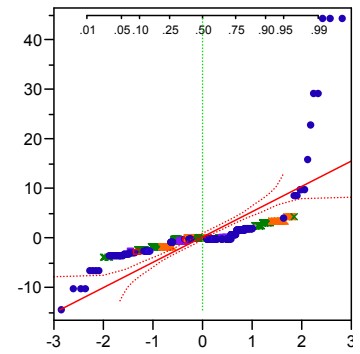
Normal Quantile Plot



Normal Quantile Plot



Normal Quantile Plot



Normal Quantile Plot

Appendix J JMP scripts for Select Models

Interactively constructed models for 1, 2, and 3 day prior training-sets (3 Mar, 2-3 Mar, 1-3 Mar)

3 Mar Model

```
If( :movAvgYpt5cm < -0.28491, If( :movAvgYpt5cm < -0.40701, If( :slopeTemp >= -3.04, 80.8, If( :slopeTemp >= -5.56, If( :slopeTemp >= -3.7, 121.2, 126.3), If( :movAvgYpt5cm < -0.49492, If( :slopeTemp >= -6.725, If( :TGslope >= 0, 131.3, 146.5), If( :movAvgYpt5cm >= -0.60115, If( :slopeTemp < -7.215, If( :movAvgXpt5cm < 0.80952, 141.4, 148.48), If( :movAvgXpt5cm >= 0.860806, If( :TGslope < 0.0199999999999999, 146.5, 151.5), 161.62)), 165.85)), If( :movAvgXpt5cm >= 0.6231166666666667, 163.31666666666667, If( :movAvgXpt5cm < 0.5771266666666667, 166.7, 183.84))))), If( :slopeTemp < -5.99, If( :movAvgYpt5cm < -0.35206, 181.84, If( :slopeTemp < -6.099999999999999, If( :movAvgXpt5cm >= 0.31013, 207.9166666666667, If( :movAvgYpt5cm >= -0.29956, 211.5125, 236.642857142857)), 243.857142857143)), 287.9)), If( :movAvgYpt5cm < -0.21775, If( :slopeTemp < -5.745, If( :slopeTemp < -5.869999999999999, If( :TGslope < 0.02000000000000065, 233.757142857143, If( :movAvgXpt5cm < 0.19902, 245.314285714286, 251.54)), 277.8), If( :slopeTemp < -5.389999999999996, If( :slopeTemp < -5.665, 300.98, 310.8777777777778), If( :movAvgXpt5cm >= 0.32845, 333.3, 353.52))), If( :slopeTemp < -4.539999999999997, If( :slopeTemp < -5.46, 282.114285714286, If( :TGslope < 0.04000000000000064, If( :slopeTemp < -4.690000000000001, 340.0333333333333, 348.5), 359.7111111111111)), If( :slopeTemp < -3.67, If( :slopeTemp < -4.25, 378.8, If( :slopeTemp < -3.914999999999999, If( :slopeTemp < -4.08, 390.5666666666667, 393.9), 400.6333333333333)), If( :slopeTemp < -2.36, If( :movAvgXpt5cm >= 0.23443, If( :movAvgXpt5cm < 0.30525, 398.98, 410.7833333333333), If( :movAvgXpt5cm >= 0.12088, 412.4166666666667, 417.16)), 435.32))))))
```

2-3 Mar Model

```
If( :movAvgYpt5cm < -0.28613, If( :movAvgYpt5cm < -0.35776, If( :slopeTemp >= -4.22096, If( :slopeTemp >= -3.04, 80.8, If( :movAvgYpt5cm >= -0.42288, 99.2, 122.22)), If( :movAvgYpt5cm < -0.49248, If( :TGslope >= -0.0199999999999998, If( :slopeTemp >= -6.299999999999999, 133.26170212766, 148.752272727273), If( :movAvgXpt5cm >= 0.84493, 149.91, 164.338461538462)), If( :movAvgXpt5cm >= 0.82051, 136.38, 178.022807017544))), If( :movAvgXpt5cm >= 2.418805, 84.2, If( :slopeTemp < -5.835, If( :movAvgXpt5cm < 0.35897, If( :movAvgYpt5cm < -0.32642, 204.772727272727, 224.521212121212), 242.8875), 300.885714285714))), If( :movAvgYpt5cm < -0.21897, If( :slopeTemp < -6.061799999999998, If( :movAvgXpt5cm < 0.285715, If( :movAvgYpt5cm < -0.233625, If( :TGslope >= 0.03999999999999892, 213.222222222222, If( :slopeTemp < -6.200000000000002, 223.111764705882, 244.805882352941)), 262.6375), If( :slopeTemp >= -6.100000000000002, 239.6111111111111, 274.15)), If( :movAvgXpt5cm >= 0.4725266666666667, 171.72, If( :slopeTemp < -5.682059999999999, 288.81875, If( :slopeTemp < -5.389999999999996, 316.3133333333333, 337.4125))))), If( :TGslope < 0.0199999999999784, 187.7, If( :slopeTemp < -4.610319999999998, If( :slopeTemp < -5.693999999999999, 281.1555555555556, If( :slopeTemp < -5.006479999999999, 331.991304347826, 353.676923076923)), If( :slopeTemp < -3.67, If( :slopeTemp < -4.1288, 375.76, 391.321621621621), 412.906896551724))))))
```

1-3 Mar Model

```
If( :movAvgYpt5cm < -0.33253, If( :movAvgYpt5cm < -0.389, If( :movAvgXpt5cm >= 1.240946666666667, If( :slopeTemp >= -3.04, 78.7409090909091, 116.312903225806), If( :movAvgXpt5cm >= 0.6434666666666667, If( :movAvgYpt5cm < -0.632585, 122.803921568627, If( :slopeTemp >= -4.22096, 130.242857142857, If( :slopeTemp < -4.9899, If( :TGslope >= -0.1200000000000002, If( :slopeTemp >= -6.725, 139.434579439252, 152.1), 157.322222222222), 167.5))), 170.890909090909), If( :slopeTemp >= -3.67376, 98.5, If( :movAvgYpt5cm < -0.3716, 186.45, If( :movAvgXpt5cm < 0.34432, 199.707692307692, 225.75))))), If( :movAvgYpt5cm < -0.21897, If( :slopeTemp < -6.080000000000004, If( :movAvgXpt5cm < 0.285715, If( :movAvgYpt5cm < -0.233625, 226.508695652174, If( :movAvgXpt5cm < 0.202075, 245.48, 293.94)), If( :TGslope < 0.02000000000000044, If( :slopeTemp >= -6.100000000000001, 234.490476190476, If( :movAvgYpt5cm < -0.308715, 224.7333333333333, 256.602702702703)), 275.654838709677)), If( :movAvgXpt5cm >= 2.5772275, 90.2, If( :slopeTemp < -5.682059999999999, If( :TGslope < 0.04000000000000026, 281.086956521739, 311), If( :slopeTemp < -4.910000000000001, 320.366129032258, 366.7875))))), If( :TGslope < 0.0199999999999784, 214.271428571429, If( :slopeTemp < -4.610319999999998, If( :slopeTemp < -5.693999999999999, 292.93125, If( :slopeTemp < -
```

5.006479999999999, 330.7, 350.120338983051)), If(:slopeTemp < -3.914999999999999, 377.0359375, 406.330434782609))))))

Automatically constructed models for 1, 2, and 3 day prior training-sets (2 Mar, 1-2 Mar, 28 Feb – 2 Mar)

2 Mar Model

If(:movAvgXpt5cm >= 0.484494, If(:slopeTemp >= -4.22096, If(:TGslope >= -0.2, 75.8, 101), If(:movAvgYpt5cm < -0.5213733333333333, If(:slopeTemp < -6.200000000000001, 126.3, If(:slopeTemp < -5.8074, If(:movAvgYpt5cm < -0.560855, If(:slopeTemp < -6.13572, 141.4, 146.5), 150.6583333333333), If(:slopeTemp >= -5.2863, If(:slopeTemp < -5.0754, 151.5, 163.62), 171.7))), If(:slopeTemp < -4.9614, If(:movAvgXpt5cm >= 0.53602, If(:TGslope >= -0.0999999999999996, If(:movAvgXpt5cm >= 0.5991033333333333, 155.58, 162.66), 171.7), 186.9), 181.8))), If(:slopeTemp < -6.061799999999998, If(:slopeTemp < -6.2, If(:movAvgYpt5cm < -0.35776, If(:TGslope >= 0, 166.7, 186.9), If(:movAvgXpt5cm < 0.27595, If(:movAvgYpt5cm < -0.309635, 196.98, If(:movAvgXpt5cm < 0.17501, 215.2625, If(:movAvgYpt5cm < -0.2714766666666667, If(:movAvgYpt5cm >= -0.281855, 212.1, 224.385714285714), 235.5))), If(:slopeTemp < -6.3, 222.2, 232.77272727272727))), If(:TGslope >= 0.03999999999999892, 225.085714285714, If(:TGslope < 0, If(:slopeTemp >= -6.1, 237.4, If(:slopeTemp >= -6.13518, 252.5, 262.6)), If(:movAvgYpt5cm < -0.26354, 264.84444444444444, If(:slopeTemp >= -6.15962, 282.8, 287.9))))), If(:slopeTemp < -5.006479999999999, If(:movAvgYpt5cm < -0.26049, If(:movAvgXpt5cm >= 0.43834, 298, 309.75), If(:slopeTemp < -5.690039999999999, 311.08, If(:TGslope < 0.01999999999999947, 317.6, If(:slopeTemp >= -5.420300000000001, 324.9, 333.3))))), If(:slopeTemp < -4.610319999999998, If(:movAvgXpt5cm >= 0.241755, 338.4, 356.075), If(:slopeTemp < -4.1288, 370.485714285714, If(:movAvgXpt5cm >= 0.1453, 378.7888888888889, 391.4))))))

1-2 Mar Model

If(:movAvgXpt5cm >= 0.484494, If(:movAvgXpt5cm >= 1.240946666666667, If(:slopeTemp >= -3.2486, 72.0125, 108.107407407407), If(:movAvgYpt5cm < -0.632585, 121.325, If(:movAvgXpt5cm >= 0.7539675, If(:slopeTemp >= -4.09328, 130.715151515152, If(:TGslope >= -0.1200000000000002, If(:slopeTemp < -4.9899, If(:movAvgYpt5cm < -0.59789, 132.5, 144.078181818182), 175.0666666666667), If(:movAvgXpt5cm < 0.8083, 143.1, 171.119230769231))), If(:movAvgYpt5cm < -0.5213733333333333, 141.881818181818, If(:movAvgYpt5cm < -0.4598175, If(:slopeTemp < -6.23, 156.2625, 177.77), 178.0375))))), If(:slopeTemp < -6.061799999999998, If(:movAvgYpt5cm < -0.32703, If(:movAvgYpt5cm < -0.38564, 173.823529411765, If(:movAvgXpt5cm < 0.33028, 195.053846153846, 216.94347826087)), If(:slopeTemp < -6.21, If(:TGslope < 0.01999999999999962, 223.196153846154, If(:TGslope < 0.05999999999999912, If(:movAvgXpt5cm < 0.3199, 227.266666666667, 252.52), 277.8)), If(:TGslope >= 0.03999999999999892, 223.4625, If(:TGslope < 0, If(:slopeTemp >= -6.1, 237.4, 257.045), If(:movAvgYpt5cm < -0.2708675, 268.0833333333333, 286.7555555555556))))), If(:slopeTemp < -5.006479999999999, If(:slopeTemp < -5.85, 295.2866666666667, If(:movAvgXpt5cm >= 0.43834, 302.328571428571, 324.315625))), If(:slopeTemp < -4.610319999999998, 348.278723404255, If(:slopeTemp < -4.209999999999996, 364.295652173913, 380.678378378378))))))

28 Feb – 2 Mar Model

If(:movAvgYpt5cm < -0.33253, If(:movAvgXpt5cm >= 0.7539675, If(:movAvgYpt5cm < -0.637046, If(:movAvgYpt5cm < -0.74726, 91.6982323232323, 118.09317898082), If(:movAvgXpt5cm >= 1.6123325, 111.002312008979, If(:TGslope >= -0.32, If(:slopeTemp >= -4.22096, If(:slopeTemp < -3, 103.022222222222, 141.428904428904), If(:TGslope >= -0.1200000000000002, 140.721230655175, 166.924348750665)), 164.125))), If(:movAvgYpt5cm < -0.39724, If(:movAvgYpt5cm < -0.49248, 156.920014094433, 173.580471380471), If(:TGslope < 0.03999999999999963, 206.25513963161, 244.444444444444))), If(:movAvgYpt5cm < -0.2271133333333333, If(:TGslope < -0.1000000000000005, 90.2, If(:slopeTemp < -6.080000000000004, If(:TGslope < 0.02000000000000044, If(:movAvgXpt5cm < 0.286935, 224.788418430884, If(:slopeTemp < -7.57, 223.484848484848, If(:slopeTemp >= -6.905000000000002, 251, 274.281274281274))), If(:movAvgYpt5cm < -0.25683, If(:TGslope < 0.03999999999999967, If(:movAvgXpt5cm < 0.2930433333333333, 213.936363636364, If(:movAvgXpt5cm >= 0.36386, 249.360606060606, 286.192480359147)), 288.08703030303), 292.618426691154))), If(:slopeTemp < -4.71, 313.124130190797, 358.58))), If(:movAvgXpt5cm >= 0.37485, 192.92, If(:slopeTemp < -5.58, If(:slopeTemp < -6.005, 304.507407407407,

334.480963480963), If(:slopeTemp < -4.20999999999996, If(:movAvgXpt5cm >= 0.298535, 328.9, If(:TGslope < 0.0400000000000141, 349.922641509434, 366.693407761829)), 380.872222222222))))))